DEFLATING THE DIMENSIONALITY CURSE IN ELECTRONIC STRUCTURE CALCULATIONS

By

ANN MELNICHUK

A DISSERTATION PRESENTED TO THE GRADUATE SCHOOL
OF THE UNIVERSITY OF FLORIDA IN PARTIAL FULFILLMENT
OF THE REQUIREMENTS FOR THE DEGREE OF
DOCTOR OF PHILOSOPHY

UNIVERSITY OF FLORIDA

2013

To my friends and loved ones

ACKNOWLEDGMENTS

I am deeply grateful for the help and direction of Dr. Rodney J. Bartlett who has been my dissertation adviser for the past six years. I thank our graduated group members: Andrew, Tom H., Josh, and Prakash from whom I have learned much and I thank our current group members: Victor, Tom W., Robert, Alexandre and Matt with whom I've had many stimulating conversations. My special thanks to Dmitry who has not only been an invaluable resource but a great friend.

I thank Ajith for tirelessly teaching our graduate students how to become better scientists, programmers, and human beings. I thank Charlie, Jon and Craig for their efforts in running the UF HPC center and teaching me much about server maintenance and the Linux environment.

Many thanks go out to my committee members with whom I've had many interesting discussions and collaborations over the years: Dr. Deumens, Dr. Bowers, Dr. Brucat and Dr. Sullivan. Finally, I'd like to extend my gratitude to the QTP members as well as to the members of the Chemistry and the Electrical and Computer Engineering departments for their encouragement and support.

TABLE OF CONTENTS

page

LIST OF TABLES

LIST OF FIGURES

Abstract of Dissertation Presented to the Graduate School
of the University of Florida in Partial Fulfillment of the
Requirements for the Degree of Doctor of Philosophy

DEFLATING THE DIMENSIONALITY CURSE IN ELECTRONIC STRUCTURE CALCULATIONS

By

Ann Melnichuk

May 2013

Chair: Rodney J. Bartlett
Major: Chemistry

Many-body problems whether classical or quantum suffer from what is known as a *dimensionality curse*. In solving physical problems, we are generally interested in quantifying interactions between physical entities and as the quantity of these entities increases, the number of interaction equations one must solve increases much faster.

The work described in this dissertation presents several solutions for the reduction of the dimension of calculations of electronic structure of molecules. Techniques and examples are drawn from calculations of excited states, UV/Vis absorption cross sections, and high-level theoretical treatment of multi-reference electronic structure problems.

The techniques described here may be combined to achieve highly accurate theoretical results for challenging examples at only a small fraction of the cost. Speed-up upwards of 500x were observed for several systems versus the established methods and several examples are presented which would not be otherwise practical to do given the current computational limitations.

CHAPTER 1
INTRODUCTION TO DIMENSIONALITY ISSUES IN QUANTUM MECHANICS

In electronic structure theory, to calculate the correlation energy between electrons is a problem which suffers from a so-called dimensionality curse as do most n-particle problems in physics. The simplest approximation to electron correlation energy is a perturbative correction of the sum of all pair of electrons interactions to a reference energy which is obtained by a variational minimization calculation for each electron in a field of $n-1$ electrons (Hatree-Fock method).

1.1 Hatree-Fock reference

Several approximations are made to the full Schrödinger Equation, $\hat{H}(r,t)\Psi(r,t) = -\frac{\partial}{\partial t}\Psi(r,t)$ to make it applicable to a molecular system. Initially, the Hamiltonian ($\hat{H}$) and the wavefunction (Ψ) are separated into a function of time and a function of space. The calculation of the ground state energy with Hartree-Fock involves only the spatial portion of the Schrödinger Equation:

$$\hat{H} = \begin{array}{ll} -\sum_A \frac{1}{2m_A}\nabla_A^2 & \text{Nuclear kinetic energy} \\ +\sum_{B<A} \frac{Z_A Z_B}{R_{AB}} & \text{Nuclear-nuclear repulsion term} \\ -\sum_{i,A} \frac{Z_A}{R_{iA}} & \text{Nuclear-electron potential term} \\ -\sum_i \frac{1}{2}\nabla_i^2 & \text{Electron kintec energy} \\ +\sum_{j<i} \frac{1}{r_{ij}} & \text{2-electron potential term} \end{array}$$

where there are A nuclei and i electrons and Z_A is the nuclear charge of the A^{th} nucleus. The time-independent Hamiltonian is further separated into an electronic part and a nuclear part. This is called the Born-Oppenheimer approximation in which the atomic nuclei are treated as a stationary potential thus producing the bound quantum well for the electrons. The BO approximation fails for cases where the potential is not bound (a continuum state) or when there exist several potentials at a point (avoided crossing).

The wavefunction of electrons only is varied until the minimum value for the energy is found. In all calculations in this dissertation the wavefunction is approximated by a

set of Gaussian functions called a basis set. The atomic basis set functions describe the atomic electronic structure to various degrees of accuracy and are unique to each atom. After the Hatree-Fock equations are solved and the minimum of the energy is obtained, the linear combination of atomic orbitals (LCAO) represent the molecular orbital electronic structure of the ground state reference.

The Hatree-Fock calculation nominally scales as $O(N^4)$ where N is the number of basis functions due to the computation of 2-electron integral quantities. The overhead is greater due to the need do call an eigensolver at each iteration for a matrix size of N^2. There are linearly scaling Hartree-Fock approaches but they are not used in this study since calculation of the reference is never the time limiting step here.

The ground state reference is ideally a single Slater determinant ($|\Psi_0\rangle = |\chi_1\chi_2\cdots\chi_N\rangle$) where χ is a molecular orbital. In the unrestricted Hartree-Fock (UHF) calculation the α and β electrons are treated as separate entities which may lead to a breaking of spin and spatial symmetry as well as a lower ground state energy than the energy from a restricted Hartree-Fock calculation (RHF) where α and β electrons are indistinguishable. In a well-behaved single reference system, the UHF and RHF solutions are virtually identical but in multi-reference systems (where more than one Slater determinant is needed to describe the electronic state), the UHF wavefunction can be dramatically different than the RHF wavefunction.

In this work, preference is given to the RHF wavefunction for closed-shell molecules because it is an eigenfunction of the spin operator which leads to whole values for the spin quantum number whereas the UHF wavefunction may lead to a contaminated spin quantum number such as 1.2, 2.4, etc. In a high-spin open-shell molecule such as a hydroxy radical, the UHF wavefunction is well behaved near the equilibrium geometry and produces $\approx$2 for the spin number up to computational accuracy. Restricted open-shell Hatree-Fock (ROHF) reference may be used to strictly impose the spin eigenfunction property of the open shell wavefunction. For difficult multi-reference cases

which also happen to be open-shell the ROHF solution tends to have convergence difficulties such as oscillating between two nearly degenerate solutions.

The RHF reference does not include any electron correlation energy. Even though the electron correlation energy is a very small portion of the total energy, the correlation energy of an electron pair is $\approx 20 kcal/mol$ which is on the order of chemically-relevant quantities. Without correlation, *ab initio* calculations tend to lose touch with reality. There are two main types of correlation: dynamic and static. The dynamic correlation manifests itself in a large number of small contributions from Slater determinants other than the ground state $|\Psi_0\rangle$. The static correlation manifests itself in cases where there are two or more Slater determinants which have a significant contribution of which $|\Psi_0\rangle$ only describes a part of the total ground state wavefunction. Post-Hartree-Fock methods which account for the contributions of other determinants are needed to obtain experimentally-relevant results. The calculation of electron correlation is where one becomes faced with a dimensional explosion of the problem.

1.2 Dimensionality issues in electronic structure

1.2.1 Ground state

For the benefit of clarity and simplicity, the following assumptions are made in the discussion that follows:

1. The system is closed shell with an even number of electrons; referred to as RHF (restricted Hartree-Fock).
2. Two indistinguishable electrons occupy each HF energy level.
3. The physical space describing an electron with respect to the other electrons generates a set of one- and two-electron integrals.

By assumption (2), we only need to calculate energy contribution from one of the electrons in an energy level and simply double it.

The integrals are calculated prior to the correlation energy calculation. They are stored as a tensor of rank 4 and have dimension of o^2v^2. The index o (number of

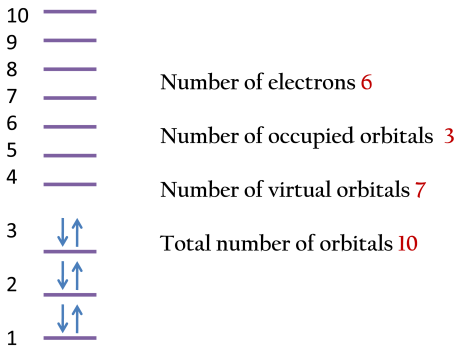

Figure 1-1. Diagram showing an example of a typical electronic structure problem

occupied orbitals) is a function of how many electrons are in the system, $o = (Num.e)/2$ and the index v is the number of virtual orbitals. Graphically, the partitioning of the o and v space is represented in Figure 1-1. Each level in Figure 1-1 denotes a filled or an empty orbital. The energy values of the levels are the eigenvalues of the RHF equations and the orbitals are the associated eigenvectors.

In order to include electron correlation, we start with the unperturbed system as shown in Figure 1-1 and allow the electrons to move from the occupied orbitals to the unoccupied orbitals. This allows for sampling of determinants other than the $|\Psi_0\rangle$ determinant.

By virtue of Brillouin's Theorem, determinants which differ from $|\Psi_0\rangle$ by moving a single electron from the occupied space to the virtual space do not directly contribute to the correlation energy because the matrix element $\langle\Psi_0|\bar{H}|\Psi_i^a\rangle$ is 0. As a first order approximation of the many body perturbation theory (MBPT2), we only allow for two electrons to move at a time; making a set of doubly-excited states known as a doubly-excited Hilbert space.

Figure 1-2 shows some of the correlation energy contributions which arise from moving a pair of electrons in the orbital space. The index notation is $E2(A, I, B, J)$ where I is the index of the orbital of origin of one of the electrons and A is the index of its

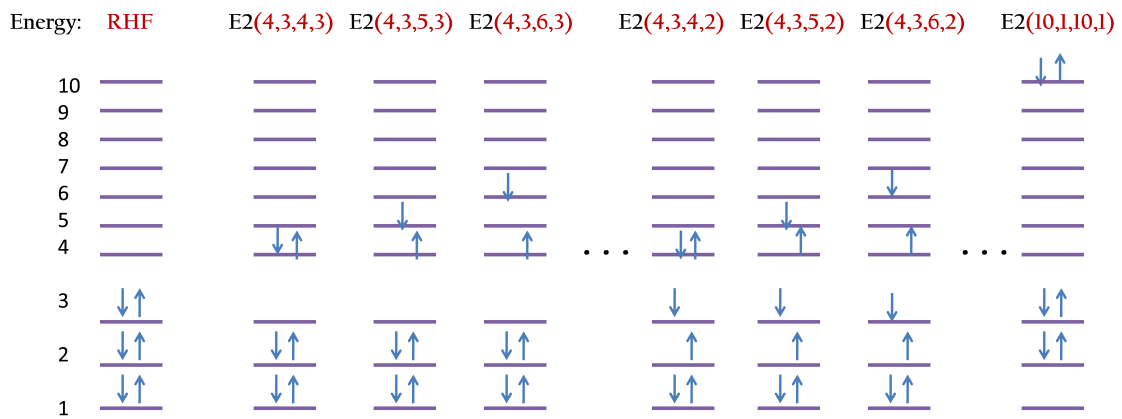

Figure 1-2. Diagram showing several elements of the Hilbert space (one pair only) starting from the zeroth order wavefunction (RHF). There are $o^2v^2 + 1$ elements in this space.

destination orbital. Index J is of the orbital of origin of the other electron and index B is of its destination orbital.

It is clear that even for a first order approximation to the correlation energy the number of contributing elements can get very large and it will be even less manageable, as we allow for more than two-particle interaction.

The following formula is used to compute the $E2$ contributions and the final value for $E2$:

$$E2(A,I,B,J) = \frac{2\,G(A,I,B,J)^2 - G(A,I,B,J) * G(B,I,A,J)}{\epsilon(I) + \epsilon(J) - \epsilon(A) - \epsilon(B)} \tag{1–1}$$

$$E2 = \sum_{A=o+1}^{bf} \sum_{I=1}^{o} \sum_{b=o+1}^{bf} \sum_{J=1}^{o} E2(A,I,B,J) \tag{1–2}$$

where G is the 2-electron integral tensor and ϵ is a vector of orbital energies. The total energy for the system is then presented as $E = E_{RHF} + E2$.

The main drawback of the MBPTn theory is the slow convergence to recover 100% of the correlation energy combined with a steeply climbing cost: MBPT2 ($O(o^2v^2)$), MBPT3 ($O(o^2v^4)$), MBPT4 ($O(o^3v^4)$). The best solution to obtain the highest percentage of correlation energy for the lowest cost is the coupled cluster (CC) theory[3, 4, 8–10, 27, 28, 84, 123, 131]. The CC methods have the advantage of being

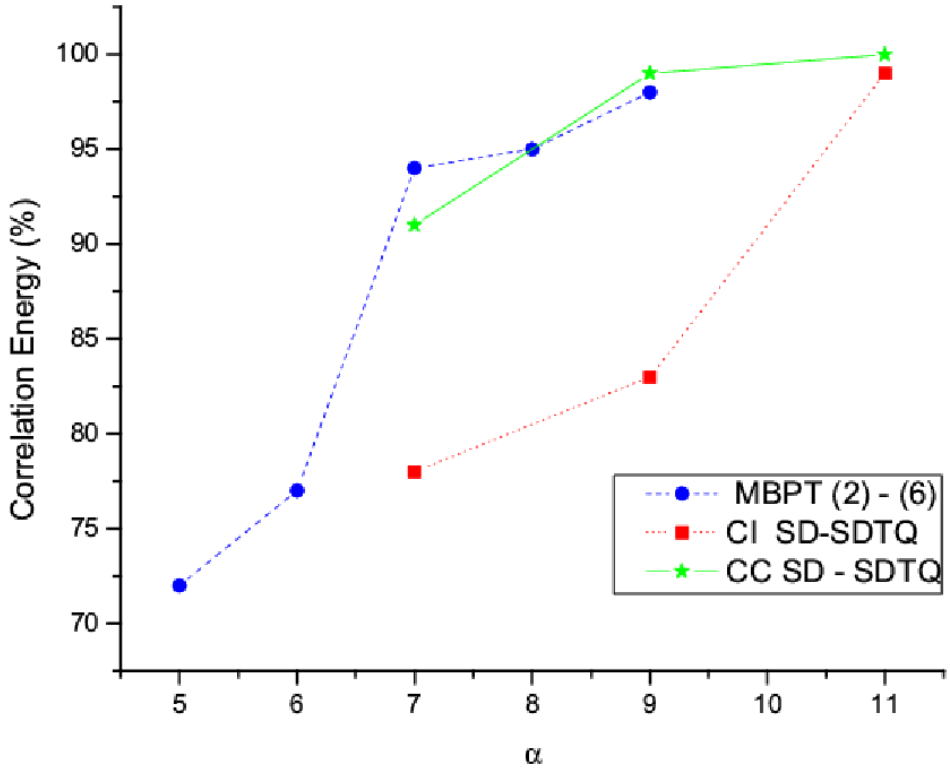

Figure 1-3. Scaling and correlation recovery of select post-Hartree-Fock methods adapted from Bartlett and Musial JCP 2007[113]

size-extensive and infinite to orders of MBPT which leads to a much faster convergence to 100% of the correlation energy[113] as shown in Figure 1-3.

In the CC ansatz the other determinants are accessed *via* a $\hat{T}$ operator which is composed of creation and annihilation operators $\alpha^\dagger$ and α. The following $\hat{T}_2$-operator creates the determinant space shown in Figure 1-2:

$$\hat{T}_2 = \frac{1}{4}\sum_{a,b,i,j} t_{ij}^{ab}\hat{\alpha}_i\hat{\alpha}_j\hat{\alpha}_a^\dagger\hat{\alpha}_b^\dagger \tag{1–3}$$

where t_{ij}^{ab} (one of many types of t-amplitudes) are the solutions to the CC equations below. The entire CC wavefunction consists of all orders of the $\hat{T}$-operator:

$$|\Psi_{CC}\rangle = e^{\hat{T}}|\Psi_0\rangle \tag{1–4}$$

$$e^{\hat{T}} \approx 1 + \hat{T}_1 + \hat{T}_2 + \frac{1}{2!}\hat{T}_1^2 + \hat{T}_3 + \hat{T}_1\hat{T}_2 + \ldots \tag{1–5}$$

Specifically, the popular singles and doubles coupled cluster method (CCSD) is:

$$|\Psi_{CCSD}\rangle = e^{\hat{T}_1 + \hat{T}_2}|\Psi_0\rangle \tag{1–6}$$

which scales as $iO(o^2v^4)$ and the CCSDT method

$$|\Psi_{CCSDT}\rangle = e^{\hat{T}_1 + \hat{T}_2 + \hat{T}_3}|\Psi_0\rangle \tag{1–7}$$

which scales as $iO(o^3v^5)$. Since both are iterative methods, i is the number of iterations needed for convergence of the t-amplitudes. For example in the CCSD method, convergence is reached when conditions $\langle\Psi_i^a|\hat{H}e^{\hat{T}_1+\hat{T}_2}|\Psi_0\rangle = 0$ and $\langle\Psi_{ij}^{ab}|\hat{H}e^{\hat{T}_1+\hat{T}_2}|\Psi_0\rangle = 0$ are satisfied by solving a set of non-linear equations.

The correlation energy is computed once convergence is reached. The CC energy is expressed by substituting a similarity-transformed Hamiltonian ($\bar{H}$) into the Schrödinger Equation:

$$e^{-\hat{T}}\hat{H}e^{\hat{T}}|\Psi_0\rangle = \bar{H}|\Psi_0\rangle = E_{CC}|\Psi_0\rangle \tag{1–8}$$

$$\langle\Psi_0|\bar{H}|\Psi_0\rangle = E_{CC}\langle\Psi_0|\Psi_0\rangle \tag{1–9}$$

$$\langle\Psi_0|\bar{H}|\Psi_0\rangle = E_{CC} \tag{1–10}$$

Equation 1–10 is true for all orders of the CC theory because higher order $\hat{T}$-operators do not make a contribution to energy since there are at most 2-particle terms in the Hamiltonian (*cf.* BakerâĂŞCampbellâĂŞHausdorff commutator relation).

The CC method described above is based on a single reference $|\Psi_0\rangle$ upon which all the contributions from other references are computed *via* the exponential ansatz. In the case where a problem is dominated by dynamic correlation, the CCSD and the subsequent CCSD(T) (CCSD with a non-iterative contribution from three terms

from the CCSDT) can recover over 99% of the correlation energy. However, due to the perturbative nature of the CC equations, cases of static correlation when several references contribute greatly to a single state, one needs to go beyond CCSD to obtain a correct description of the problem. In such cases the CC calculations become unmanageably expensive. Any non-iterative methods based on a single reference tend to fail dramatically for multi-reference problems as well. A classic example of this is the ozone molecule which has four major determinants in the ground state at equilibrium. In order to get quantitatively correct vibrational frequencies, one needs to solve CCSDTQ equations.

How to use single-reference CC theory to tackle cases where static *and* dynamic types of correlation are present will be the subject of Chapters 5 and 6 of this dissertation.

1.2.2 Excited state

In this work, vertical excitation energies are computed using configuration interaction with singles (CIS) [46], equation-of-motion singles and doubles (EOM-CCSD) [148] methods and the similarity transformed equation-of-motion (STEOM-CCSD) method [6] to compute excited state energies. The computation of excited states suffers from a similar dimensional explosion problem as the ground state CC theory. Chapter 2 describes several examples regarding the accuracy of these methods.

The CIS method is the least expensive since only singly-excited determinants are included for. In essence, the CIS method finds high-energy solutions to the Hartree-Fock equations and as such does not include any explicit electron correlation. The CIS excitation energy for a k^{th} target excited state is:

$$\omega_k = \Delta E_i^a(CIS) = E_0(HF) - \epsilon_i + \epsilon_a - \langle ia||ia\rangle \tag{1–11}$$

where i can be any occupied molecular orbital and a can be any virtual molecular orbital. While CIS does not account for electron correlation, the wavefunction generated by CIS is often used as a starting guess for solving the EOM-CC equations.

The EOM-CC method can be used to compute the energy and properties of a k^{th} target excited state whether it be electron attachment (EA-EOM), ionization potential (IP-EOM) or excitation (EE-EOM) with electron correlation. It applies a linear excitation operator ($\hat{R}_k$) on a ground state coupled cluster wavefunction:

$$\hat{H}\hat{R}_k e^{\hat{T}}|\Psi_0\rangle = \Delta E_k \hat{R}_k e^{\hat{T}}|\Psi_0\rangle \tag{1–12}$$

or in terms of $\bar{H}$:

$$\bar{H}\hat{R}_k|\Psi_0\rangle = \Delta E_k \hat{R}_k|\Psi_0\rangle \tag{1–13}$$

where $\hat{R}_k$ is:

$$\begin{aligned}\hat{R}_k &= \hat{R}_0 + \hat{R}_1 + \hat{R}_2 + \ldots \\ &= \hat{R}_0 + \textstyle\sum_{i,a} r_i^a \hat{\alpha}_i \hat{\alpha}_a^\dagger + \sum j < i,\, b < a r_{ij}^{ab} \hat{\alpha}_i \hat{\alpha}_j \hat{\alpha}_a^\dagger \hat{\alpha}_b^\dagger + \ldots\end{aligned}$$

Unlike the $\hat{T}$-operator the $\hat{R}$-operator does not have non-linear terms such as $\hat{R}_1\hat{R}_2$. The similarity to the ground state CC equations is that $\hat{R}$-operator can also be truncated to some order leading to EOM-CCSD (scales like CCSD for EE and $N_k iO(o^2v^3)$ for IP and $N_k iO(ov^4)$ for EA) and EOM-CCSDT (scales like CCSDT for EE and $N_k iO(o^3v^4)$ for IP and $N_k iO(o^2v^5)$ for EA) where i is the number of steps required to converge to a state and N_k is the number of excited states requested.

Due to the linear nature of the $\hat{R}$-operator, EOM-CC is somewhat less robust that CC theory for the ground state at the same order of expansion. This feature makes it difficult for EOM-CCSD to get highly accurate excitation energies for charge transfer (CT) states and for multiply-excited states. EOM-CCSDx[114] is a recent fix to the EOM-CC ansatz for dealing better with singly-excited charge transfer states. Generally, one needs to be able to solve EOM-CCSDT and beyond to get the most accurate representation of CT and multiply-excited states which gets very expensive.

STEOM-CC is an approximate approach which can greatly reduce the dimension of the EE-EOM through active space selection. Other benefits include: 1) natural

treatment of CT states 2) indirect inclusion of some triples 3) capability to solve for many k-states with virtually no overhead. The main drawback is the dependence on the completeness of the active space. Chapter 2 shows a few examples of CT states where STEOM-CCSD is superior to EOM-CCSD in accuracy and Chapter 5 addresses ways to automatically select active spaces which can be applicable to a STEOM-CC calculation.

The steps to calculate STEOM-CCSD excitation energies are (adapted from [6]):

- Solve the ground state CCSD equations
- Store $\bar{H}$ on the disk
- Choose active occupied orbitals and solve the IP-EOM-CCSD equations. Store the resulting $\hat{R}_k$(IP) in an $\hat{S}^-$-operator.
- Choose active virtual orbitals and solve the EA-EOM-CCSD equations. Store the resulting $\hat{R}_k$(EA) in an $\hat{S}^+$-operator.
- Perform a similarity transform on $\bar{H}$: $\hat{G} = e^{-(\hat{S}^- + \hat{S}^+)} \bar{H} e^{(\hat{S}^- + \hat{S}^+)}$
- Diagonalize $\hat{G}$ over a set of $\hat{\alpha}_i \hat{\alpha}_a^\dagger |\Psi_0\rangle$ configurations where orbitals i and a belong to the active space.

The STEOM-CCSD calculation has scaling of $N_{IP} iO(o^2v^3) + N_{EA} iO(ov^4) + jO(ov)$, the latter term being the diagonalization of $\hat{G}$-matrix step. Since both EA and IP steps nominally scale as $O(N^5)$ and the EE scales as $O(N^6)$, STEOM is guaranteed to be faster if several excited states are requested and the computational disparity between EOM and STEOM grows as the number of EOM-CCSD roots becomes larger.

1.3 Dimensionality issues in molecular structure

The first example of this is in calculating the vibronic energies of molecules. Any non-linear molecule has $3N - 6$ vibrational degrees of freedom where N is the number of atoms in the molecule. From each vibrational level of the ground state, one can get to any symmetry-allowed vibrational levels of the excited state, thus creating the spectral line broadening seen in UV/Vis spectroscopy. For large molecules, calculation of all the possible couplings of vibronic states can be computationally prohibitive and doing so for

dissociative excited states precludes the use of the quadratic potential energy surface (PES) approximations which make these calculations at all feasible.

In this work, a method is introduced which analyses the ground state vibrational energy levels to determine their level of coupling. The levels which couple strongly are pre-selected to go to the next step in the process. Analytical fits are made for the pre-selected vibrational modes for the ground state and excited state PES as well as the dipole strength surface. Vibronic excitation cross section is then computed using discrete variable representation (DVR). Temperature-dependent broadening can be calculated using Boltzmann-weighted averaging of the absorption cross sections from each of the ground state vibrational energy levels.

The combination of coupling pre-screening and analytical fits of the surfaces makes this approach scale as αn where α is the time it takes to compute the energy surface (to be done with whatever level of theory necessary for good results) and n is the number of pre-screened degrees of freedom for the functional group relevant to the study.

1.4 Implementation techniques and software used

In this work both serial ACES II [147] and the parallel ACES III [80, 92, 93] are used. The author's modification and implementation of active-space CC methods are done within ACES II.

The discrete variable representation (DVR) method[90] is adapted to vibronic spectroscopy methods and an original stand-alone program is written in F90 with an interface to the ACES II program.

An automatic active space selection algorithm is written using the R scripting language with an interface to the ACES II program.

CHAPTER 2
CHARGE TRANSFER EXCITED STATES

2.1 Background

Chemical reactions that take place on excited state potential energy surfaces are the subject of many experimental and theoretical studies, since reactivity might be greatly enhanced by the electronic excitation of one or more of the substrates. One class of these reactions is excited state proton transfer (ESPT) which is summarized by the Förster Cycle [47] shown in Figure 2-1.

The correct description of CT is of interest in several studies. Questions addressed include the assessment of the degree of CT in the first excited state, assumed to be significant by [44], as well as in other potential CT states. Also, since it is known that TD-DFT cannot describe such states correctly, more sophisticated methods like EOM-CC and STEOM-CC are applied here.

2.2 Background on examples

The free molecules are shown in Figure 2-2. The ammonia complex is formed by creating a hydrogen bond between the nitrogen and the proton on the hydroxy group. Only the *cis* isomer of the β-naphthol is considered.

Previous theoretical studies of phenol-ammonia clusters have been carried out for the ground state, the first $\pi \rightarrow \pi^*$ excited state and the $\pi \rightarrow \sigma^*$ excited state [32, 141, 142]. The first two phenol excited states were also characterized at the CASSCF level of theory [51]. Experimental studies of phenol and phenol ammonia clusters are abundant in the literature [65, 68, 108, 119, 127, 143, 154]. The α-naphthol ammonia clusters have been studied with resonance-enhanced multiphoton ionization (REMPI), resonant two-photon ionization (R2PI), laser induced fluorescence (LIF), and fluorescence emission spectroscopy [24, 25, 56, 58, 63, 72, 150] with support from *ab inito* study [56, 150]. The β-naphthol ammonia clusters have been studied with REMPI, R2PI, fluorescence emission spectroscopy, and with UV absorption and emission in an

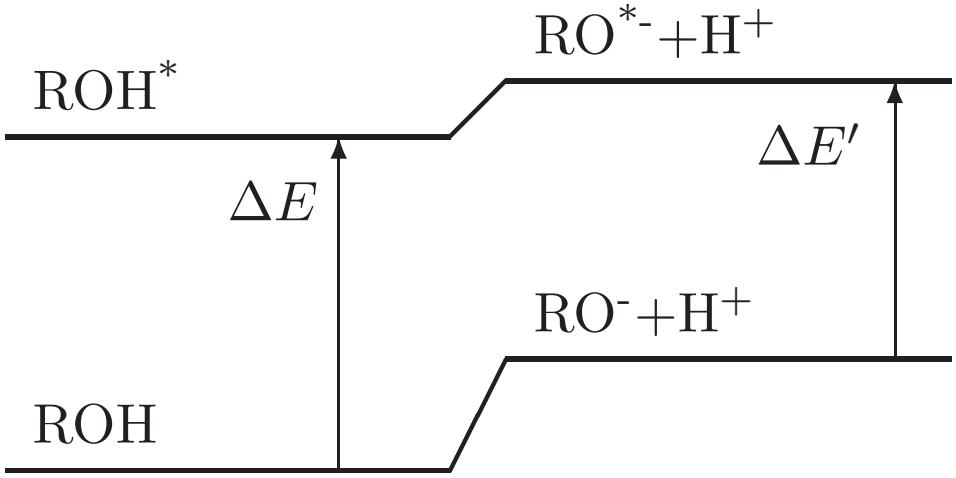

Figure 2-1. Visualization of the Förster Cycle where ROH is the photoacid. In this work the R groups considered are benzyl, α-naphthyl, or β-naphthyl. $\Delta E'$ is shown to be red-shifted from ΔE.

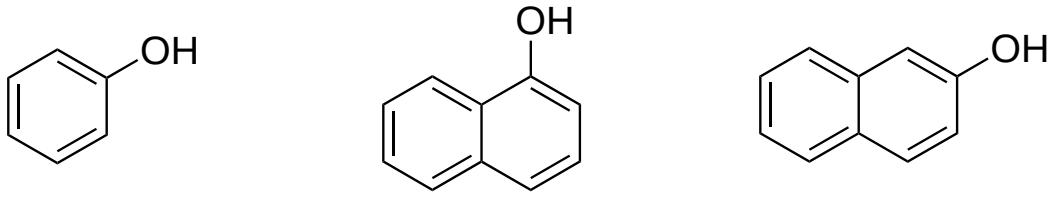

Figure 2-2. Structures of phenol, α-naphthol, and β-naphthol.

Argon matrix [19, 36, 44, 67, 104, 129]; and in solution [144]. For further information on spectroscopic techniques used to study solvation red-shifts in the gas phase consult Dissent *et al.* [34]. For a review of ESPT of phenol and naphthol photoacids see the following references [1, 33, 73, 85, 153, 166].

Recently available high resolution gas phase spectra of β-naphthol and the β-naphthol-ammonia complex show a solvatochromic red shift of 585 cm^{-1} in the energy of fluorescence of the first excited state. Fleisher *et al.* explain the observed red-shift by a charge transfer (CT) between the solute and the solvent. They analyze the difference between the EDM of the ground state and the excited state of the complex, compared

to the difference between the EDM of the ground state and the excited state of the free molecule.

By decomposing the EDM into four components: the dipole moments of the naphthol, the ammonia, and the induced dipole moment; the difference between the total dipole moment of the complex and the sum of the four components listed was considered the dipole moment of charge transfer. Such an empirical model neglects several features that predictive levels of *ab intio* theory can resolve. The argument for charge transfer being responsible for the red-shift of excited states of hydrogen bonded species is an old one, dating back to Nagakura and Gouterman (1957) for phenol, α-naphthol, and β-naphthol specifically [117]. The wavefunction-based description and classification of CT donors and acceptors dates back to Mulliken (1952) whose methods are widely accepted [112]. However, the conclusion of Fleisher *et al.* gas phase experiment is that CT is responsible for the red-shift of the first excited state while the conclusion of Solntsev *et al.* in condensed phase experiments is that Hydrogen bonding interactions are responsible for the red-shift of the first excited state. In this paper we address this discrepancy. While it is accepted that the $\pi \rightarrow \sigma^*$ transitions are charge transfer the discussion of the CT character of $\pi \rightarrow \pi^*$ transitions continues despite early CNDO calculations suggesting that it is not the case [13].

A similar theoretical study is done for the α isomer of naphthol since it is known that this isomer is less photo-acidic than the β isomer [73, 117] and therefore may display different excited state properties. There have been several previous DFT, CIS, CASSCF and CASPT2 studies of the phenol excited stated but no EOM-CCSD or STEOM-CCSD study have been performed. The coupled cluster methods should provide more definitive results than the previous methods cited. Most of the experimental literature cited here reports the 0-0 vibronic transition but not the vertical absorption (or emission) thus making a direct comparison to theoretical values difficult. Fortunately, the excitation energy shifts due to the presence of the ammonia solvent molecules appear to be little

affected whether the shift is calculated from the 0-0 vibronic band or from some other band (5 - 25 wavenumber error) [25, 36] so a comparison of the shifts between theory and experiment is reasonable. Furthermore, in a number of experimental studies it is noted that the 0-0 peak is the highest intensity peak thus making it a vertical transition for the first excited state. Since the first excited state of the aromatic compounds in this study is expected to be a $\pi \rightarrow \pi^*$ transition, we do not expect a big geometry change between the ground and the excited state, meaning that the vertical excitation energy will not be radically different than the 0-0 band energy.

2.3 Methods

We begin with phenol and its ammonia complex. Phenol acts as a photoacid in a similar way as naphthol (see the review of David *et al.* [33]). This system is accessible to all of the excited state capabilities of ACES II without compromising the essence of the problem. The ground state geometries are optimized using CCSD with a DZP basis whose exponents of polarization functions are taken from correlated calculations [134]. Vertical excitation energies are computed using configuration interaction with singles (CIS) [46], EOM-CCSD and STEOM-CCSD methods to compute excited state energies.

For comparison, a TD-DFT [48] calculation using a hybrid B3LYP [12] functional. All DFT calculations are performed using GAMESS [137] software. A DZP basis modified with diffuse functions is used in excited state calculations in order to properly describe any Rydberg states.

The ground state geometries of α-naphthol and β-naphthol and their ammonia complexes are optimized using MBPT(2) [7, 55] with a 6-31++G** basis set [54]. Single point energy calculations are performed on the optimized geometries with CCSD/6-31++G** and with CCSD(T)/6-31++G** [11]. Geometry optimization and single point energy calculations are done with ACES III. Excitation energies are computed using CIS and EOM-CCSD methods.

A restricted Hartee-Fock (RHF) reference is used for all coupled cluster calculations. Electric dipole moments are calculated with EOM-CCSD and STEOM-CCSD in ACES II.

All parallel geometry optimization calculations are accomplished on the University of Florida High Performance Computing Center with AMD Opteron (2.2 GHz) nodes. The resource requests are modest (24-64 processors) so that the performance of ACES III may be ascertained in an average working environment even though it has been shown that ACES III scales exceptionally well on tens-of-thousands of processors [93]. The excited state parallel calculations are accomplished on Cray XE6 AMD Opteron (2.3 GHz) nodes at the Arctic Supercomputer Center with 256-512 processors. The orbital plots are done using the MacMolPlt software package [16].

2.4 Results and discussion

2.4.1 *Ab initio* spectrum of phenol

The excited state energy and properties are determined for the free phenol molecule and the phenol-ammonia complex. The nature of the first four excited states is determined from orbital analysis and from the electric dipole moment. The differences in energies and properties due to the solvation of phenol by a single solvent molecule (in this case ammonia) are documented. The ground state geometries are optimized at the CCSD/DZP level unless stated otherwise. The optimized geometric parameters for the free phenol and the phenol-ammonia complex are listed in Table 2-1 and the labels are shown in Figure 2-3.

The equilibrium geometries are in good agreement with the experimental values [81] as well as with the previous theoretical studies [32, 51, 142]. The CCSD/DZP method yields a smaller Hydrogen bond length (1.8912 Å) as opposed to the CASSCF results: 2.042 Å (Sobolewski and Domcke) and 2.07 Å (Daigoku *et al.*).

The results of the excited state calculations are presented in Table 2-2. See Figure 2-4 for the plots of the orbitals. The superscript x signifies that the excited state and the orbitals are those of the complex. The orbitals with the highest coefficients for

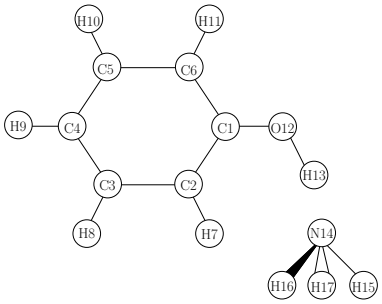

Figure 2-3. The atomic labels corresponding to Table 2-1.

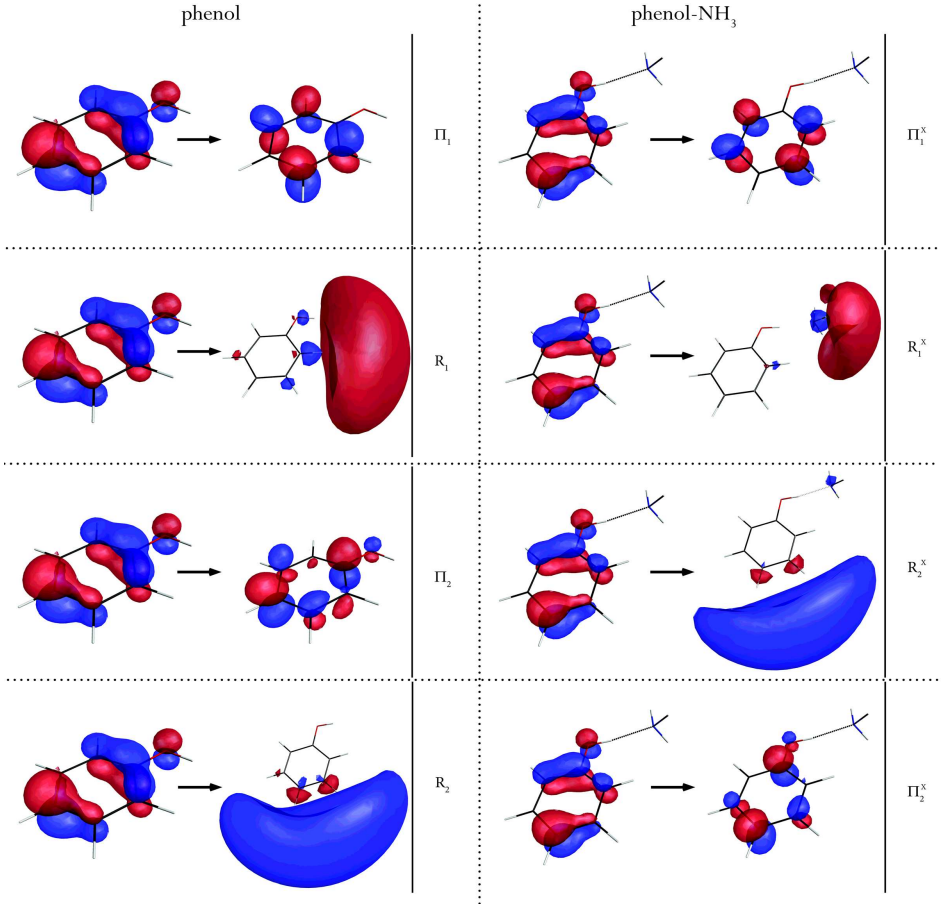

Figure 2-4. Hatree-Fock orbitals of free-phenol and phenol-ammonia cluster corresponding to the excitations listed in Table 2-2. The superscript x signifies that the excited state and the orbitals are those of the complex. The designation Π stands for a $\pi \rightarrow \pi^*$ valence transition and the designation R stands for a Rydberg state.

Table 2-1. Optimized geometry parameters for free phenol and phenol-ammonia complex with CCSD/DZP. The distances are in Angstrom and the angles are in degrees.

Coordinate	Phenol	Phenol-NH_3
C_1, C_2	1.4054	1.4094
C_2, C_3	1.4061	1.4052
C_3, C_4	1.4031	1.4037
C_4, C_5	1.4073	1.4070
C_5, C_6	1.4019	1.4016
C_2, H_7	1.0927	1.0909
C_3, H_8	1.0909	1.0915
C_4, H_9	1.0900	1.0901
C_5, H_{10}	1.0910	1.0915
C_6, H_{11}	1.0898	1.0901
C_1, O_{12}	1.3707	1.3583
O_{12}, H_{13}	0.9622	0.9775
H_{13}, N_{14}	-	1.8912
N_{14}, H_{15}	-	1.0195
N_{14}, H_{16}	-	1.0195
N_{14}, H_{17}	-	1.0195
$\angle C_1$, C_2, C_3	119.7	120.0
$\angle C_2$, C_3, C_4	120.6	120.8
$\angle C_3$, C_4, C_5	119.2	119.0
$\angle C_4$, C_5, C_6	120.8	120.8
$\angle H_7$, C_2, C_1	120.0	119.8
$\angle H_8$, C_3, C_2	119.3	119.3
$\angle H_9$, C_4, C_3	120.4	120.5
$\angle H_{10}$, C_5, C_6	119.3	119.3
$\angle H_{11}$, C_6, C_1	119.0	118.7
$\angle O_{12}$, C_1, C_6	117.1	117.6
$\angle H_{13}$, O_{12}, C_1	108.1	109.6
$\angle N_{14}$, H_{13}, O_{12}	-	170.5
$\angle H_{15}$, N_{14}, H_{13}	-	106.9
$\angle H_{16}$, N_{14}, H_{15}	-	105.7
$\angle H_{17}$, N_{14}, H_{15}	-	105.7
$\measuredangle H_{16}$, N_{14}, H_{15}, H_{13}	-	-124.0
$\measuredangle H_{17}$, N_{14}, H_{15}, H_{16}	-	-112.0

Table 2-2. The excitation energy is reported in eV. The oscillator strength (f) is unit-less. The values for ΔEDM are reported in Debye. The ground state EDM for phenol is 1.32 D and the ground state EDM for phenol-NH_3 is 3.97 D for correlated methods. The ground state r^2 for phenol is 705.9 and the ground state r^2 for phenol-NH_3 is 1469.4. The excited state labels and orbitals correspond to Figure 2-4. All calculations are performed at the optimized ground state geometry at the CCSD/DZP level with DZP++ basis set. The designation Π stands for a $\pi \rightarrow \pi^*$ valence transition and the designation R stands for a Rydberg state. The superscript x signifies that the excited state and the orbitals are those of the complex.

	State	B3LYP		CIS		EOM-CCSD				STEOM-CCSD			
		E(eV)	f	E(eV)	f	E(eV)	f	ΔEDM(D)	δr^2	E(eV)	f	ΔEDM(D)	Δr^2
Phenol	Π_1	4.95	0.031	5.81	0.047	4.90	0.021	0.07	0.6	4.41	0.018	0.13	0.5
	R_1	5.21	0.000	6.28	0.001	5.66	0.000	9.41	38.9	5.57	0.000	9.27	39.0
	R_2	5.65	0.004	6.56	0.017	6.18	0.005	7.19	43.5	6.11	0.000	7.36	44.3
	Π_2	5.71	0.032	6.08	0.002	6.23	0.049	0.11	4.6	6.06	0.079	0.75	4.0
Ph-NH_3	Π_1^x	4.84	0.038	5.73	0.061	4.83	0.025	0.44	-0.1	4.34	0.024	0.56	-0.2
	R_1^x	4.39	0.000	6.10	0.002	5.48	0.000	5.19	56.9	5.37	0.000	5.36	57.7
	R_2^x	5.26	0.003	6.34	0.017	5.85	0.006	5.20	56.5	5.76	0.006	5.61	56.3
	Π_2^x	5.58	0.053	6.03	0.007	6.04	0.070	0.07	7.6	5.83	0.121	1.07	6.0

each excited state are used to identify the states listed in Figure 2-4 and Table 2-2. A CT excited state would be expected when in the pair of orbitals with the dominant contribution to the transition matrix, one would be on the solute and one on the solvent. Depending on the direction of CT, such states would be dominated by a transition from either an occupied orbital on the phenol to a virtual orbital on the solvent (such as R_1^x) or from an occupied orbital on the solvent to a virtual orbital on the phenol. R_1^x is the first state which is observed to involve a transition between the phenol occupied orbital and a virtual orbital on the ammonia. This is a Rydberg state and due to a minimal orbital overlap does not have a significant oscillator strength.

The main difference in the TD-DFT spectra is the underestimation of the vertical excitation energies as well as the significant lowering of the excitation energy of the CT state (R_1^x) compared to the wavefunction spectra. The CIS energies are significantly higher than the EOM-CCSD and STEOM-CCSD results and the oscillator strengths of R_2, R_2^x, Π_2 and Π_2^x states are reversed. This is well illustrated in Figure 2-5 which shows the line spectra for several of the methods listed in Table 2-2 as compared to the first two $\pi \rightarrow \pi^*$ states from Kimura and Nagakura [69]. The experimental values for excitation energies and oscillator strength for Π_1 and Π_2 states were 4.6 eV (f=0.020) and 5.77 eV (f=0.132) respectively. The experimental data points are fitted with a Gaussian lineshape for better visualization. Since this was a condensed phase spectrum, the agreement between calculated values and experimental value is not expected to be perfect, but it should be at least qualitatively right since the heptane solvent is not polar and should not add noticeable solvation effects. The best agreement is shown by the STEOM-CCSD method which gets both energies and oscillator strengths qualitatively correct. The ratio of oscillator strength in the EOM-CCSD spectrum between Π_1 and Π_2 states is lower than experiment but the energies are still on target. The CIS spectrum gets neither the energies nor the oscillator strengths qualitatively correct and while

TD-DFT/B3LYP energies are certainly better than CIS, the oscillator strengths are not consistent with experiment.

The excitation energy and oscillator strength for Π_1 is consistent with several CASSCF and CASPT2 calculations [32, 51, 142]. However, the R_1 while being consistent with the CASPT2 calculations of Sobolewski and Domcke as well as Daigoku *et al.* does not match the second excited state found by the CASPT2 calculation of Granucci *et al.*. The correlated methods match the energy and the orbital assignments of the CASPT2 results of Sobolewski and Domcke and (Daigoku *et al.*): 5.77 eV (5.81 eV) and 5.47 eV (5.76 eV) for R_1 and R_1^x respectively. However, for the R_1 state, the correlated methods do not match the excitation energies of the CASPT2 results of Granucci *et al.*, which is 6.26 eV and closer in energy to either the R_2 or the Π_2 state. Upon further investigation, the second excited state in Granucci *et al.* is the Π_2 state, which is the second excited state in A'' symmetry, but not the second state overall. The confusion was caused by a mistake in the symmetry assignments of excited states in Tables 2 and 3 in the paper of Granucci *et al.*: the first and second states were assigned to a B and A symmetry respectively in Table 2 and both were assigned to B symmetry in Table 3. After the corrected assignment is made, the agreement between the EOM-CCSD results and all CASSCF methods is rather good though higher than the STEOM-CCSD results.

Excited state properties are summarized in Table 2-2. The ground state EDM for phenol is 1.32 D and the ground state EDM for phenol-NH_3 is 3.97 D for correlated methods. The ground state r^2 for phenol is 705.9 and the ground state r^2 for phenol-NH_3 is 1469.4. The difference between the size of the ground state and the excited state, Δr^2 is reported for EOM-CCSD and STEOM-CCSD results. Large Δr^2 values relative to the ground state indicate Rydberg states while small Δr^2 values signify that the excited states are valence-type transitions. The Δr^2 values of CT states tend to fall in-between, but in this case the CT state also happens to be a Rydberg state. The R_1

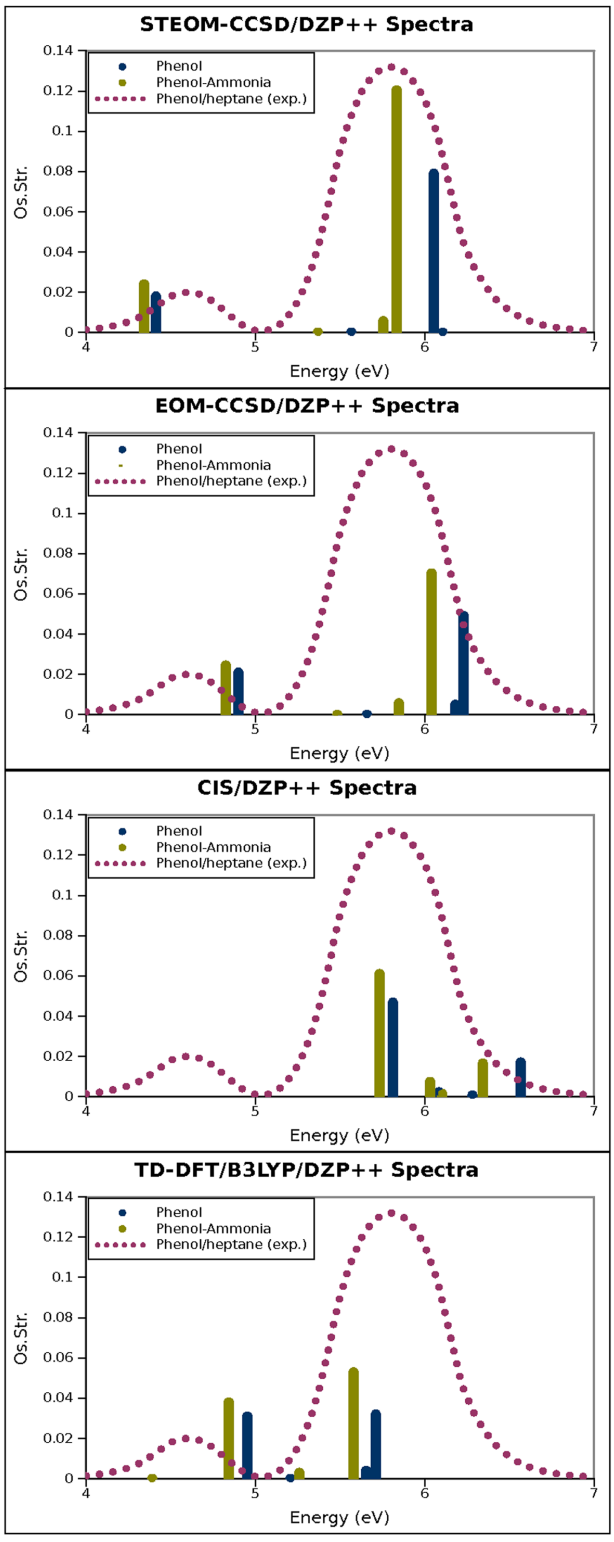

Figure 2-5. Vertical excitation spectra using the CIS, TD-DFT/B3LYP, EOM-CCSD, and STEOM-CCSD methods listed in Table 2-2. The experimental curve is adapted from Kimura and Nagakura [69] which shows Π_1 and Π_2 states of phenol in heptane solvent fitted with a Gaussian lineshape.

may be characterized as a charge transfer state between the benzyl and the hydroxide groups based on the Δr^2 value and the molecular orbitals involved. It is related to the R_1^x CT state between phenol and ammonia. Note the large change in EDM for this state as the electron density moves from the π system to a σ^* orbital.

The third excited state (R_2) of free phenol also has a large increase in EDM due to an appreciable movement of electron density between the π system and the diffuse σ^* orbital. However, the added ammonia molecule is not involved in this state. For the phenol-NH_3 complex the EDM substantially increases for the R_1^x state due to electron density movement between the solvent ammonia and the phenol. Therefore, while a large difference in EDM can be an indicator of CT between solvent and solute (R_1^x) it can also be an indicator of CT to a diffuse orbital (R_1,R_2,R_2^x).

Π_1, Π_1^x, Π_2 and Π_2^x states show a modest increase in EDM. The increase in EDM follows from charge re-distribution on the ring causing charge build-up at one or more atomic centers. These observations show that the changes in EDM are very susceptible to electrostatics and CT is not always necessary to invoke if a large change in EDM is found.

The change in EDM is regarded as the main reason for the excitation energy shifts of molecules in solution. The change in the ΔEDM between the free molecule and its ammonia complex is:

$$\Delta(\Delta EDM_k) = (\Delta EDM_k)_c - (\Delta EDM_k)_f \tag{2–1}$$

for each k^{th} excited state.

Note that the ΔΔEDM for both Rydberg states is negative signifying that the relative dipole moment of the complex tightens with respect to the relative EDM of the free molecule. For the R_1 state, which is related to the R_1^x CT state, the ΔΔEDM is -4.22 D while for the R_2 state, which is related to the R_2^x state, the ΔΔEDM is only -1.99 D. This result follows from R_2 not being as affected by the addition of solvent and retaining its

orbital character (refer to Figure 2-4) while the character of the R_1 state changes from involving a diffuse σ^* orbital on the phenol to a σ^* orbital on the ammonia. The ΔΔEDM values for the Π transitions are positive but small in magnitude compared to those of the Rydberg states signifying that the addition of one solvent molecule causes moderate changes in the charge distribution of these excited states. All of the excited states show an energy red-shift associated with the addition of ammonia, however, the sign of ΔΔEDM may be positive or negative.

The properties calculated with the EOM-CCSD method are consistent with those calculated with the STEOM-CCSD method. The ΔEDM values for STEOM-CCSD tend to be slightly larger in magnitude than those for EOM-CCSD. The oscillator strength also tends to be greater than the EOM-CCSD calculation. The results in Figure 2-5 slightly favor the STEOM-CCSD method but the oscillator strength, Δr^2, and ΔEDM values are not radically different between the two. The STEOM-CCSD calculation scales better with system size than EOM-CCSD and offers not only a possible accuracy boost but a computational advantage as well.

2.4.2 *Ab initio* spectra of α-naphthol and β-naphthol

The geometries of the α and β isomers of free naphthol and the ammonia-naphthol complex are optimized at the MBPT(2) level of theory using the parallel version of ACES. Only 24 to 48 processors are used depending on resource availability and near to linear scaling was observed across different number of processors in cases where the same calculation had to be repeated on different numbers of cores. The single point energy is calculated at the CCSD and CCSD(T) levels of theory. The designations used for the isomers are αN for α-naphthol, αNC for α-naphthol-ammonia complex, βN for β-naphthol, and βNC for β-naphthol-ammonia complex. The ground state energy values for naphthol and the ammonia-naphthol complexes are listed in Table 2-3.

The importance of using a correlated method for the ground state is illustrated in Table 2-3. The Hartree-Fock energy shows the β isomer to be lower in energy than

Table 2-3. The geometries are optimized at MBPT(2)/6-31++G** level of theory. All energy values for post-Hartree Fock methods are reported as correlation energies. The energy is reported in atomic units. The δE between the αN and βN and the αNC and βNC is reported in kcal/mol units.

Method	αN	αNC	βN	βNC
E_{HF}	-458.23920	-514.45124	-458.23955	-514.45131
δE	0.22	0.04	0	0
$E_{MBPT(2)}$	-1.51927	-1.71753	-1.51860	-1.71706
δE	0	0	0.20	0.25
E_{CCSD}	-1.56343	-1.77486	-1.56292	-1.77453
δE	0	0	0.10	0.16
$E_{CCSD(T)}$	-1.63505	-1.85147	-1.63445	-1.85105
δE	0	0	0.16	0.22

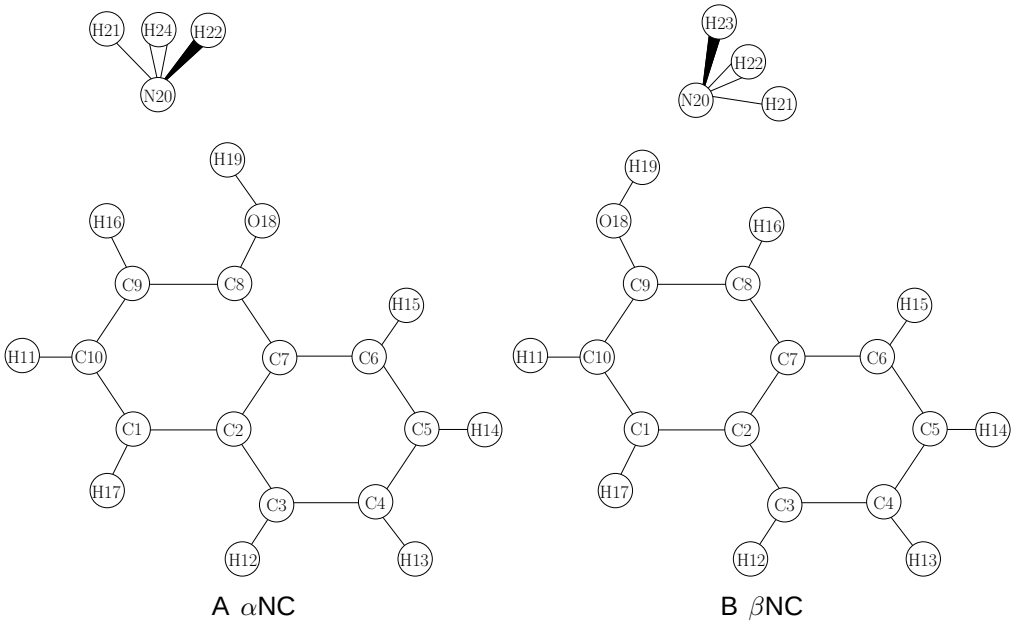

Figure 2-6. The atomic labels corresponding to Table 2-4.

the α isomer but with the addition of correlation, the relative energies are reversed. Quantitatively, the relative energies of the CCSD(T) method are closer to those of the MBPT(2) method making it our choice for geometry optimization.

The optimized geometric parameters for the naphthol molecules and their ammonia complexes are listed in Table 2-4 and the labels are shown in Figure 2-6.

Table 2-4. Optimized geometry parameters for free and complexed α-naphthol and β-naphthol with MBPT(2)/6-31++G**. The distances are in Angstrom and the angles are in degrees.

Coordinate	αN	αNC	βN	βNC
C_1, C_2	1.4205	1.4274	1.4212	1.4211
C_2, C_3	1.4197	1.4184	1.4189	1.4188
C_3, C_4	1.3817	1.3826	1.3820	1.3823
C_4, C_5	1.4147	1.4149	1.4149	1.4150
C_5, C_6	1.3824	1.3819	1.3823	1.3825
C_6, C_7	1.4185	1.4201	1.4198	1.4204
C_7, C_8	1.4235	1.4202	1.4197	1.4192
C_8, C_9	1.3818	1.3861	1.3811	1.3854
C_9, C_{10}	1.4145	1.4139	1.4155	1.4186
C_{10}, C_1	1.3800	1.3861	1.3782	1.3782
C_{10}, H_{11}	1.0830	1.0823	1.0825	1.0828
C_3, H_{12}	1.0845	1.0817	1.0844	1.0846
C_4, H_{13}	1.0831	1.0834	1.0831	1.0832
C_5, H_{14}	1.0832	1.0833	1.0832	1.0834
C_6, H_{15}	1.0816	1.0848	1.0847	1.0851
C_8, H_{16}	1.0848	1.0839	1.0859	1.0843
C_9, H_{17}	1.0837	1.0836	1.0843	1.0846
C_1, O_{18}	1.3780	1.3644	1.3766	1.3642
O_{12}, H_{13}	0.9672	0.9667	0.9671	0.9864
H_{13}, N_{14}	-	1.8641	-	1.8678
N_{14}, H_{15}	-	1.0139	-	1.0141
N_{14}, H_{16}	-	1.0142	-	1.0142
N_{14}, H_{17}	-	1.0142	-	1.0142
$\angle C_1, C_2, C_3$	121.9	121.5	122.2	122.3
$\angle C_2, C_3, C_4$	121.0	120.3	120.7	120.8
$\angle C_3, C_4, C_5$	120.2	120.5	120.2	120.1
$\angle C_4, C_5, C_6$	120.6	120.1	120.4	120.3
$\angle C_5, C_6, C_7$	120.1	121.1	120.8	121.1
$\angle C_6, C_7, C_8$	122.0	121.9	121.9	121.9
$\angle C_7, C_8, C_9$	121.1	120.0	120.3	120.6
$\angle C_9, C_{10}, C_1$	120.7	120.4	119.9	120.5
$\angle H_{11}, C_{10}, C_1$	120.2	119.6	121.5	121.3
$\angle H_{12}, C_3, C_4$	120.3	121.0	120.4	120.4
$\angle H_{13}, C_4, C_3$	120.0	119.8	120.0	120.1
$\angle H_{14}, C_5, C_6$	119.7	120.0	119.9	119.9
$\angle H_{15}, C_6, C_5$	120.8	120.2	120.2	120.1
$\angle H_{16}, C_8, C_9$	120.0	120.7	120.5	120.2
$\angle H_{17}, C_9, C_8$	120.6	120.0	119.8	119.9
$\angle O_{18}, C_1, C_2$	115.9	116.4	123.5	123.9
$\angle H_{19}, O_{18}, C_1$	108.9	110.8	109.2	110.9
$\angle N_{20}, H_{19}, O_{18}$	-	169.5	-	169.9
$\angle H_{21}, N_{20}, H_{19}$	-	118.3	-	118.0
$\angle H_{22}, N_{20}, H_{21}$	-	107.1	-	107.1
$\angle H_{23}, N_{20}, H_{21}$	-	107.1	-	107.1
$\measuredangle H_{22}, N_{20}, H_{21}, H_{19}$	-	-122.6	-	-122.7
$\measuredangle H_{23}, N_{20}, H_{21}, H_{22}$	-	-114.7	-	-114.7

The presence of the solvent ammonia molecule has the expected effect on the geometry of β-naphthol. The carbon-carbon bonds are lengthened by an average of 0.009 Å in the complex but the greatest deformation is experienced by the CO bond (contracted by 0.0124 Å) and the OH bond (expanded by 0.0193 Å). This kind of geometry deformation would contribute to the 586 cm^{-1} red-shift observed by Fleisher *et al..* as well as the observed increase in the EDM for ground and excited states. This change in geometry is not included in the dipole moment vector addition analysis since the free β-naphthol used there was at its equilibrium geometry. The ammonia solvent has a slightly different effect on the α-naphthol isomer. The CO bond contracts by 0.0136 Å but the OH bond contracts by 0.0005 Å, thus even though the CO bond strengthens with the addition of solvent, the OH bond does not weaken. The optimized geometry parameters are consistent with the previous theoretical calculations [56, 104, 150] with the exception of the results from DFT methods. The αNC intermolecular Hydrogen bond was computed to be 1.789 Å with the PW91/6-31G(d,p) method (Henseler *et al..*) and 1.837 Å with the B3LYP/6-311++G(d,p) method (Tanner *et al..*). The MBPT(2) calculation of Henseler *et al..* with 6-31G(d,p) basis set yielded a Hydrogen bond of 1.919 Å. This indicates that the accuracy of the intramolecular bond distance is as affected by basis set as it is by the choice of *ab initio* method. The Hydrogen bond of βNC was calculated to be 1.905 Å by Matsumoto *et al..* with the HF/6-31G method.

Table 2-5 lists the *ab initio* excitation energy values as well as several properties of the three lowest excited states. The dominant orbitals for each excitation correspond to the orbitals shown in Figures 2-7 and 2-8. A CT state for the naphthol complex would involve a transition dominated by either an orbital on the ammonia going to an orbital on the naphthol or an orbital on the naphthol going to an orbital on the ammonia, similar to the situation for phenol. The R_1 and R_1^x state show CT behavior according to the

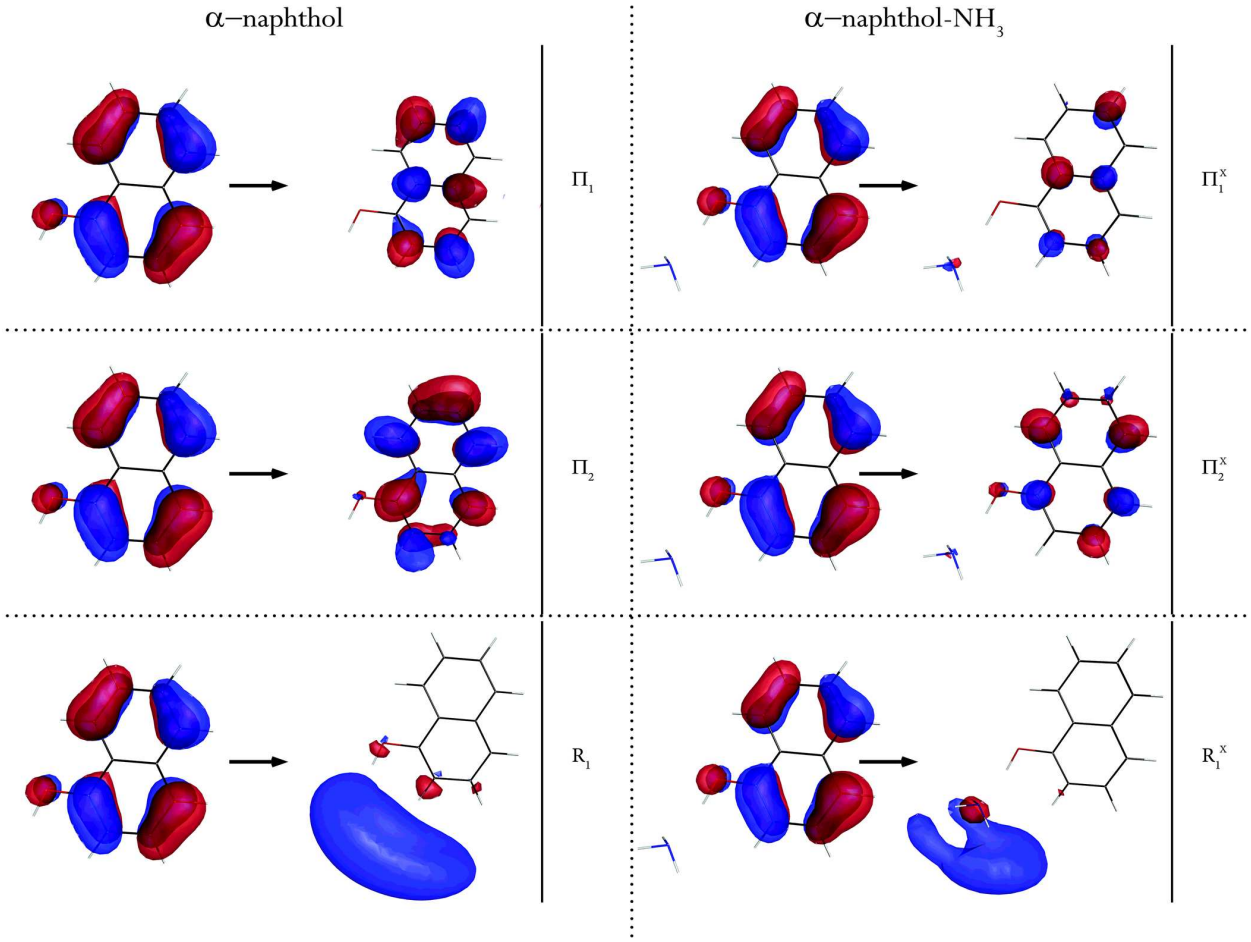

Figure 2-7. Hatree-Fock orbitals of α-naphthol corresponding to the excitations listed in Table 2-5.

molecular orbital analysis. All units and designations in Table 2-5 are the same as those in Table 2-2.

The discrepancy between the EOM and the STEOM excitation energies is worse for the naphthol molecules than for the phenol. The $\pi \rightarrow \pi^*$ transitions on the naphthol molecules have more double excitation character than the ones on the phenol due to the π system being more extensive. EOM-CCSD performs much better for single excitations than for those with appreciable double excitation character. Triples excitations are required to improve the latter [120]. The agreement in energy is the worst for the R_1 state of α-naphthol. In this case, it is most likely that the STEOM-CCSD value is about 0.1 eV too low. This is the only state where the % singles (a projection of the

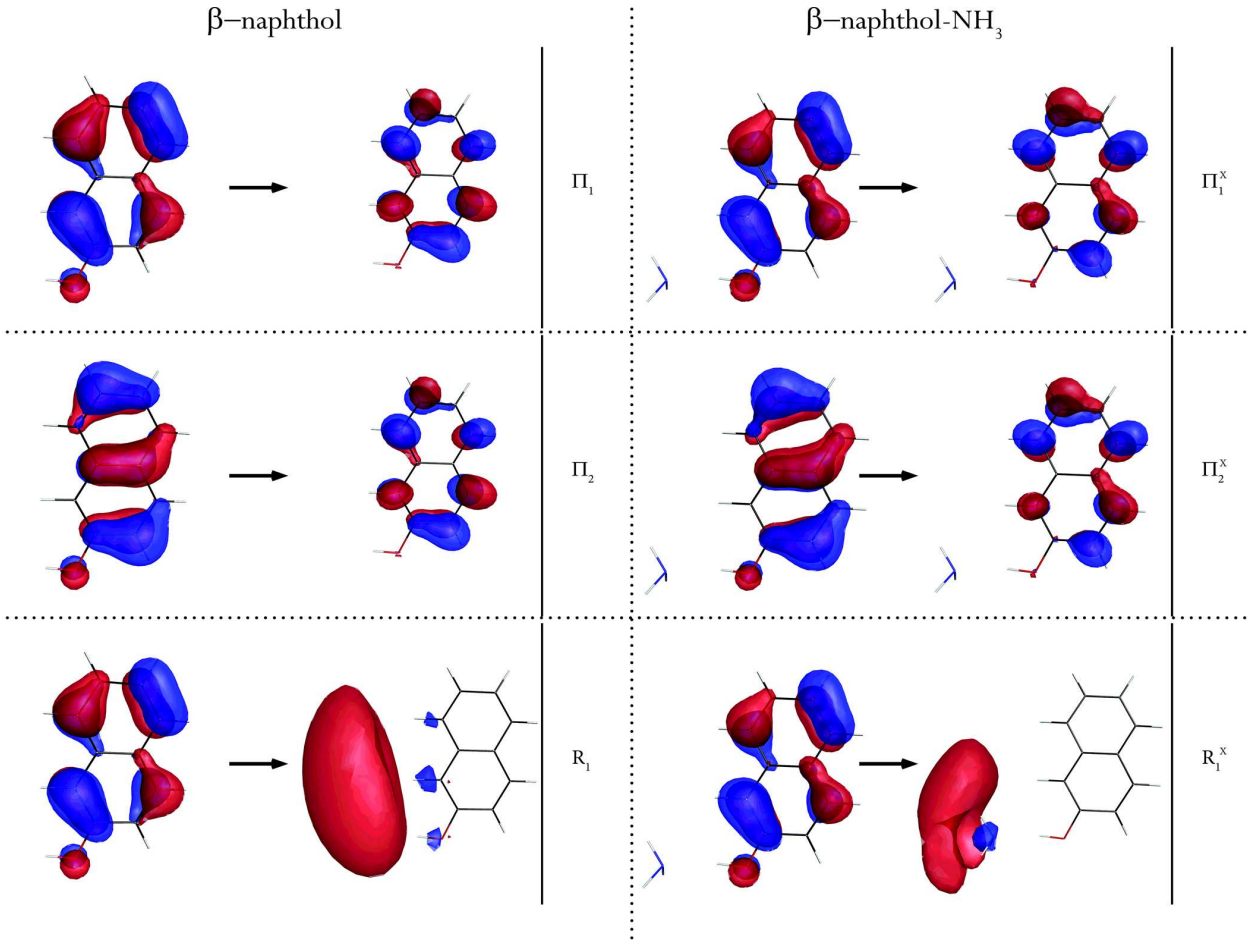

Figure 2-8. Hatree-Fock orbitals of β-naphthol corresponding to the excitations listed in Table 2-5.

STEOM-CCSD wavefunction on a space of singly-excited determinants) is as low as 71% whereas for all of the other states it is 88% and above. The STEOM-CCSD ΔEDM value for R_1 is also underestimated: the ΔEDM for R_1 is 10.95 D with EOM-CCSD which exceeds the error range shown in Table 2-2 for phenol. Generally, when the % singles value dips below 85%, a triples correction is necessary to rescue the energy and properties values for that state.

The change in EDM of the first excited state of β-naphthol is different than from the CIS calculations of Fleisher *et al.*. The ΔEDM values from Fleisher *et al.* are 0.16 D for the free β-naphthol and 1.05 D for the ammonia complex. As shown in this work, the CIS method lacks the necessary accuracy to compute the small differences in

Table 2-5. The excitation energy is reported in eV. The oscillator strength (f) is unit-less. The values for ΔEDM are reported in Debye. The excited state labels and orbitals correspond to Figure 2-7 and Figure 2-8.

	State	EOM-CCSD		STEOM-CCSD			
		EE(eV)	f	EE(eV)	f	$\Delta EDM(D)$	Δr^2
αN	Π_1	4.33	0.009	3.87	0.006	0.49	0.6
	Π_2	4.89	0.093	4.66	0.124	3.45	2.4
	R_1	5.22	0.000	4.97	0.000	8.34	54.0
αNC	Π_1^x	4.30	0.012	3.84	0.011	0.56	3.3
	Π_2^x	4.76	0.084	4.50	0.135	4.01	7.6
	R_1^x	5.04	0.000	4.95	0.000	7.51	67.7
βN	Π_1	4.29	0.015	3.81	0.015	0.34	-0.4
	Π_2	5.10	0.052	4.90	0.075	0.69	1.2
	R_1	5.33	0.000	5.23	0.000	11.54	41.9
βNC	Π_1^x	4.22	0.026	3.76	0.021	0.85	-0.2
	Π_2^x	5.05	0.048	4.82	0.072	2.03	3.3
	R_1^x	5.13	0.000	5.00	0.000	8.00	50.5

properties. Using the STEOM-CCSD/DZP++ level of theory, we compute the ΔEDM of 0.34 D for the free β-naphthol and 0.85 D for the ammonia complex; a much less dramatic difference with ΔΔEDM of only 0.51 D which is more consistent with Suppan [149]. One half of a Debye difference is actually small when compared to a ΔΔEDM value of a true CT state such as R_1.

2.4.3 Comparison to experimental results

The first (and in some cases the second) excited states of phenol, α-naphthol, β-naphthol and their ammonia complexes have been documented experimentally with a variety of methods in the gas phase, Argon matrix, and in solution. The Π_1 state has been probed by both absorption and emission spectroscopic techniques and the 0-0 vibronic band reported. The collated experimental results are presented in Table 2-6.

The agreement between the STEOM values and the experimental values for the first excited state is excellent, despite the exclusion of the adiabatic correction from vertical excitation to the 0-0 vibronic excitation. We also have good agreement with the results from non-polar solvents as well as the Argon matrix experiments. For the second excited

Table 2-6. The excitation energies from experiments are presented for first and second excited states of phenol (Ph), phenol-NH_3 (PhC), α-naphthol (αN), β-naphthol (βN), α-naphthol-NH_3 (αNC), and β-naphthol-NH_3 (βNC). The units are eV and the sources of the values are: a:[65, 68, 119, 154]; b:[127]; c:[65, 68, 143]; d:[24, 25, 58]; e:[67, 104]; f:[117] (heptane); g:[24, 25, 58, 63, 72]; h:[144] (hexanes); i:[36]; j:[19] (Ar matrix); k:[44, 129]; l:[69]; m:this work (vertical excitation) STEOM-CCSD/DZP++; n:this work (vertical excitation) EOM-CCSD/DZP++

State	Ph	PhC	αN	αNC	βN	βNC
	4.51[a]	4.20[b]	3.90[d]	3.87[g]	3.75[h]	3.61[h]
		4.43[c]	3.87[e]		3.83[e]	3.72[i]
			3.85[f]		3.79[i]	3.76[j]
Π_1					3.81[j]	3.76[k]
					3.78[f]	
	4.41[m]	4.34[m]	3.87[m]	3.85[m]	3.81[m]	3.76[m]
	4.90[n]	4.83[n]	4.33[n]	4.30[n]	4.29[n]	4.22[n]
	5.77[l]		4.28[f]		4.35[f]	
Π_2	6.06[m]		4.66[m]		4.82[m]	
	6.23[n]		4.89[n]		5.10[n]	

state the agreement is less clear since we only have an experimental result in solution. The relative energy for the second excited state compares well: $\Pi_2^{\alpha N} < \Pi_2^{\beta N} < \Pi_2^{Ph}$.

Table 2-7 shows the excitation energy shifts for phenol and the two naphthol isomers. The energy shifts are provided in wavenumber units:

$$\Delta(E_k) = (E_k)_c - (E_k)_f \tag{2–2}$$

for each k^{th} excited state.

The agreement in energies between EOM-CCSD and STEOM-CCSD methods is generally good except for the R_1 state of α-naphthol. The EOM-CCSD red-shifts are more consistent with experiment than the STEOM-CCSD despite the experimental absolute excitation energies being closer to the STEOM results. This can be explained by the active space dependence of the STEOM calculation. The slight change in the orbitals between the free molecules and the complex is enough to introduce an error on the order of 100-200 cm^{-1} in the STEOM-CCSD values; R_1 of α-naphthol being an outlier

for reasons explained in the previous section. Since there is no active space choice in the EOM scheme, the energy differences are in closer agreement with experiment. The agreement in energies is rather good considering that 100 cm^{-1} is equivalent to 0.01 eV which exceeds the accuracy of any of these calculations. However, we can hope that the error will largely cancel for relative energy values. This kind of error cancellation allows obtaining reasonable agreement between the calculated red-shifts and the experimental red-shifts. The TD-DFT/B3LYP values show little consistency: the ΔE of the Π_1 state of phenol is -879 cm^{-1}.

The red-shift due to the ammonia solvent of the first excited state (Π_1) may be compared with experimental values. The STEOM and EOM values for phenol and β-naphthol are underestimated by about 100 cm^{-1}, however, there is also a large variation in these values among the various experimental results, especially for the β-naphthol, perhaps due to some difficulties in the assignment of the *cis/trans* isomers [36, 104]. The standard deviation of the red-shift is much less for the α-naphthol isomer. Despite these issues, the relative energies agree very well: the red-shift of Π_1 of β-naphthol is about twice the magnitude of the red-shift of Π_1 of α-naphthol for the theoretical correlated methods as well as for experiment. The values from the B3LYP method show no correlation to any experimental or correlated method. Several large basis set calculations of excited state energies were performed for phenol but they were not significantly closer to the experimental values than the ones done with DZP++ basis. Therefore, we deem DZP++ adequate in describing the several lowest excited states.

2.5 Conclusion

Recent high-resolution spectroscopy studies of β-naphthol, α-napthol, and phenol show a solvatochromic effect in the first excited state with just one solvent molecule present. This presents an opportunity to compare experimental solvent effects with *ab inito* theory without making crude solvent model approximations. We can also begin to apply the term “solvatochromic”, which is generally reserved for the condensed phase,

Table 2-7. The excitation energy differences between the phenol-ammonia complex and free phenol and the excitation energy differences between the α and β naphthol-ammonia complex and free naphthol are reported in wavenumber units. The experimental values sources are: a:[65],b:[68]; c:[143]; d:[58]; e:[24, 25]; f:[44, 67, 129]; g:[36]; h:[19] (Ar matrix).

	State	EOM-CCSD ΔEE	STEOM-CCSD ΔEE	EXP ΔEE
PhC	Π_1	-581	-564	-635[a],-642[b],-650[c]
	R_1	-1403	-1588	
	R_2	-2719	-2882	
	Π_2	-1528	-1778	
αNC	Π_1	-243	-177	-240[d],-236[e]
	Π_2	-1096	-1286	
	R_1	-1467	-205	
βNC	Π_1	-505	-432	-586[f],-606[g],-409[h]
	Π_2	-453	-637	
	R_1	-1623	-1811	

to these gas-phase experiments and *ab initio* calculations since there are obvious solvent effects present.

Based on an orbital analysis of the ground and excited states, it is determined that only a marginal charge transfer occurs between the solvent and the solute molecules for the first two $\pi \rightarrow \pi^*$ states. The amplified change in EDM in the presence of one ammonia solvent molecule points to some differences in charge distribution on the naphthol (or phenol) fragment of the complex but not due to charge transfer.

We also show that the CIS method, which is often used for *ab initio* spectroscopy of larger molecules, does not posses sufficient accuracy based on (1) its comparison with higher level theory and experimental values and (2) the incorrect description of the Hatree-Fock ground state of α and β isomers of naphthol. If one is computationally restricted to a single particle theory even TD-DFT is a better choice provided that no CT states are considered and with the caveat that oscillator strengths may be questionable. The STEOM-CCSD method offers a computational advantage since it scales as $\approx 2n^5$ as opposed to EOM-CCSD which scales as $\approx n^6$ where n is the

number of orbitals. The calculation of the CCSD ground state wavefunction ($\approx n^6$) is required for both methods. STEOM-CCSD also offers advantages for excited states with significant mixing and double-excitation character such as the $\pi \rightarrow \pi^*$ states in this study. However, for computing small differences (on the scale of less than 0.2 eV) in energy between *different* molecules, the EOM-CCSD method offers a potential advantage over STEOM-CCSD because a complete orbital space is always included in the EOM framework while STEOM depends on a selection of orbitals.

CHAPTER 3
ABSORPTION CROSS SECTION

3.1 Background

The photodissociation rates of volatile organic and inorganic compounds are critically important in modeling the composition of the atmosphere, in addressing global warming, ozone depletion, and other phenomena. The absorption cross section in the spectral range of solar flux is needed to calculate the photodissociation rate constant

$$J = \int_{\lambda} \phi_{\lambda} \sigma_{\lambda} F_{\lambda} d\lambda \tag{3–1}$$

where λ is the incident wavelength, σ is the absorption cross section, ϕ is the quantum yield of photodissociation and F is the solar actinic flux.

The photodissociation rate constant and its dependence on temperature can be measured provided a pure sample is obtained and the absorption cross section at various temperatures is known[100, 105]. The pure sample condition becomes increasingly difficult to satisfy as the size, complexity and stability of the compound in question impede attempts to synthesize it. Currently, the absorption cross sections that are used to determine the photodissociation rates of complex or unstable molecules are unknown and are crudely estimated. An example of the problems arising from poor estimates are the photodissociation rate values for organic peroxides that are directly derived from the absorption cross sections of hydrogen peroxide and methyl peroxide simply due to their experimental availability, bypassing the difficulties in obtaining the experimental cross sections of the actual molecules[66]. Using estimated values as opposed to the true values can lead to serious inaccuracies in the steady state models of the atmosphere.

Normally, when an absorption cross section is calculated with *ab inito* methods a vibronic model can be used to include some molecular motion. In order to compute a photodissociation absorption cross section for relatively large species several

complications of the vibronic model need be resolved. None of the currently available software can properly handle the dissociative excited state surface, and few can correctly handle a torsional potential since it does not naturally lend itself to a quadratic or quartic expansion but rather should be expanded with a set of trig functions[43, 75]. Even if this model is made to work with the types of PESs involved in photodissociation, there is still the aspect of finding roots of a very large matrix which may not be sparse when there are many strong vibronic couplings present.

The most widely used programs that have the capability to simulate an absorption spectrum are VIBRON[121] and HOTFCHT[14]. All of these programs require a calculation of the harmonic normal modes of the absorbing state which works well enough for excited state potential energy surfaces which have a stationary point, but do not perform well for dissociative potential energy surfaces. The LEVEL[82] program works for bound and quasi-bound potentials and has been successfully applied to a variety of diatomic molecules.

3.2 Methods

3.2.1 Approach to the problem

In order to calculate the absorption cross section for large molecules several simplifications need to be made. The recurring theme is that we are trying to remove as many non-vital vibrational degrees of freedom as possible. These assumptions are explained below and will be illustrated throughout the NaOH example.

1. *Consider the dissociative coordinate as the primary coordinate.* This is the obvious choice since we are initially interested in those cross sections which lead to dissociation. This method can be extended to use any degree of freedom as the primary coordinate.

2. *Compute the absorption cross section of the primary mode.* This will be the zeroth-order solution. The discrete variable representation method (DVR)is used to compute the Frank-Condon overlap integrals for a dissociative mode.

3. *Consider only those vibrations which are significantly thermally populated.* In practice, this would involve a subset of vibrations of energy equal or lower than

the energy of the stretch along which dissociation takes place. By *equal* we mean within some tolerance which is optimal for a given temperature. For example, if one is interested in going to very high temperatures, modes higher in energy than the primary mode should be considered.

4. *Determine the impact each secondary mode has on the excitation energies of interest as well as the corresponding dipole transition moments.* If the impact is less than some tolerance, remove that normal mode from the subset. This will now define the subset of secondary modes. Any degree of freedom which is not explicitly a part of the secondary modes' subset will be relaxed in all partial geometry optimization calculations so that any small effect these modes have can be partially reflected in the final answer.

5. *Add the effects of other degrees of freedom by perturbing the primary mode ground state and excited state potentials.* This can be done by extrapolating or fitting the curves used to determine the impacts in step IV.

6. *Temperature effects can be introduced at this stage.* This step involves redistributing energy quanta among the vibrational levels of the primary mode and the various secondary modes.

3.2.2 Discrete variable representation

The discrete variable representation (DVR) method[90] has been used to solve the vibrational Hamiltonian for a variety of small chemical compounds provided a potential energy surface is known as well as expanded to work up to N=16 vibrational degrees of freedom[132, 133, 164]. It can be used to find vibrational wavefunctions on a dissociative surface[29, 110]. DVR works by a numerical discretization of the kinetic energy operator and the potential into N segments. The detailed derivation of the DVR using the Fourier grid Hamiltonian method can be found elsewhere[29, 103]. The discretized form of the kinetic energy operator is shown below where m is the reduced mass and Δx is the size of the grid on which the potentials are placed.

$$T_{ii'} = \frac{\hbar^2}{2m\Delta x^2}(-1)^{(i-i')} \times \begin{cases} \frac{\pi^2}{3} & \text{for } i = i' \\ \frac{2}{(i-i')^2} & \text{for } i \neq i' \end{cases} \tag{3–2}$$

The Hamiltonian that is diagonalized is shown below where V is the potential function used to fit the *ab intio* data points. The Hamiltonian below in in atomic units.

$$H_{ii'} = T_{ii'} + V_{ii'}\delta_{ii'} = \frac{(-1)^{(i-i')}}{2dx^2} \times \left\{ \begin{array}{ll} \frac{\pi^2}{3} & \text{for } i = i' \\ \frac{2}{(i-i')^2} & \text{for } i \neq i' \end{array} \right\} + V_{ii'}\delta_{ii'} \tag{3–3}$$

The results are sensitive to the resolution of the grid. Since this is a very fast calculation, it is easy to vary the number of grid points until the eigenvalues in the energy range of interest converge. In this work, 501 grid points are enough to reach convergence.

3.2.3 Discrete absorption cross section

One can rewrite Equation 3–1 to include the temperature dependence of the photodissociation rate constant:

$$J = \int_{\lambda} \phi_{\lambda} \sigma_{\lambda,T} F_{\lambda} d\lambda \tag{3–4}$$

where the temperature dependence is added via the absorption cross section term. The absorption cross section can be written as:

$$\sigma(\lambda, T) = \sum_{k}^{K} \{ \langle \Psi^k | \mu | \Psi^0 \rangle \sum_{m=0}^{M} \sum_{n=0}^{N(T)} \langle \Phi_k^m | \Phi_0^n \rangle \} \tag{3–5}$$

where μ is the electronic transition moment obtained from the electronic wavefunctions Ψ, and Φ are the vibrational wavefunctions. The summations are over K-electronic excited states, M-vibrational states on the excited PES and N-vibrational states on the ground PES where $N(T)$ is the maximum occupied vibrational levels at temperature, T. The temperature dependence of the absorption cross section comes from varying the population of the ground state vibrational energy levels. EOM-CCSD will be used to compute the electronic transition moment and a DVR code developed by the author will be used to compute the Frank Condon integrals.

In order to facilitate comparison between the experimental and the theoretical absorption cross sections it is best to express all intensities as unit-less oscillator

strengths as opposed to transition dipole moments. The relationship between the two quantities is:

$$f_{0k} = \{\frac{8\pi^2 m_e c g_n}{3he^2}\}\omega_{0k}\mu_{0k} \tag{3–6}$$

ω_{0k} is the excitation energy, μ_{0k} is the dipole strength, c is the speed of light, e is the elementary charge, m_e is the mass of an electron, h is the Planck constant, and g_n is the electronic degeneracy of the excited state.

The experimental data may also be expressed as the oscillator strength [22] provided that the molar extinction coefficient is known:

$$f_{0k} = \{\frac{2303 m_e c^2}{\pi N_A e^2}\}F\int_{\omega_1}^{\omega 2} \epsilon d\omega \tag{3–7}$$

Here, N_A is Avogadro's number, F is the correction for the refractive index, which can be set to 1 since this applies to a diffuse gas, and ϵ is the molar extinction coefficient in the units of $L/mol \cdot cm$. The quantities obtained from Equation 3–6 and Equation 3–7 the experimental and theoretical vertical excitation intensities may be compared and the agreement is known to be good based on examples currently found in the literature[17, 45].

3.2.4 Combine DVR and the discrete absorption cross section

Care must be taken to properly combine the electronic structure results (oscillator strength) with the DVR results (Frank Condon) such that both are expressed as a function of ω and lie on the same grid. There are several ways to achieve this and one such way is described here.

Solving the Hamiltonian as written in Equation 3–3 will produce the following set of Frank Condon integrals:

$$FC_{im} = \{\sum_j \phi_{mj}\phi_{ji}\}^2 \tag{3–8}$$

where ϕ_{mj} is the eigenvector corresponding to the m^{th} energy level of the ground state potential energy surface and ϕ_{ji} is the eigenvector corresponding to the i^{th} energy level

of the excited state potential energy surface. These integrals are normalized such that $\sum_i FC_{im} = 1$. The difference of eigenvalues for the ground and excited state are used to build the ω_i vector: $E_i - E_k = \omega_i$.

The oscillator strengths are calculated as a function of geometry for each electronic transition. However, only the value at the equilibrium geometry corresponds to the experimental value determined using Equation 3–7, which is an integral of the cross section. What is needed is a way to map the oscillator strength value to the area of the cross section, preferably in cgs units. First, rearrange Equation 3–7 to reflect the cgs units:

$$f_{0k} = \{\frac{m_e c^2}{\pi e^2}\} F \int_{\omega_1}^{\omega 2} \sigma \, d\omega \tag{3–9}$$

where σ is the absorption cross section in $cm^2/molecule$. Now, rearrange to solve for σ discretely:

$$\tilde{\sigma}_i = \{\frac{\pi e^2 g_n}{m_e c^2}\} \frac{F_i}{\omega_{i+1} - \omega_i} \tag{3–10}$$

Note that this $\tilde{\sigma}$ is a discrete electronic part of the total σ. The ω in the denominator comes from the eigenvalues of the DVR Hamiltonian. The oscillator strength is also discrete and obtained from *ab initio* calculations which is why g_n appears in this equation. At this point, F_i is the oscillator strength which corresponds to each $m \rightarrow i$ transition and is estimated by a weighted average oscillator strength, $\bar{f}_i$:

$$\bar{f}_i = \frac{\sum_j f_i \times |\phi_{mj}\phi_{ji}|}{\sum_j |\phi_{mj}\phi_{ji}|} \tag{3–11}$$

Combining Equations 3–10 and 3–11 allows the electronic part of σ to be placed on the same grid as the Franck-Condon part of σ such that the largest contribution to F_i are coming from the portions of the oscillator strength surface with the greatest Franck-Condon overlap. The total absorption cross section for each electronic transition

which can be compared with experiment is then obtained by combining the electronic and vibrational parts:

$$\sigma_{0k} = \sum_i \tilde{\sigma}_i \times \sum_m c_m^T F C_{im} \tag{3–12}$$

The subscript m will be greater than one when more than one ground state vibrational energy level is populated. The population of the m-states are weighted by a set of temperature-dependent constants c_m, which correspond to the Boltzmann distribution at a given temperature. In the case of $T = 0K$, m will always be set to 1 corresponding to the first vibrational level.

The final cross sections for each k^{th} excited state are to be convoluted to obtain a theoretical spectrum in the desired spectral range.

One consistency check for the procedure outlined above is to use Equations 3–7 or 3–9 to find the oscillator strength once the calculated absorption cross section is obtained. If everything is done right in the code, the fits to the PES are adequate, and the grid is fine enough, the f_{DVR} should be close to the calculated f for each transition. Furthermore, improving upon fits to the potentials (by using more points for example) as well as increasing the resolution of the grid should converge the f_{DVR} to the correct value.

CHAPTER 4
ABSORPTION CROSS SECTION EXAMPLES

4.1 Sodium Hydroxide

We propose a method for computing absorption cross sections for dissociative surfaces which are geared toward describing a larger molecule with more than 10 vibrational degrees of freedom. As an illustration of the methodology we choose a small molecule, sodium hydroxide. Photodissociation of gaseous NaOH as well as other sodium oxide compounds is an important atmospheric process in the mesosphere[128], and the absorption cross sections leading to photodissociation have been obtained experimentally using flame absorption[2] and laser spectroscopy[139]. The pertinent experimental results are from the laser spectroscopy study of Self and Plane.

4.1.1 Electronic structure calculations

The starting point for calculating an absorption spectrum is to begin with single point vertical excitation energies. From the energy range of the experimental spectrum in Figure 4-1, we see that three low energy excited states are required to create a theoretical spectrum in the near UV spectral range. These states, their symmetry and character are listed in Table 4-1. The error bars from the experimental data show a great deal of uncertainty in the intensity especially in the peak at 220 nm. In this example the agreement between the calculated and the theoretical oscillator strength is not as good as it has been for other molecules found in the literature[17, 45, 130]. A high resolution absorbtion cross section of NaOH would be desireable to obtain for comparison. As it presently stands, the calculated oscillator strength is about two times greater than the experimental value.

Table 4-1. Characteristics of the low energy excited states of NaOH.

State	Symmetry	Character	Type	Electronic Degeneracy	EOM-CCSD/ POL (nm)	f calc.	f exp.
A	$^1\Sigma(0) \rightarrow ^1\Pi(1)$	Valence	$\pi \rightarrow \sigma*$	2	344.5	0.054	0.017
B	$^1\Sigma(0) \rightarrow ^1\Pi(2)$	Rydberg	$\pi \rightarrow \sigma*$	2	239.2	0.092	0.060
C	$^1\Sigma(0) \rightarrow ^1\Sigma(1)$	Rydberg	$\pi \rightarrow \pi*$	1	227.3	0.026	

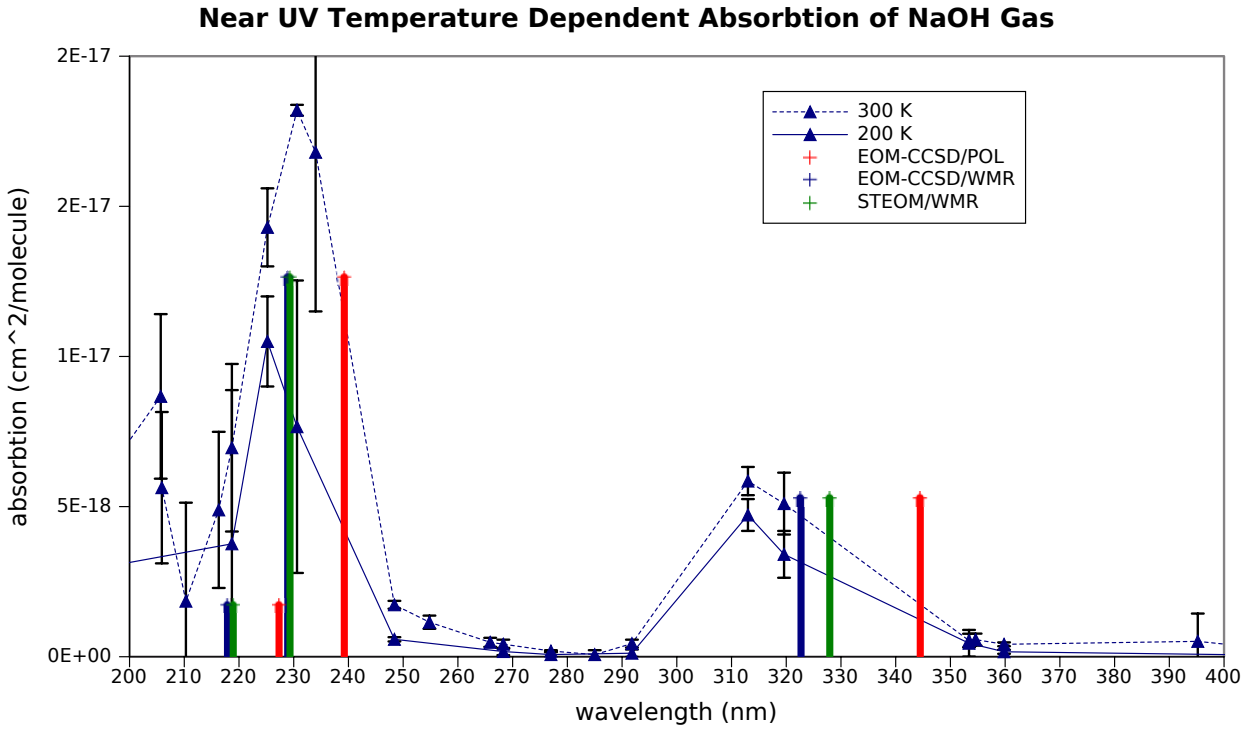

Figure 4-1. The POL basis set does a reasonable job of describing the Rydberg excited states in the 220 nm region but it underestimates the energy gap of the valence state. The results from EOM and STEOM calculations with WMR basis are in good agreement with each other as well as with the experiment. The dipole transition moments remain largely unaffected by the choice of basis set. Vertical excitation intensities are approximate but reflect the theoretical relative intensities.

The geometry is optimized at the CCSD level of theory using the POL basis set [136]. The R_{NaO}=1.9493 Å and R_{OH}=0.9589 Å. The best available experimental NaOH geometry[79] is R_{NaO}=1.9500 Å. This geometry is also in good agreement with the geometries listed in the work of Lee and Wright who employ a variety of high-end methods and basis sets[83] which suggests that CCSD/POL is adequate to proceed as far as geometry is concerned. Keeping in mind that the method outlined below is geared for larger molecules, the best optimized geometry will often be a DFT geometry done with a modest basis set.

The excitation energies are calculated using the EOM-CCSD method and POL basis set has proven to be a good choice for describing excitation energies and dipole

Table 4-2. Near-UV EOM-CCSD excitation energies for NaOH.

State	POL		aug-cc-pVDZ		aug-cc-pVTZ		WMR		MAD		Exp.
	eV	nm	eV	nm	eV	nm	eV	nm	eV	nm	nm
A	3.60	344.50	3.65	340.10	3.81	325.70	3.84	322.70	0.10	9.00	313
B	5.18	239.20	5.18	239.30	5.34	232.10	5.42	228.30	0.10	4.50	230
C	5.45	227.30	5.45	227.50	5.61	220.90	5.70	217.90	0.10	4.00	225

Table 4-3. Near-UV STEOM excitation energies for NaOH.

State	POL		aug-cc-pVDZ		aug-cc-pVTZ		WMR		MAD		Exp.
	eV	nm	eV	nm	eV	nm	eV	nm	eV	nm	nm
A	3.53	351.10	3.58	346.50	3.76	329.40	3.78	327.90	0.11	10.10	313
B	5.15	240.60	5.16	240.20	5.30	233.70	5.41	229.30	0.10	4.40	230
C	5.26	235.60	5.44	227.70	5.59	221.70	5.66	218.90	0.14	5.70	225

moment strengths. Since NaOH is a small molecule, we are also able to calculate the spectrum with the aug-cc-pVXZ (X=D,T)[37, 161] basis sets of Dunning Jr. and with the WMR[158] basis set of Widmark *et al.* This may not be possible to do for the large molecules that are our objective so we will always present the EOM-CCSD/POL result as an expected electronic structure level of accuracy along with any energy corrections made to it based on the results from a more complete basis set calculation. The best results are shown in Figure 4-1 and a comprehensive list of results is summarized in Table 4-2 and Table 4-3.

It should be noted that for both EOM and STEOM calculations the mean average deviation is on the order of 0.1 eV. However, the error in the calculated absorption cross section is sensitive to the spectral range: the lower energy wavelengths carry a higher error than the higher energy wavelengths as reflected in the MAD values for the energies in nanometer units. Since there are no significant differences between STEOM-CCSD and EOM-CCSD methods for the excited states considered in this work, EOM-CCSD/POL is used in all subsequent calculations with the final energies of the calculated spectrum shifted to the best results from Table 4-2 and Table 4-3. The energy adjustments for the absorption peaks are: -21.8 nm for the A state, -9.9 nm for the B state and -9.4 nm for the C state.

There is no reason to suppose that doubly excited states are significant contributors since the average excitation level (AEL)[148] is not greater than 1.07 in any of the EOM-CCSD calculations for the excited states considered.

4.1.2 Absorption Cross Section Model

This portion of the results section will illustrate the validity of assumptions made in the methodology section using NaOH as an example.

4.1.2.1 Dissociative coordinate as the primary coordinate

Figure 4-2 shows the behavior of the low energy excited states as a function of distance between the sodium and oxygen atoms. Eleven single point calculations are performed for the distances ranging from 1.7 Å to 5.0 Å. The energy surfaces are computed using CCSD and EOM-CCSD methods with a restricted Hartree-Fock (RHF) reference in the vicinity of the equilibrium geometry and an unrestricted Hartree-Fock (UHF) reference past the Na-O distance of 2.5 Å at which the bond begins to break.

The valence state is purely dissociative and the Rydberg states are weakly bound. The ground state surface is fit with a Morse potential with the unbound limit set to the sum of the calculated energies of Na and OH radicals (shown as a point at 6.0 Å in Figure 4-2). The excited state surfaces are fitted with Equation 4–1 which allows a good fit for a fully dissociative surface, as well as for a weakly bound surface by setting parameter B to zero.

$$V(x) = A + Bx^{-3} + C\exp(-Dx) \tag{4–1}$$

The dipole transition moments are fit using a 6^{th} order polynomial. The R^2 values of the fits are greater than 0.998 with the worst fit being the Rydberg states due to a small energy gap at the UHF-RHF junction on the energy surfaces. The UHF-RHF energy gap at Na-O distance of 2.5 Å for the ground state PES is 0.23 mH, for the excited states A it is 4.2 mH, and for states B and C it is 7.2 mH.

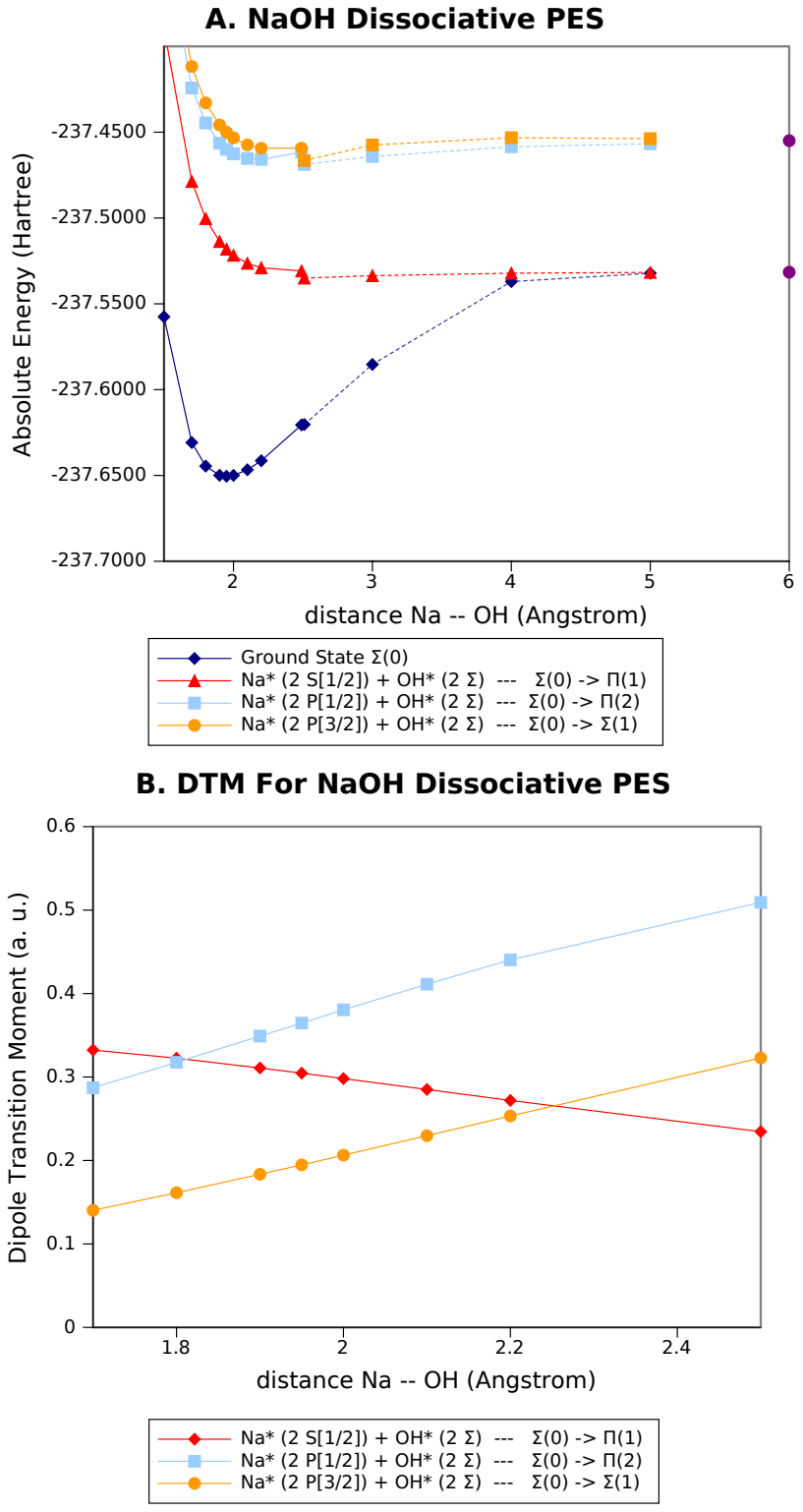

Figure 4-2. Energies and dipole transition moments of NaOH along its dissociative coordinate. Solid lines for RHF solutions and dashed lines are UHF solutions. The points at 6.0 Å represent the total energies of the dissociated products. The are no surface crossings observed.

4.1.2.2 Compute the absorption cross section of the primary mode

At this point, a zeroth order approximation to the spectrum may be determined. Since the primary mode chosen was a dissociative mode, the theoretical spectrum will have the form of a continuum cross section centered at the vertical excitation of the equilibrium geometry augmented by the dipole transition moment intensity. One can also make a different choice for the primary mode and let it be the bending coordinate, in which case the spectrum will have fine structure of the vibronic progression. Since the experiment was not done at a high enough resolution to yield vibronic peaks and we are interested in photodissociation; the choice of primary mode remains the Na-OH stretch.

Using the above-mentioned fitting parameters for the energy and dipole strength surfaces the cross section is calculated using a DVR program implemented in FORTRAN specifically for this purpose. The resulting cross section is shown in Figure 4-3.

The energy adjustments from POL to the WMR basis set are as follow: A (-21.8 nm), B (-9.9 nm), and C (-9.4 nm). These energies will be used for the rest of the data.

4.1.2.3 Consider significantly thermally populated vibrations

The calculated absorption cross section coming from the primary mode alone is in fairly good agreement with the experimentally obtained cross section. It may be sufficient for this molecule. To further improve the results we need to look at the other vibrational degrees of freedom and what (if any) effect they have on the cross section.

Including the effects of other vibrational modes to the dissociative mode will broaden the energy range of each peak as well as make the intensities more representative of what is experimentally observed. For example, this step would be vital in getting an accurate absorption cross section for a forbidden excited state which is vibronically allowed.

Vibrational energies can be found in two ways: 1) harmonic frequencies are calculated using ACES II and 2) anharmonic frequencies are determined from DVR.

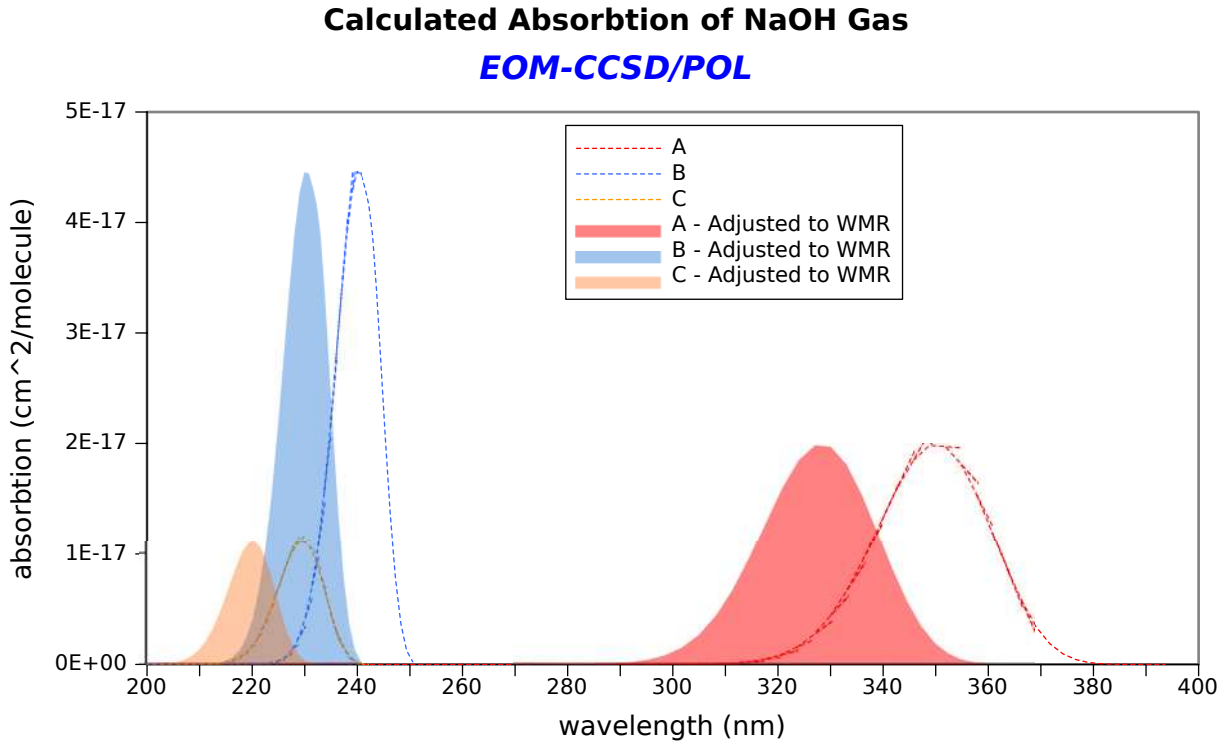

Figure 4-3. These cross sections are obtained from the FC overlap between the ZPE vibrational wavefunction of the ground state and the dissociative continuum of the exited states weighed by the dipole transition moment. The surfaces are computed at the EOM-CCSD/POL level of theory and the resulting cross sections are shown as dashed lines. Only the energies are adjusted to the best calculated values.

Table 4-4. Characteristics of the vibrational frequencies of NaOH.

Mode	Symmetry	Type	CCSD/POL (cm^{-1})	DVR (cm^{-1})	Exp.(cm^{-1})[a]	Comments
1	Π	Bend	272.31	284.7	300	Include.
2	Σ	Na-O Str.	559.83	526.6	540	Primary mode.
3	Σ	O-H Str.	3969.79	–	3637	Exclude.

These values are consistent with each other as well as with experimental data as listed on Table 4-4.

The bending mode is the only low energy mode in this molecule and it will be considered in the next steps. The OH stretching mode is too high in energy to be significantly populated and have an impact on the absorption cross section so it will not be included. The stretching mode has considerable anharmonic character so that the Morse potential fit to the ground state PES provides better agreement with the

experimental frequency than with the *ab initio* result. The bending mode is fit with a quartic potential. The difference in vibrational energy frequencies between the *ab inito* and the DVR values is 35 wavenumbers for the stretching mode which is attributed to anharmonicity of the PES. The bending mode is much better described by a harmonic potential yields a much smaller error between the *ab initio* and the DVR values. The bending mode was fit with a quartic function. Energy errors for vibrational modes on the order of 50 wavenumers introduce less than 0.5 nm error to the absorption cross section in the worst case scenario.

4.1.2.4 Determine the impact of each secondary mode

In case of NaOH, the bending mode is the only one selected to be in the secondary-mode set. For larger molecules, there will be more low-energy vibrational degrees of freedom to consider so further analysis of normal modes is needed to weed out only the important degrees of freedom. Inclusion of vibrational modes which strongly couple to the excited state potential energy surfaces is vital for an accurate absorption cross section. Emphasis is placed on the screening being both quick and accurate to minimize the number of *ab initio* calculations that need to be performed. This involves picking each mode in the second set and calculating a few key points along its surface. For each set of points the impact of the molecular geometry deformation along a particular mode on the excitation energy and the dipole transition moment is determined.

The number of actual calculations can be optimally minimized to a few key points on a surface: *cis* and *trans* conformers for dihedral rotation modes, a +/- 30 degree deformation in each direction is appropriate for bending modes and +/- 0.5 Å for stretching modes. Since this approach is still in the testing stage, the above parameters are not to be taken as absolutes but as a staring point. Symmetry and breaking thereof will need some attention paid to it since symmetric modes and asymmetric modes will have slightly different behaviors. Furthermore, there are special vibrational modes

Table 4-5. The impact of the bending normal mode has on the excited state potential energy surfaces and the dipole transition moments.

Excited State	*A*	*B*	*C*	*A'*	*B'*	*Na-O-H Angle*
EE (nm)	325.8	237.8	232.1	349.7	245.9	120
EE (nm)	344.5	239.3	227.4	344.5	239.3	180
EE (nm)	325.8	237.8	232.1	349.7	245.9	240
Impact (nm)	10.80	0.86	2.71	3.00	3.81	
DTM (a.u.)	0.66	0.03	0.13	0.34	0.02	120
DTM (a.u.)	0.30	0.05	0.19	0.30	0.05	180
DTM (a.u.)	0.66	0.03	0.13	0.34	0.02	240
Impact (a.u.)	0.69	0.23	0.18	0.08	0.35	

that need to be taken into consideration such the umbrella mode of ammonia or the ring-breathing mode of benzene.

The first step is to get a list of vibrations which have the most impact and to exclude the ones that have little or no effect. If there is a reason and capability to do more points on the surfaces which matter most then computer time may be allocated more efficiently to get better surfaces for modes with have a greater impact. Table 4-5 shows how this procedure works for the bending mode of NaOH.

It is clear from Table 4-5 that the error in energy of the zeroth order cross section (Figure 4-3) is no grater than 10.8 nm. The lower energy valence excited state is most affected by the bending mode and the errors in the Rydberg states are more tolerable. The dipole transition moment for A and B states is significantly affected by the bending mode which would have impact on intensities. Figure 4-4 shows the energy surfaces and the dipole transition moment surfaces as a function of the bending mode while keeping the R_{NaO} at it equilibrium value and relaxing the R_{OH}.

For a small molecule such as sodium hydroxide it is inexpensive to compute several more points along the bending mode, but is not necessary to do since we are only interested in the range of the potentials which are close to the equilibrium. If a high temperature spectrum were of interest where a significant fraction of higher vibrational levels are populated, then it would make sense to have more points. The agreement

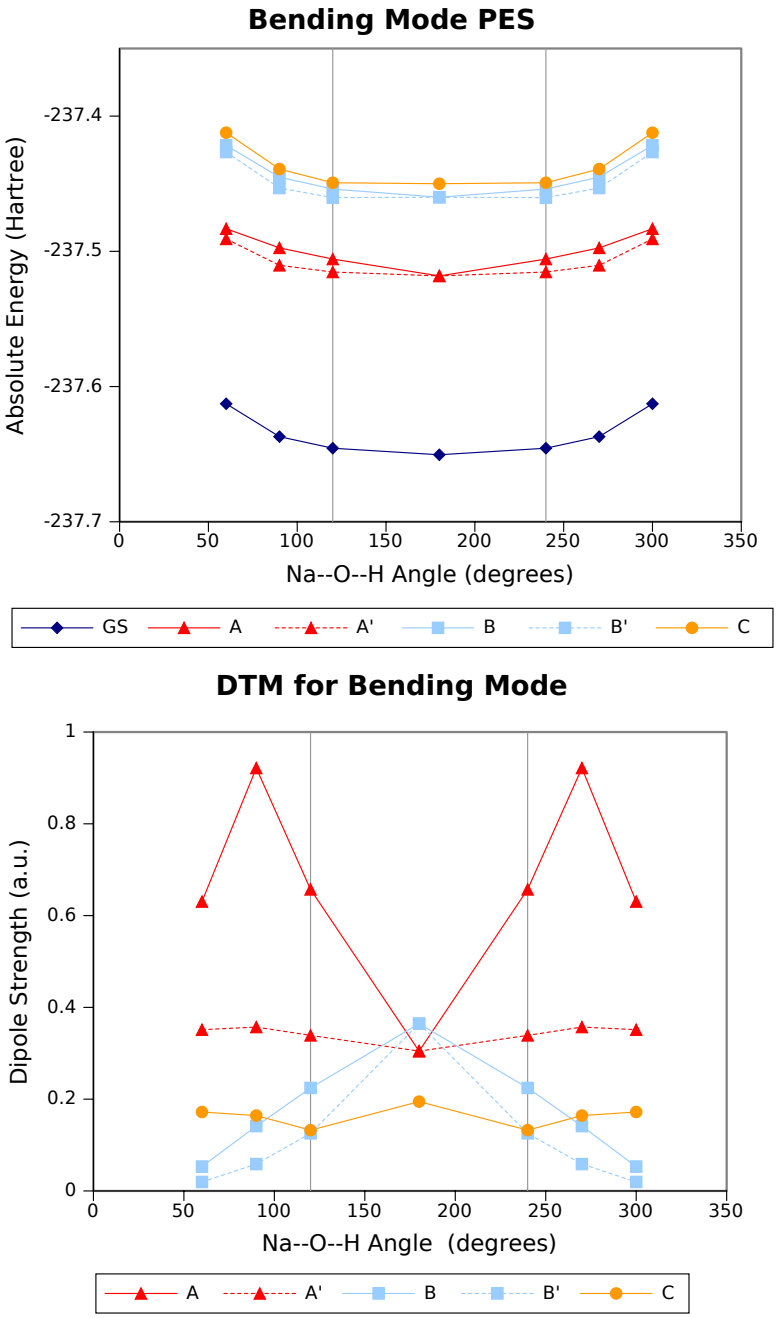

Figure 4-4. Energies and dipole transition moments of NaOH along its bending coordinate. The points which are listed in the table are the three points encompassed by the vertical lines. Several more points were done for completeness but were not necessary for accuracy.

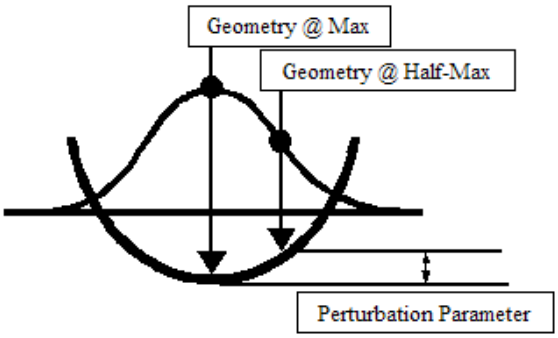

Figure 4-5. This is a cartoon of a vibrational wavefunction in a potential (in this case the potential of the bending mode). The change in the surface energy between the equilibrium geometry and the geometry of the half-maximum is what is added onto the zeroth order dissociative potential for the ground and excited states. The dipole strength potential is multiplied by the fraction of the $DTM_{Half-Max}/DTM_{Max}$.

between the DVR vibrational energy for this mode and the *ab initio* frequency suggests that three points provide a good enough fit. A large discrepancy between the energy values would be a signal to do more points for a better potential.

4.1.2.5 Add the effects of other degrees of freedom

The fitting parameters of the energy surfaces and the dipole transition moments for excited and ground states are used to perturb the zeroth-order dissociative state and recalculate Frank-Condon overlaps. This calculation is done at two points as illustrated in Figure 4-5: the original equilibrium geometry overlap (which corresponds to the maximum of the vibrational wavefunction) is given a weight factor of 0.50 and a weight factor of 0.25 is assigned to the two half-maximum points. Due to the symmetry in the bend, this distribution simplifies to 50% of the intensity coming from the point at the maximum and another 50% of the intensity coming from one of the points at the half-maximum.

Due to the breaking of the electronic degeneracy for states A and B, the distribution is 50% of the intensity coming from the point at the maximum, 25% of the intensity

Table 4-6. Oscillator strengths calculated from the DVR cross sections.

State	Single Point	ZPE	ZPE+P1	Convoluted	*f* exp. (200 K)	*f* exp. (300 K)
A	0.054	0.051	0.051	0.051	0.017	0.023
B	0.092	0.095	0.084	0.108	0.060	0.106
C	0.026	0.027	0.024			

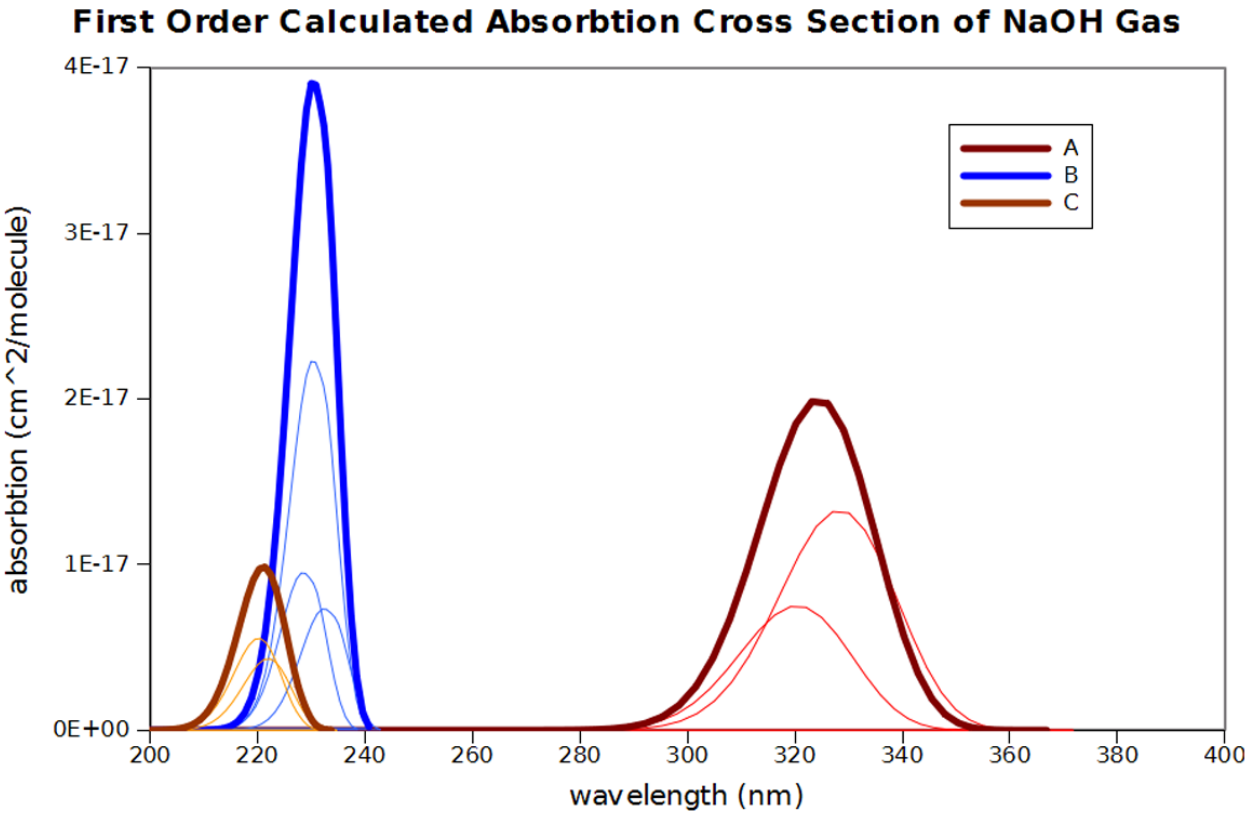

Figure 4-6. The convoluted cross sections are shown in thick lines. This is the 1st order spectrum.

coming from one of the points at the half-maximum from one symmetry (A and B) and another 25% of the intensity coming from one of the points from the other symmetry (A' and B'). Finally, the peaks are convoluted into one cross section for each excited state as shown in Figure 4-6. The resulting convoluted spectrum is correct in the 1st order. Taking more points: 66% /33% Max would be 2nd order, 75%/50%/25% would be 3rd and so forth.

4.1.2.6 Temperature effects can be introduced at this stage.

The spectrum in Figure 4-6 does not have any temperature effects since only the first vibrational levels are populated. Temperature effects may be added by putting quanta into higher vibrational levels and recalculating the weights. No extra time is required for this as all Frank Condon integrals are calculated at once. At 200 K the contribution from the second vibrational level of the primary and the secondary modes to the absorption cross section is only about 10% of the total intensity which is not very noticeable. Only when the temperature used in determining the Boltzmann distribution is raised above 500 K does any significant change in peak intensity occur.

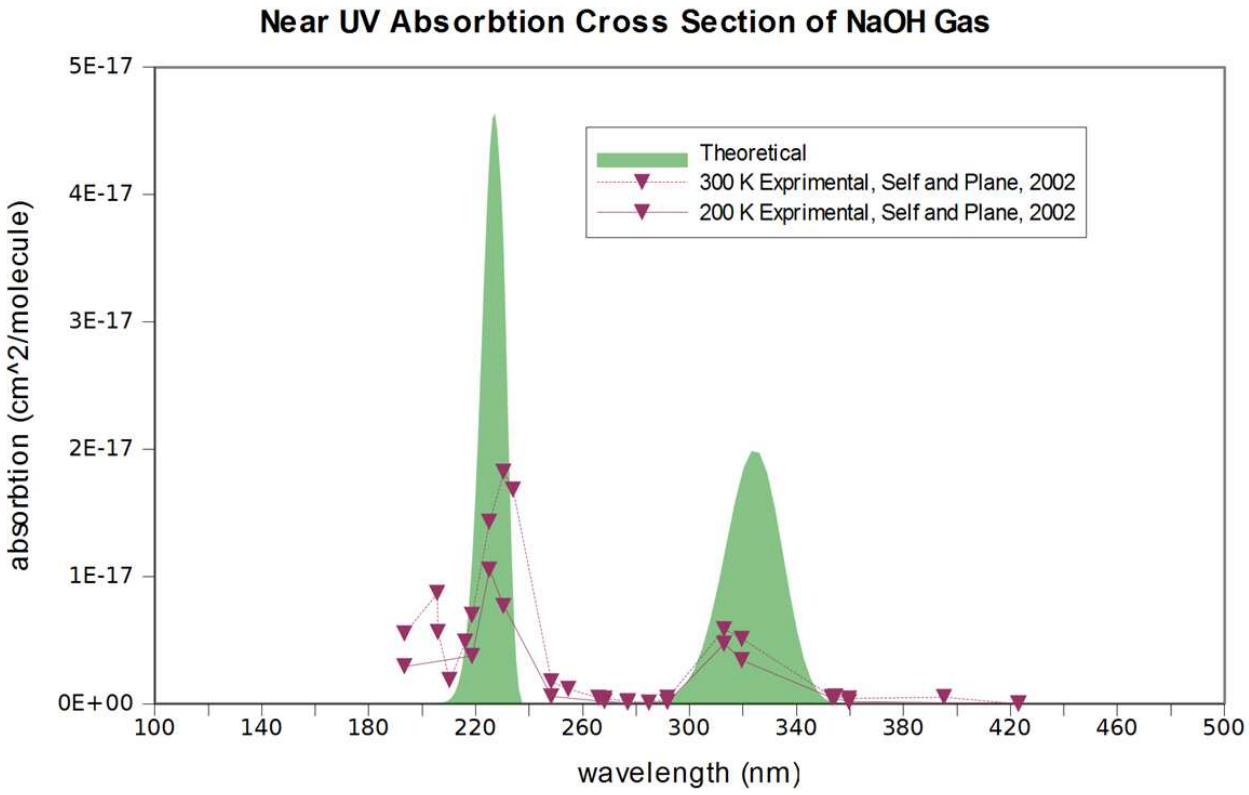

Figure 4-7. The convoluted cross section is shown with the experimental cross section

According to Self and Plane the significant increase in intensity for the peak at 220 nm is due to the increase in the Frank-Condon overlap. This assertion is based on the fact that their CIS/6-311+G(2d,p) calculation of the geometries of ground state and excited state showed that while the ground state in linear, the excited state is bent.

In the present work, the ground state and excited state potential energy surfaces in Figure 4-4 show a lack of a true double minimum on the excited state PES[1] which means that a linear geometry is preferred for the excited states in the energy range of the absorption cross section. Furthermore, the dipole strength for excitations B and C tends to diminish as a function of angle thereby reducing the total intensity (as opposed to increasing it). This is in support of the conclusion that hot bands originating from populating the bending mode will not lead to a significant increase in intensity for B and C states, but possibly for the A state. The higher intensity cross section observed by Self and Plane at 300 K may not be due to a temperature dependence but to the fact that it is a higher resolution experiment and slightly more accurate.

The consistency check described in the Methods section is done and results presented in Table 4-6. It appears that as the peaks get broadened, the integrated oscillator strengths become slightly lower but no major discrepancies are noted. The final theoretical spectrum is presented in Figure 4-7.

4.2 Water: example of a bound system

In the previous section, it was shown that the frequency pre-selection in combination with the DVR vibronic spectrum provides a very good representation of a photodissociative absorption cross section. In this section, I will show that this approach also works on a bound absorption cross section.

The water molecule has three vibrational frequencies: symmetric stretch (3657 cm^{-1}), bend (1595 cm^{-1}) and asymmetric stretch (3756 cm^{-1}); the reference experimental geometry is $R_{OH} = 0.958$ Å and $\angle HOH = 104.478$ [62]. Using the experimental

[1] The energy surfaces in Figure 4-4 were calculated with the constraint $\mathrm{that} R_{NaO}$ is at it equilibrium. These surface were recomputed such that R_{NaO} and R_{OH} were allowed to relax and no double minimum was found

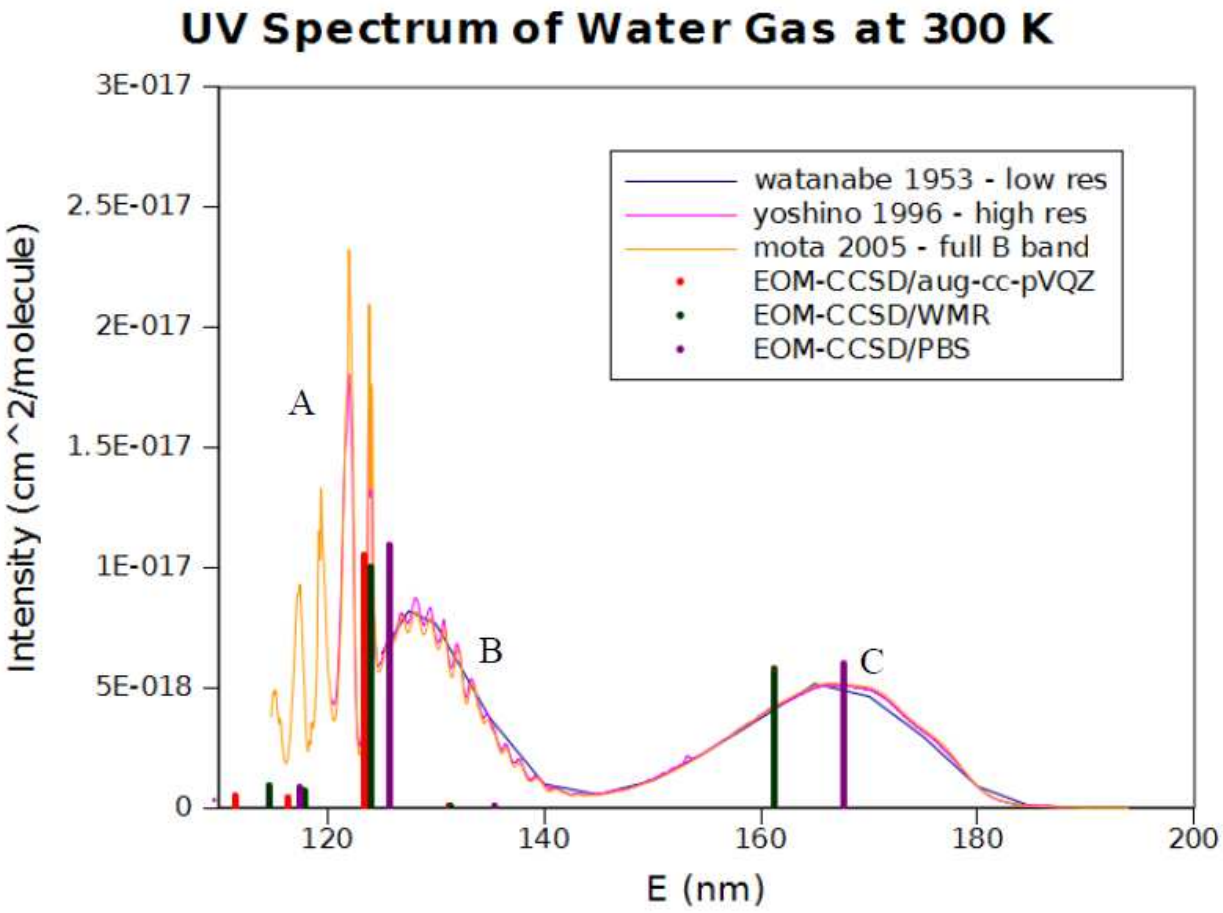

Figure 4-8. A collection of several experimental VUV absorption cross sections for water: Watanabe *et al.* [156], Yoshino *et al.* [163] and Mota *et al.* [111]. The theoretical stick spectrum for several selected basis sets are shown.

geometry the photoelectronic spectrum computed with EOM-CCSD is shown in Figure 4-8 along with several experimental absorption cross sections.

The decomposition of the experimental spectra is as follows. There is no disagreement about the peak at C, it is a $^1B_1(b_1 \rightarrow 3pb_2)$ allowed excitation. The calculated vertical excitation corresponds to the peak at A which is another allowed excitation $^1A_1(3a_1 \rightarrow 3sa_1)$. This excited state overlaps with the peak at B which corresponds to an electronically forbidden excited state (vibronically allowed) $^1A_2(b_1 \rightarrow 3pb_2)$ [26, 89]. Table 4-7 shows the Hartree-Fock orbital energies and symmetry labels from WMR basis set to help follow the excited state assignments.

Table 4-7. Molecular orbitals of water HF/WMR.

Energy (a.u.)	*Energy (eV)*	*Label*
-20.5632996227	-559.5560829301	1a1
-1.3544751515	-36.8571593129	2a2
-0.7202241618	-19.5983046595	b2
-0.5853340530	-15.9277565337	3a1
-0.5107691418	-13.8987412302	b1
0.0320045368	0.8708881161	3s a1
0.0500758245	1.3626330761	3p b2

Unfortunately, it's not easy to unambiguously de-convolute these peaks and get a precise oscillator strength value since a portion of the intensity from the $^1A_1$ excited state be a significant portion of the intensity of the $^1A_2$ state.

The vibronic spectrum at 500 K is calculated for the $^1A_2$ state to show the dipole-forbidden state become vibronically allowed as a demonstration of the approach described in Chapter 3. The bending mode is chosen as the primary mode and the OH-stretch is chosen as a perturbation. The vibronic spectrum is shown in Figure 4-9. The spectral lines show a matching broadness and peak characteristics as the experimental cross section.

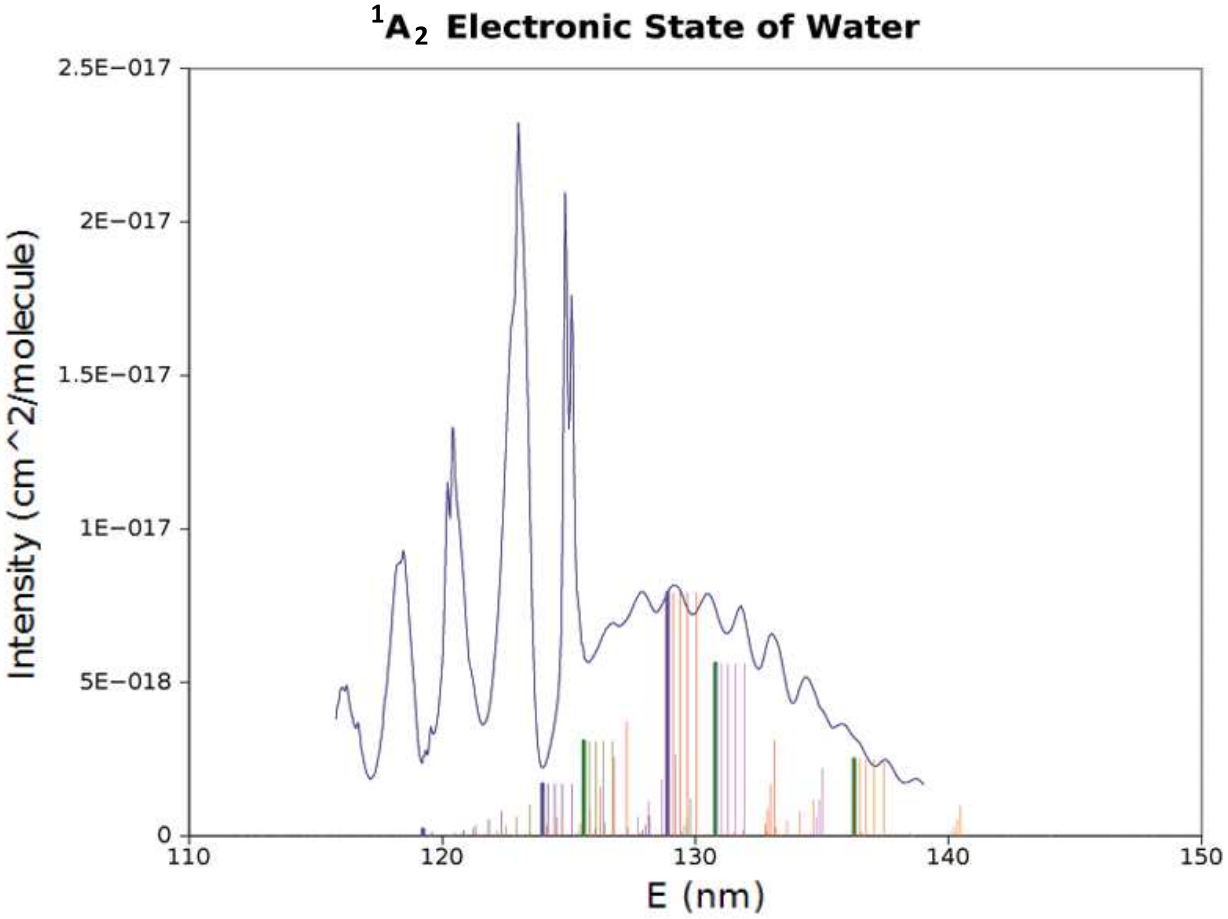

Figure 4-9. Bold lines: OH stretch vibrational levels, $v_{str} = 0$ (blue), $v_{str} = 1$ (green). Fine lines: vibrational levels at $v_{str} = 0$ and $v_{str} = 1$. The experimental spectrum is by Mota *et al.* [111].

CHAPTER 5
SINGLE REFERENCE CC FOR MULTI-REFERENCE PROBLEMS

5.1 Background

Traditional high order single reference coupled cluster theory (CCSDT, CCSDTQ, CCSDTQP, etc.)[3–5, 8–10, 27, 28, 84, 123, 131] can successfully solve multi-reference problems such as bond breaking at a sufficient level of approximation. For a recent and comprehensive review of single-reference and multi-reference methods used for the description of bond breaking see [5, 38, 99, 126]. The recovery of the correlation energy using coupled cluster (CC) methods is much more rapid than those of configuration interaction (CI) due to the exponential nature of the CC wavefunction. However, including all higher order excitations is not the solution, because of computational demands. Hence, steps have been taken to limit the most expensive procedures to a small orbital space such as is done in CCSDt'q' and with addition of intermediate indexes in CCSDtq[124, 125]; as well as with Tailored-CC method (TCCSD)[59, 71] methods; the later being related to the RMR approach of Li and Paldus[87].

5.2 Tailored-CC extension

The methods described below are depicted pictorially in Figure 5-1 where it is easy to see the main differences among them.

A single bond dissociation relative to an RHF reference is considered a type of multi-reference problem where the significant determinants originate in the σ,σ^* space of the two electron, two orbital ([2,2]) space. The TCCSD scheme uses the FCI coefficients for the active space problem and imposes them onto a full space CCSD calculation:

$$|\Psi_{\mathrm{TCC}}\rangle = |e(^{\mathrm{ext}}\hat{T}_1 + ^{\mathrm{ext}}\hat{T}_2)e(^{\mathrm{FCI}}\hat{T}_1 + ^{\mathrm{FCI}}\hat{T}_2)|\Psi_0\rangle \tag{5–1}$$

Computationally, the Tailored-CC wavefunction is obtained in two parts: first the active space amplitudes labeled with *fci* are determined

$$|\Psi_{\mathrm{FCI}}\rangle = |e(^{\mathrm{FCI}}\hat{T}_1 + ^{\mathrm{FCI}}\hat{T}_2)|\Psi_0\rangle \tag{5–2}$$

then, Equation 5–1 is solved for the external amplitudes while keeping the amplitudes obtained from Equation 5–2 constant. The FCI for a [2,2] problem is equivalent to a CCSD or a CISD calculation. If a CCSD calculation is done in the active space, the two t-amplitudes ($t_1\{\sigma,\sigma^*\}$, and $t_2\{\sigma,\sigma^*\}$) are directly used in the subsequent restricted CCSD calculation; if a CISD calculation is done in the active space, the t-amplitudes are derived from CI coefficients *via* the cluster decomposition analysis: $T_1 = C_1$ and $T_2 = C_2 - C_1^2/2$. Either way is acceptable to obtain the active space t-amplitudes.

The decoupling between the active [2,2] space and the full space can be pathological in the TCCSD method which becomes one of the major drawbacks of an otherwise efficient way of introducing higher orders of correlation. This decoupling manifests itself in a large non-parallelism error (NPE), measured as the difference between the maximum and the minimum error along the potential energy surface.

Our solution is to introduce some additional coupling between the [2,2] active space and the full space (see Figure 5-1 regarding the discussion below). This is done with a CCSDT calculation in an extended active space or what is known as a CCsdt calculation. The amplitudes associated with a [2,2] determinant are saved from that CCsdt calculation and the full space CCSD equations are allowed to relax while keeping the amplitudes from the CCsdt constant. This approach is called XTCCSD for "eXtended TCCSD". In order to determine active space independent errors associated with the Tailored-CCSD procedure, we use the entire orbital space to do the CCSDT calculation from which the [2,2]-related t-amplitudes are taken ($\bar{\text{X}}$TCCSD). This calculation also provides the CCSDT values as a reference.

Another way to use the extended active space is to save all the amplitudes from the CCsdt calculation and use them to tailor the subsequent full space CCSD calculation. This will lead to a very different NPE and relative energy error since now the absolute energy value will be closer to the reference CCSDT value. We call this FXTCCSD for "Fully eXtended TCCSD" The calculation time tends to be slightly shorter than that of

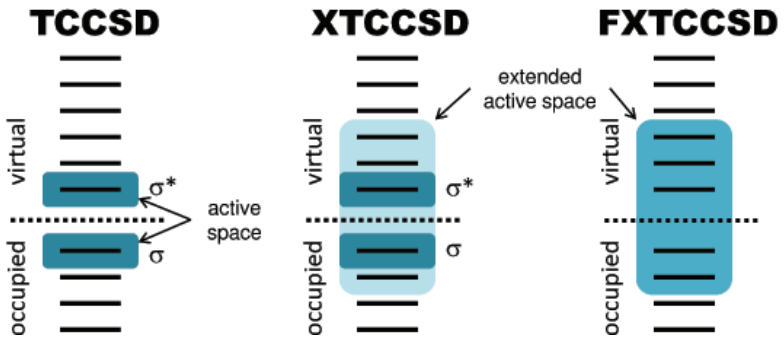

Figure 5-1. A cartoon representation of the methods used. The traditional Tailored-CC is on the left with a single bond active space indicated by the σ and σ^* orbitals. The extended active space is indicated for XTCCSD and FXTCCSD methods. In XTCCSD, the active space amplitudes are saved but are calculated with a CCsdt calculation in the extended space. In FXTCCSD, the entire set of amplitudes from the extended space is saved.

XTCCSD because there are fewer amplitudes to converge in the second step, usually taking fewer iterations.

The main advantage of the FXTCCSD approach is when the active space is not necessarily well defined *a priori*. Unlike in the clear case of σ-bond dissociation, sometimes the user does not know which of the determinants constitute the multi-reference problem. This is one of the general drawbacks of active space methods, especially for difficult and/or unfamiliar molecules, since what tends to happen is the active space is varied by the user until some agreement with experiment might be reached. We believe that this is not what the function of a predictive theory ought to be and insist that the choice of active space should be based on numerical results alone and not on any chemical intuition so as not to create inherently biased results. To that end, we propose an automated active space determining algorithm (ASDA) which finds a set of appropriate extended active spaces based on statistical analysis of the orbital energies of the reference used by the coupled cluster calculations. The user can either pick an extended active space from the ASDA set or let the selection process do so automatically.

There were several attempts to automate selection of active spaces published prior to this work which include an adaptive coupled cluster scheme[97], a scheme based on overlap integrals of the reference[76, 140] and a particular orbital contributions (POC) analysis[98].

5.3 Extended space choice

The main function of the ASDA is to find the first "big" energy gap in the virtual (or occupied) orbitals with the logic being that after that gap the denominators lose most of their significance by becoming too large. So all significant transitions are treated with a higher level of theory (CCSDT) and all the other ones with a lower level of theory (CCSD).

The following discussion details an automated way of picking an active space for either the extended tailored coupled cluster method (XTCCSD) or the fully extended tailored coupled cluster method (FXTCCSD) both of which are described in the previous section.

A generic amplitude may be described as:

$$T_o^v = \frac{t * v}{\epsilon_o - \epsilon_v} \tag{5–3}$$

Where t is a coupled cluster amplitude coefficient, v is either the Fock or 2-electron integral, ϵ_o are orbital energy contributions from the occupied space and ϵ_v are orbital energy contributions from the virtual space. The generic amplitude does not distinguish excitation level: *e.g.* $\epsilon_o = \epsilon_i + \epsilon_j$ and $\epsilon_v = \epsilon_b + \epsilon_b$ for a selected t_{ij}^{ab}. Since the orbital energy difference appears in the denominator, we conclude that the more positive the value of ϵ_v is, the less that amplitude term will contribute to the total ground state energy since as $\epsilon_o - \epsilon_v \to \infty$, $T \to 0$. Due to this property, it is common practice to exclude core orbitals from the coupled cluster and configuration interaction calculations.

The extended active space as used by the XTCCSD and FXTCCSD methods needs to be established such that the cutoff is in the mid-valence, which is less obvious

than a simple core orbital exclusion. This is especially so in the virtual space where energy levels may be closely packed. We employ a statistical analysis of the distribution of energy values of virtual orbitals to determine the best places for the active space boundary.

The examples in the Results section illustrate numerically how each of the steps are accomplished and it is pertinent to say that while the reference orbitals here are Hartree-Fock, it is not a necessity. The statistical model draws from the available set of orbitals so the only condition for success is that there be enough of them to present a meaningful distribution.

The Hartree-Fock orbitals are separated into occupied and virtual sets. For the molecules studied here, there are not enough occupied orbitals to offer a meaningful distribution so only the core orbitals are excluded from the extended active space for the occupied block. The virtual orbitals are sorted in order of increasing energy values such that the orbital energy may be expressed as a function of orbital number, $E(n)$.

The numerical derivative of the ordered orbital energy is then:

$$\frac{dE(n)}{dn} = \frac{E(n+1) - E(n)}{(n+1) - n} \tag{5–4}$$

Since dn is always one (though for a molecule with thousands of basis functions, we may want to make it greater than one), Equation 5–4 becomes:

$$dE(n) = E(n+1) - E(n) \tag{5–5}$$

The significance of the contribution containing the n^{th} orbital is measured by the reciprocal of the energy

$$R(n) = dE(n)^{-1} \tag{5–6}$$

where the larger the value for $R(n)$, the more significant is the contribution from denominators containing the n^{th} orbital. Core orbitals are excluded from further analysis.

The distribution of $R(n)$ is exponential, therefore to achieve a normal distribution, $R(n)$ is transformed to $ln(R(n))$.

The kernel density estimation (KDE) and quantile-quantile (QQ) plots show that the distribution of the $ln(R(n))$ data points is close to a normal distribution, but not always unimodal, especially at points away from equilibrium. Having multiple modes at the dissociation limit is not surprising considering that the energy levels of atomic orbitals are inherently bi-modal (n-levels (large energy gaps) and n-manifold levels (small energy gaps)). At equilibrium the molecular orbitals are coupled through the linear combination of atomic orbitals procedure, and thus tend to produce smoother distributions. If multiple modes are detected, the ASDA will only consider the mode which samples the biggest gaps in the distribution.

The $ln(R(n))$ data are fit to either a unimodal or multimodal normal distribution and the mean (μ) and the standard deviation (σ) computed. The range of interest is $\bar{U} = \mu - \sigma$ for the upper-bound cutoff to the active space. The $\bar{U}$ is then transformed back to the energy domain $dE_{\bar{U}} = \exp(-\bar{U})$. The $n^{th} + 1$ orbital of any $dE(n) > dE_{\bar{U}}$ is saved to a list as a contender for marking the active space cutoff.

The final output from ASDA is a list of orbitals which fulfill the condition of being on the upper side of a significantly (by more than one standard deviation) large energy gap. The program will attempt to go with the first cutoff orbital on the list and check to make sure that at least 20% of the total number of basis functions is included and that all large amplitudes from a second order many-body calculation (MBPT(2)) are within the active space. If any of the above conditions fail, the active space is expanded to the next cutoff candidate on the list and the checks are repeated. These checks are an unfortunate consequence of basis set contractions which can lead to early gaps in the virtual space energy manifold.

At this point the active space calculation will proceed as described in the previous subsection. Depending on the purpose of the calculation, the user can always intervene

and choose which of the possible cutoffs to use. For example, if the final goal is to generate a PES, in order to minimize discontinuities one can choose a cutoff which is common to all the points on the PES which we will refer to as an intersection (∩) active space. This choice leads to better NPE but can be more expensive. If the goal is to determine the energy difference between two points, one can choose a consistent active space (like in a PES generation) or one can let the ASDA choose the minimal cutoff space. Both choices are evaluated in the results section and accuracy is weighted by computational advantage. In any case, we highly discourage picking a cutoff orbital which is not on the ASDA output list just to satisfy active space size consistency.

5.4 Statistical analysis techniques

This section contains the background necessary to understand the statistical analysis performed by ASDA.

5.4.1 Quantile-quantile plot

A Quantile-Quantile Plot, or QQ Plot, is a plot comparing the probability distribution of two sets of data. Quantiles are points taken at regular intervals from a data sample, the most familiar of which is the 2-quantile or the median.

Generally, a QQ Plot will compare the distribution of a data set with a theoretical distribution (normal, gamma, Poisson, geometric, etc.). If the plot forms a straight line with a slope of 1 and intercept of 0, then we can conclude that the data follows whatever theoretical distribution it was compared with.

It is easy to see outliers on a QQ Plot and any other peculiarities of the data such as if it follows a combination of probability distributions. The main reason for evaluating the QQ plot is to make sure that the standard deviation which is used as a cutoff parameter is calculated for the correct probability distribution of the data.

5.4.2 Kernel density estimation

The following explanation is adapted from a book called *Density Estimation* by B. W. Silverman[95].

A data set can be presented as a histogram. A better representation of this data is to determine a uniform distribution fit to it. To accomplish that, we define a kernel K:

$$\int_{-\infty}^{\infty} K(x)dx = 1 \tag{5–7}$$

In the case of normally distributed data, the kernel used is a normal density function. The idea is to assign a normal probability density function (a Gaussian) to every data point, X_i. These Gaussian functions are convoluted to produce the KDE plot via:

$$KDE(x) = \frac{1}{nh}\sum_{i=1}^{n} K(\frac{x - X_i}{h}) \tag{5–8}$$

where h is the width of the Gaussian, generally referred to as a smoothing parameter or bandwidth. The benefits include continuity and the ease of interpretation of the data distribution since KDE avoids the jagged edges of a histogram. For the purpose of evaluating the results from ASDA, the KDE plot is superior to a histogram plot because it is easy to see the modality of the distribution (*i.e.* how many peaks).

CHAPTER 6
ACTIVE SPACE CC EXAMPLES

In this work we explore the errors that arise from the traditional TCCSD and improve upon it while keeping the computational cost manageable. FH (hydrogen fluoride) and F_2 (molecular fluorine) are chosen as classic examples of a single bond-breaking MR problem.

6.1 Hydrogen fluoride

The FH example is useful because its PES is very well documented in the literature[49, 60, 64, 71, 88, 91, 97, 101, 126, 135, 138] and it provides a good platform for error analysis of any new method. The experimental dissociation energy is known[23, 31, 165] and has been calculated to high accuracy with the quantum Monte Carlo method[94]. Unfortunately, most of the available calculations are done with very small basis sets due either to computational limitations of the methods used, or to the limitation of the FCI[10] with which the comparison is usually made. This work demonstrates that larger basis sets may cause problems with convergence and make errors that might be small with double-zeta-type basis gain significance. Even triple-zeta basis sets are not adequate to reach a result which is comparable to experiment.

The CCSDT method has been shown to successfully compute the dissociative PES of a single bond[5]. We further test this method's viability by comparing several points on the PES to the FCI method for FH with the cc-pVDZ basis set. The energy error between the CCSDT and the FCI method for FH at the dissociation limit (3.20 Å) is 0.2 mE_h and CCSDT is known to recover more than 99% correlation energy at equilibrium.

Figure 6-1 shows the dissociative PES energy error with respect to CCSDT of FH from 0.0.917 Å to 3.20 Å computed with TCCSD, CASCCSD[64], CASCISD(MRCI)[20, 122] and CCSD.

Table 6.1 shows the dissociation energy values computed with the methods described above. The MRCI energy lies slightly higher but the D_e value is acceptable so while the absolute energy is a bit too high, the relative energy may yet be trustworthy. The error of the CASCCSD method is close to that of the CCSD in the equilibrium region but it does not diverge as the CCSD does.

There are several formulas which can be used to extrapolate correlation energy but it is unclear which is appropriate for the methods based on Tailored-CC. Furthermore, the errors of these extrapolations can be larger than the error between the largest basis set calculation in this work and experiment[41]. For example, the CCSDT correlation energy may be extrapolated by at least three well known methods:

$$E_{\text{corr}}^{\infty}[\text{T,Q,5}] = a + bX^{-3} \tag{6–1}$$

$$E_{\text{corr}}^{\infty}[\text{T,Q,5}] = a + bX^{-c} \tag{6–2}$$

where function parameters a, b, and/or c are fitted to the cardinal [T,Q,5] numbers of the cc-pVXZ basis set. Also a two-point extrapolation can be used using the cc-pVQZ and cc-pV5Z energies:

$$E_{\text{corr}}^{\infty}[\text{Q,5}] = \frac{4^3 * E_{\text{corr}}[4] - 5^3 * E_{\text{corr}}[5]}{4^3 - 5^3} \tag{6–3}$$

Hatree-Fock energies can be extrapolated with the exponential decay formula:

$$E_{\text{HF}}^{\infty} = a + b * exp(-c * X) \tag{6–4}$$

Using Equation 6–4 with Equations 6–1, 6–2, or 6–3; the D_e values for CCSDT are: 227.72 mE_h, 230.50 mE_h, or 228.77 mE_h respectively. The conclusion is that while the CCSDT probably overshoots the experimental reference by some small amount, it is unclear from the uncertainty in the extrapolation formulas by how much. This is consistent with the conclusion of Halkier *et al.*.[53] where a $(T, Q, 5)$ extrapolation could

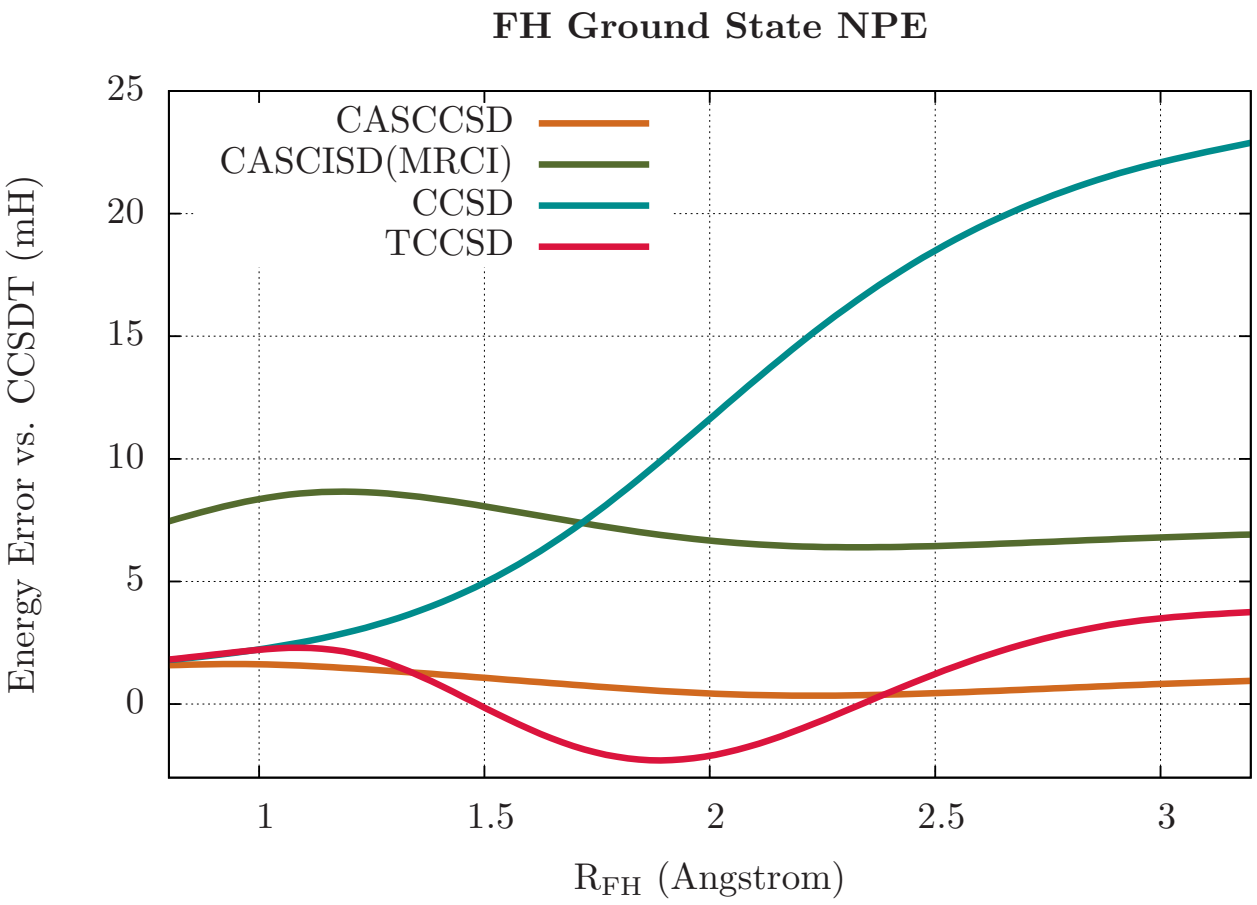

Figure 6-1. Dissociative PES energy error with respect to CCSDT of FH from 0.917 Å to 3.20 Å computed with [2,2]FCI-Tailored-CCSD, CASCCSD, CASCISD(MRCI), and CCSD. Basis set is cc-pVDZ.

have ≈3 mE_h of error and a two-point $(Q, 5)$ extrapolation could have ≈1.5 mE_h of error. Several mE_h errors between different extrapolation techniques is also evident in the comprehensive basis set extrapolation evaluation study of Feller *el al*.[41] It is possible that conventional formulas such as the ones listed above are not sufficient to describe molecules such as FH or F_2 due to rather poor RHF reference. Since the unextrapolated CCSDT value is 226.16 mE_h which is already within a mE_h difference from the experimental and the Quantum Monte Carlo values, there is no useful information to be gained by doing these approximate basis set extrapolations.

Table 6-1. Dissociation energy for hydrogen fluoride. Energies are reported in mE_h units.

	cc-pVDZ	cc-pVTZ	cc-pVQZ	cc-pV5Z
CCSD	222.55	246.10	252.45	255.04
CCSDT	201.68	219.87	224.41	226.16
CASCCSD	201.0			
CASCISD(MRCI)	200.6			
TCCSD	203.38	221.38	225.69	227.45
$\bar{X}$TCCSD	202.22	220.04	224.51	226.70
XTCCSD	201.88	219.10	223.69	225.65
FXTCCSD	203.34	220.61	225.50	226.89
experimental values[a]		225.92[b]	225.82[c]	
Quantum Monte Carlo		226.3[d]		

[a] Experimental values are reported minus the atomic SO coupling of -0.605580 mE_h and relativistic corrections of -0.302784 mE_h[42]
[b] From Ref. [23]; [c] From Ref. [31, 165]; [d] From Ref. [94].

Table 6-2. NPE for hydrogen fluoride. Energies are reported in mE_h units.

	cc-pVDZ	cc-pVTZ	cc-pVQZ
TCCSD	6.0	5.5	5.4
$\bar{X}$TCCSD	0.6	1.9	2.8
XTCCSD	1.8	2.0	2.8
FXTCCSD[a]	1.7	0.9	1.1

[a] For the cc-pVQZ the NPE is reported for the consistent active space, the NPE for minimal space is 2.5 mE_h. For the other basis sets the minimal active space is also the consistent active space.

6.1.1 Source of NPE in TCCSD

The NPE of the TCCSD is $\approx$6 mE_h which is larger than the error between CCSD and CCSDT at equilibrium. There are two sources of error in the TCCSD method: 1) the error that comes from the lack of coupling between the active and inactive space in the FCI calculation; 2) the error that comes from the full space CCSD calculation which, based on the error around equilibrium, should be $\approx$2 mE_h.

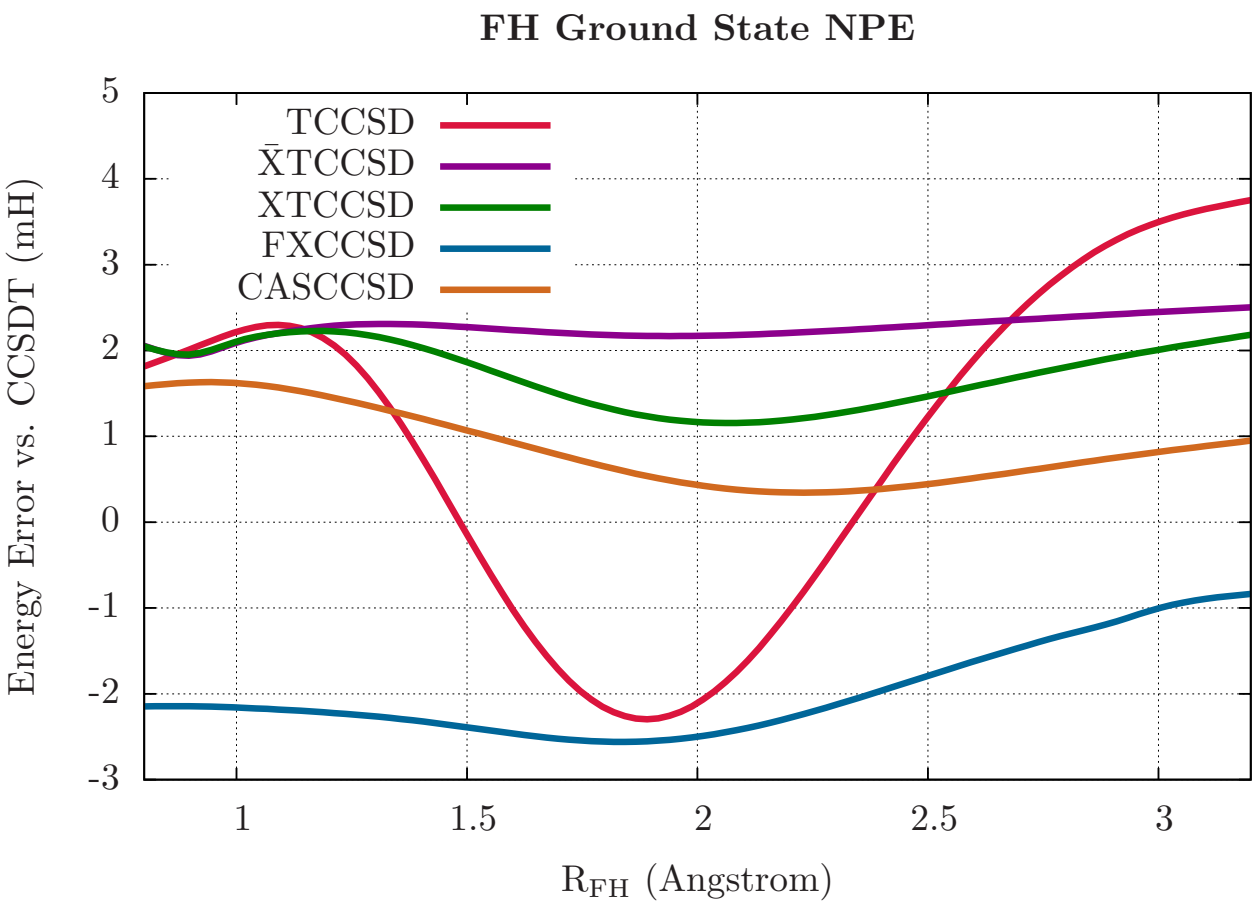

Figure 6-2. Dissociative PES energy error with respect to CCSDT of FH from 0.917 Å to 3.20 Å computed with TCCSD, X̄TCCSD, XTCCSD, FXTCCSD and CASCCSD. Basis set is cc-pVDZ.

In order to address the first issue, we compare the $t_1\{\sigma,\sigma^*\}$, and $t_2\{\sigma,\sigma^*\}$ from the [2,2]FCI calculation to the $t_1\{\sigma,\sigma^*\}$, and $t_2\{\sigma,\sigma^*\}$ from the CCSDT in Figure 6-4. There is a large deviation between the t-amplitudes from the full CCSDT calculation and that of the [2,2]FCI calculation which suggests that there are regions on the PES where the coupling between the σ, σ^* orbitals and the other orbitals is significant. To verify that this is the cause for the NPE, we extract the $t_1\{\sigma,\sigma^*\}$, and $t_2\{\sigma,\sigma^*\}$ from the CCSDT calculation and follow with the restricted full space CCSD calculation (the second step of the TCCSD calculation). The NPE curves obtained with X̄TCCSD are included in Figures 6-2 and 6-3.

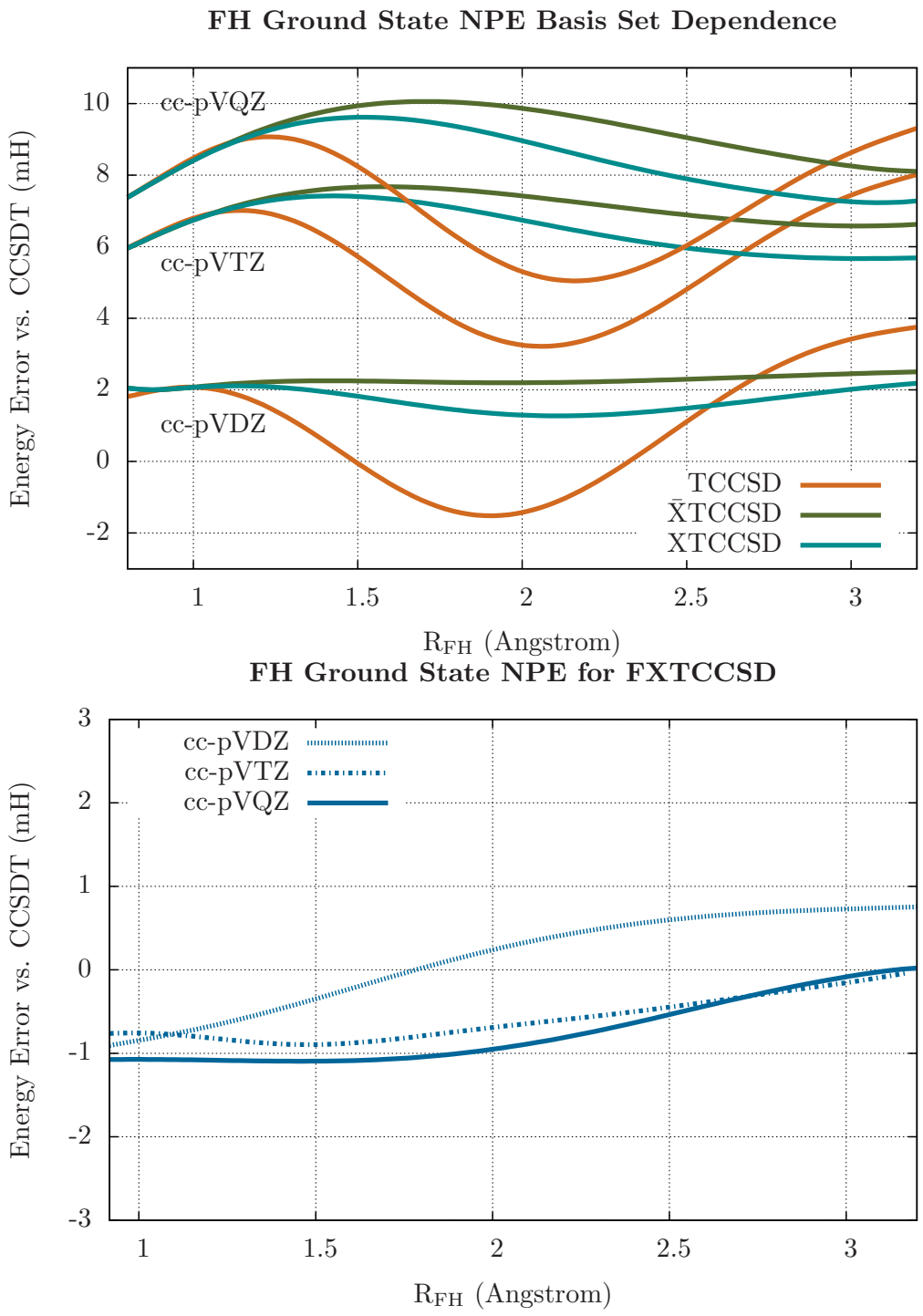

Figure 6-3. Dissociative PES energy error with respect to CCSDT of FH from 0.80 Å to 3.20 Å computed with TCCSD, $\bar{X}$TCCSD, XTCCSD and FXTCCSD. Basis sets are cc-pVXZ(X=2,3,4).

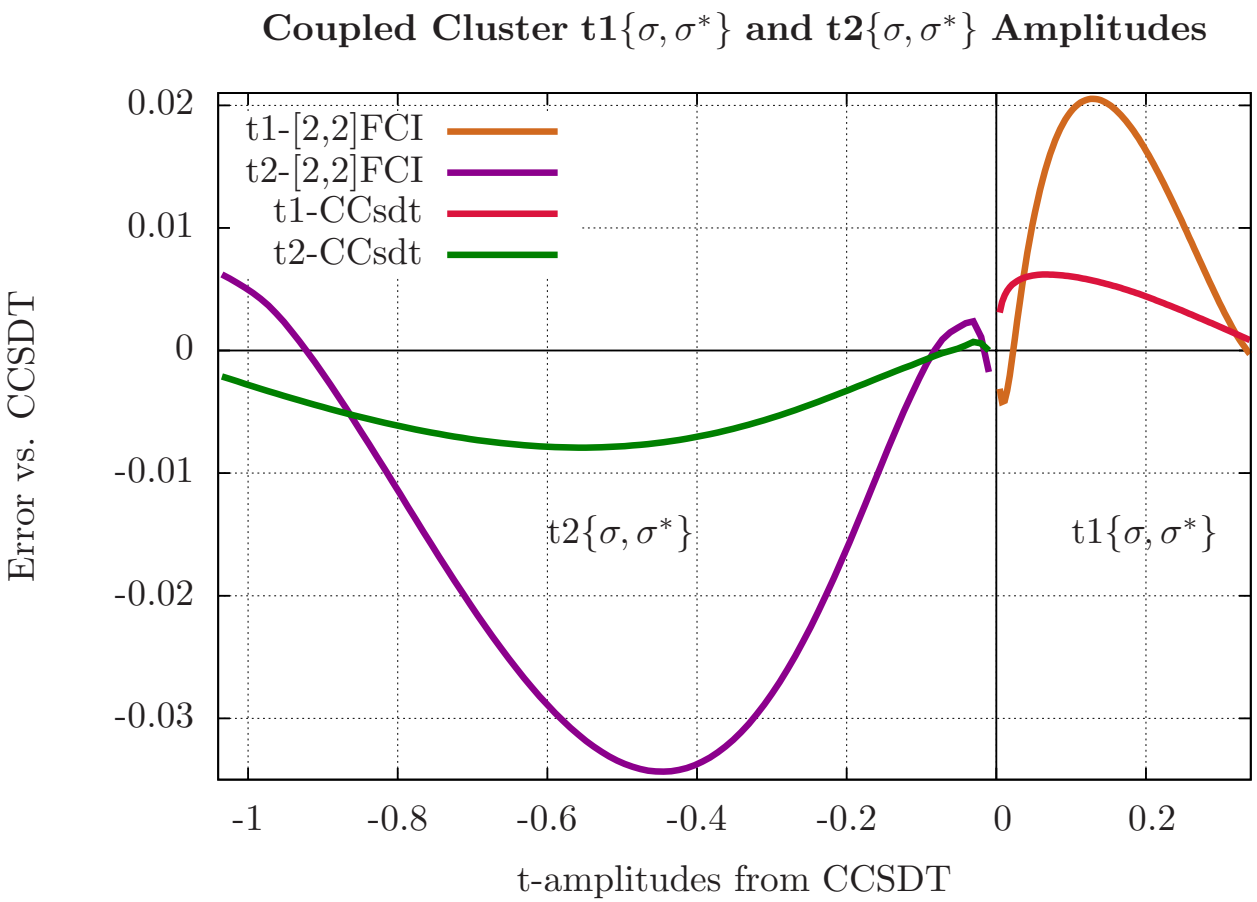

Figure 6-4. Amplitudes from the dissociative PES calculations of FH from 0.917 Å to 3.20 Å. The error between [2,2]FCI amplitudes, CCsdt amplitudes and CCSDT amplitudes are plotted vs the CCSDT amplitude values. Basis set is cc-pVDZ.

The $\bar{X}$TCCSD method has significantly reduced the NPE and the majority of the remaining error ($\approx$2 mE_h) is associated with CCSD. Unfortunately, this is not a very cost-effective approach. It is clear that in order to reduce the NPE, some correlation between the [2,2] space and the extended space must be allowed to occur but not all of that space need be required. For this reason an extended active space is introduced. It must be small enough to allow a timely execution of the CCSDT calculation but large enough to capture the correlation of the orbitals which participate in the σ-bond. The method which thus reduces the NPE *via* the extended active space is XTCCSD.

In order to determine the influence of basis set choice on NPE, the PES for FH dissociation is also computed with a cc-pVTZ, cc-pVQZ, and cc-pV5Z basis sets. The same trend as shown in Figure 6-4 is observed across each basis set. Looking at the NPE across the basis sets in Figure 6-3 and Table 6.1 we see a difference in trend between the TCCSD method (at the high extreme of de-coupling) and the $\bar{X}$TCCSD method (at the low extreme of de-coupling) with the NPE character of the XTCCSD method much closer to that of $\bar{X}$TCCSD than to CCSD.

6.1.2 FXTCCSD

While XTCCSD has done a good job of reducing NPE and obtaining the experimental D_e values, there can be benefits to keeping the entire extended space and not just the orbitals associated with the [2,2] problem. The first reason is to lower the absolute error between XTCCSD and CCSDT which is mainly due to the error between CCSD and CCSDT. The second reason is to treat a few other less important determinants at a higher level of theory because it may not always be obvious which determinants make up the MR problem. The NPE curves obtained with FXTCCSD are included in Figures 6-2 and 6-3.

The main drawback of the FXTCCSD method is that it is more sensitive to the active space choice than the XTCCSD method. The maximum error in XTCCSD due to active space choice can be estimated by simply looking at the difference between it and the reference $\bar{X}$TCCSD method which uses the entire space. The effects are minor since only two amplitudes are affected. In FXTCCSD the external space amplitudes relax *via* CCSD with respect to the whole extended active space amplitudes and small effects on the energy (not the main MR effect) are compounded.

6.1.3 Active space choice

The ASDA as described in the Methods section is used to perform statistical analysis on the reference orbital energies to determine the bounds of the active space.

Since FH has so few electrons, only the one core orbital is dropped from the occupied space and ASDA works on the virtual space.

Figure 6-5 shows the results for a few points along the PES. In an effort to deal with multimodal distributions, the energy gap threshold is incrementally increased, until all points belonging to the mode with the largest energy gaps are isolated. This progression can be seen in the kernel density plots of $ln(R(n))$ as the data set goes from including all energy differences (pink) to including only the large energy differences (green). When the program determines that the distribution is unimodal (by any standard modality test such as Hartigan's dip test), it stops increasing the threshold. Another approach is to estimate the number of modes, use a multi-modal distribution curve-fitting procedure such as the mixtools R package, and only use the results from the mode with the lowest mean. Either approach yields the cutoffs employed in this study and though some small variation may be possible, none have yet been seen. The former approach is used in this study as it is more in agreement with the philosophy of minimizing user intervention.

The QQ plots in Figure 6-5 show that the distribution is very close to being normal and one can even see the different modes by looking at the clustering of the data along the 1,1 diagonal. The outliers at the higher values of the QQ plots show a few orbitals nearly degenerate to each other with an energy difference slightly greater than 0.1 mE_h which is the first threshold used to discard degenerate orbitals.

A typical output from ASDA produces a list of candidate orbitals like so:

```
++++++++
Possible Cutoff Orbitals at rFH= 1.30
Cutoff: 0.622599112125938
31 49 60 61 72 73
0.7435471 0.7033709 0.9927676 2.240253 0.9165902 1.311481
++++++++
Possible Cutoff Orbitals at rFH= 1.40
```

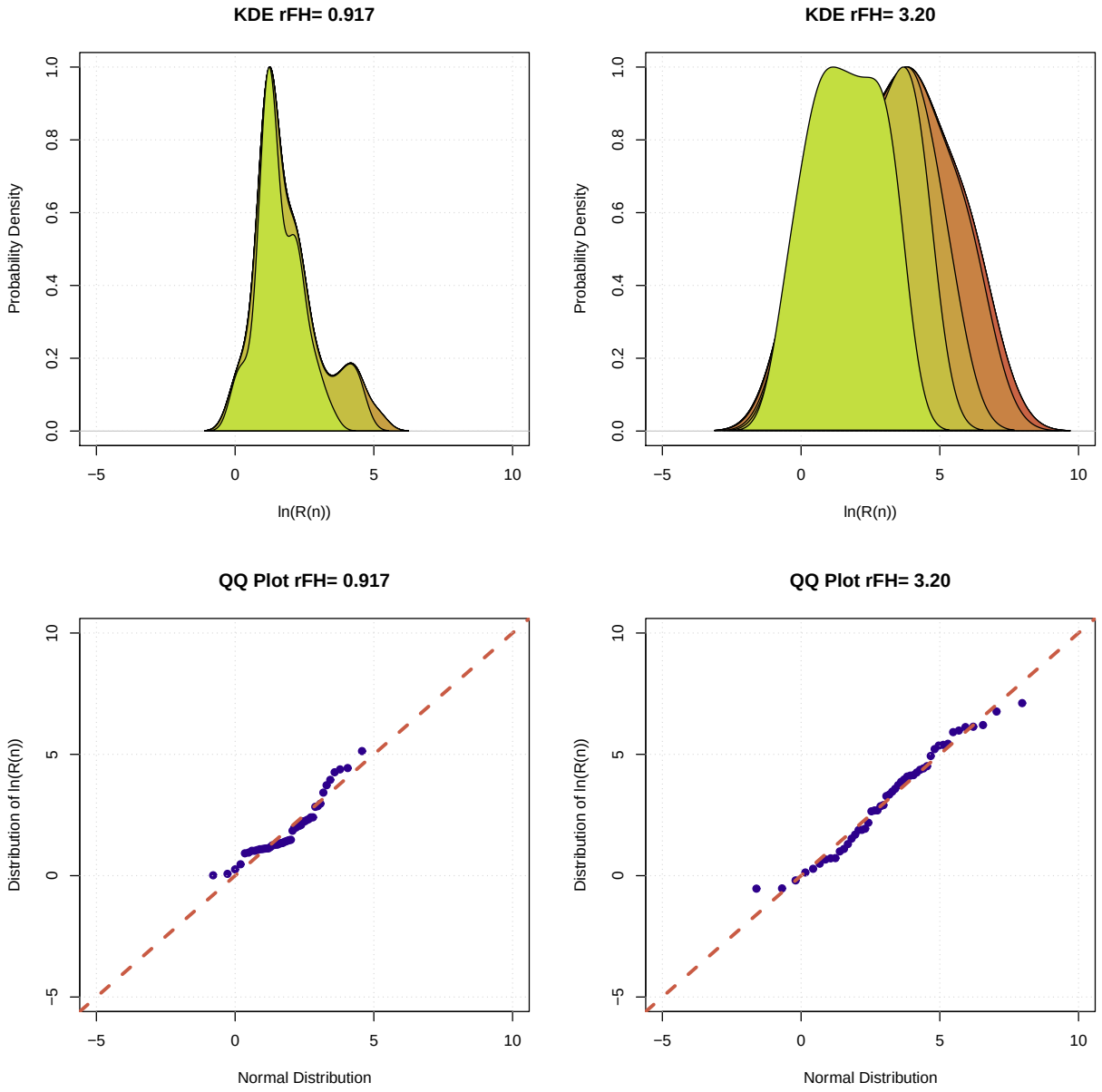

Figure 6-5. Graphical output from ASDA is shown for the equilibrium and dissociation limit geometries of FH at cc-pVQZ basis. The KDE plot of $ln(R(n))$ is plotted for data which includes all energy differences (pink) and progresses toward the data set which includes only the large energy differences (green). The QQ plots show that the probability distribution of $ln(R(n))$ is normal.

```
Cutoff: 0.681974319543561
31 49 61 72 73
0.7040421 0.7261902 2.76404 0.8659455 1.416099
+++++++++
```

This output shows that the lowest possible cutoff happens at orbital 31. It also shows that the cutoff threshold has increased from 0.6226 H to 0.6820 H going from 1.30 Å to 1.40 Å points on the PES. The last line is the set of energy differences between the orbital listed and its predecessor so it becomes apparent that while orbitals 31, 49, and 60 (at 1.30 Å) are slightly larger than the cutoff threshold; orbital 61 has a much larger gap. If the user wants to intervene and pick orbital 61 as the cutoff provided the computational cost is manageable, he or she can do so at this time.

The distribution patterns do not change much for the series of cc-pVXZ basis sets so the results shown here for the cc-pVQZ are typical. However, past the cc-pVTZ basis set there begins to be a difference between the minimal active space cutoff and a cutoff that is consistent with the entire PES. Generally, this is dominated by the difference of cutoffs at equilibrium and at the dissociation limit as shown in the FH cc-pV5Z example:

```
++++++++
Possible Cutoff Orbitals at rFH= 0.917
Average: 1.47006758809646
Cutoff: 0.701681769183348
60 68 83 104 107 108 114 118 121 124 125 138 142 145
0.9844741 0.7715318 0.9273001 0.7234571 0.8695963
1.001046 0.7500163 1.077662 0.8322482 0.868769 0.7360771
2.498539 1.192338 1.434257
++++++++
Possible Cutoff Orbitals at rFH= 3.20
Average: 0.53723213211244
```

```
Cutoff: 1.71685675760544
108 111 125 141
2.905959 2.110185 4.525748 3.324365
+++++++++
```

Here, the minimal cutoff would be 60 at equilibrium and 108 at dissociation which leads to a 0.55 mE_h error with CCSDT for D_e. An intersection cutoff would require that both calculations be performed with 108 for cutoff leading to an error of 0.71 mE_h; a marginal difference. These are summarized in Table 6.1.3. It is clear from this table that there is no great benefit for the calculation of D_e to use a consistent active space for the FH example. The NPE is a bit larger for the minimal active space choices mainly due to the difficult middle portion of the PES where a lot of surface crossings begin to happen and solutions may become unstable. However, for the two extremities, the relative error to CCSDT is about the same in both cases of active space selection.

The reduced active space fraction of the total space generally becomes smaller as the basis set becomes larger. Because of this, larger differences in computation time are observed as the basis set size increases between the CCSDT calculation and the Tailored-CC methods. Table 6.1.3 summarizes the reduction in orbital space as well as the subsequent speed-up of the calculation compared to the equivalent CCSDT calculation.

The XTCCSD method is not nearly as sensitive to the active space choice so the minimum possible extended space is always used. The timings of the XTCCSD are in the same range as the ones for FXTCCSD. The TCCSD method has a speedup of about 50x compared to CCSDT for the cc-pVQZ and cc-pV5Z basis which reduces to 8x for the cc-pVTZ basis.

6.2 Fluorine molecule

F_2 is chosen because the UHF solution is not bound and the RHF solution is only bound due to its incorrect separation. Therefore it provides a test of a single bond

Table 6-3. Orbital space and performance for hydrogen fluoride.

cc-pVXZ[a]	$[e,o]^{FS}$	$[e,o]^{AS}$	% Reduced	Speedup	Abs. Err.[c]	D_e Err.[c]
D	[10,19]	[8,12]	37	–[b]	0.91	1.66
T	[10,44]	[8,29]	34	5x	0.76	0.74
Q$^{\cap}$	[10,85]	[8,58]	32	18x	1.07	1.09
Q	[10,85]	[8,47]	45	45x	1.09	1.08
5$^{\cap}$	[10,146]	[8,106]	27	7x	1.28	0.71
5	[10,146]	[8,58]	60	24x	1.16	0.55

[a] The $\cap$ superscript stands for results obtained with the lowest common cutoff; [b] The calculation used for the speed benchmark is the energy computation at equilibrium geometry;
[c] With respect to the CCSDT reference values in mE_h units.

dissociation potential energy surface (PES)[21, 40, 60, 88, 91, 126, 135, 138], and is more difficult to compute with larger basis sets. There is also a very large error in the dissociation energy for CCSD with the RHF reference being notoriously bad. Again, most of the available calculations are done with very small basis sets with the exception of Bytautas *et al.*[21] and Evangelista *et al.*.[39] who have done a CBS extrapolation for the F_2 PES. The experimental value for the dissociation energy of F_2 is well established[62, 162].

The ground state dissociation PES of F_2 is a notoriously difficult problem for single reference coupled cluster methods. The CCSD error in the dissociation energy is about the same magnitude as the actual dissociation energy. Even the dissociation energy of the CCSDT is known to be a few mE_h higher than the FCI depending on which basis set is used.

In TCCSD, the majority of the amplitudes (other than the [2,2] dominant ones) are calculated at the CCSD level but despite that fact, the Tailored-CC absolute energy values are closer to the CCSDT values than the CCSD values along the PES. Furthermore, the relative energy (D_e) of the extended Tailored methods are in excellent agreement with the CCSDT values.

Table 6-4. Dissociation energy for molecular fluorine. Energies are reported in mE_h units.

	cc-pVDZ	cc-pVTZ	cc-pVQZ	cc-pV5Z
CCSD	84.07	110.14	119.90	119.87
CCSDT	43.43	57.84	61.00	62.42
TCCSD	54.02	67.36	69.48	69.33
XTCCSD	45.98	59.91	62.67	63.88
FXTCCSD	44.32	58.15	60.84	62.23
experimental values		62.56[a]	62.13[b]	

[a] From REf. [21, 162]; [b] From Huber and Hertzberg[62] minus atomic spin-orbit coupling of -1.22705 mE_h and relativistic effect of -0.031871 mE_h[42]

Table 6-4 shows the calculated dissociation energy of F_2 for all basis sets including the CBS values. As the basis set increases, the D_e from the CCSD calculation remains about twice as large as the D_e from the Tailored-CC methods and CCSDT. The TCCSD overshoots the experimental results by about $\approx$7 mE_h but with the addition of active space extension, that error goes down to $\approx$2 mE_h. Based on the conclusion of Bytautas *et al.*. and Evangelista, there should be a small ($\approx$2 mE_h) error in the dissociation of F_2 when treated with CCSDT due to the very strong multi-reference character of this problem that can be ameliorated by the addition of quadruples, pentuples, etc. In the CBS limit in Table 6-4 the CCSDT calculation is in very good agreement with experimental values once the spin-orbit coupling has been subtracted from the experimental values. There is some room for improvement over CCSDT for the potential energy curve in the middle range (2.20 Å to 3.00 Å) where there is still an unphysical $\approx$1 mE_h bump, which is indicative of the multi-reference aspects in the F_2 PES.

The errors between the various methods are more apparent in the F_2 example than in the FH example due to a stronger multi-reference character a and larger number of basis functions. These errors are apparent in the wrong energy of CCSD as well as in the struggling TCCSD. In order to determine the influence of basis set, the NPE

Table 6-5. NPE for molecular fluorine. Energies are reported in mE_h units.

	cc-pVDZ	cc-pVTZ
TCCSD	12.5	12.6
$\bar{X}$TCCSD	3.5	3.8
XTCCSD	2.7	2.6
FXTCCSD	1.3	0.5

with respect to CCSDT is plotted for the two basis sets where it is practical to compute the CCSDT PES: cc-pVDZ and cc-pVTZ as shown in Figure 6-6 and in Table 6-5. The basis-dependent trend of the NPE for the molecular fluorine case is observed to be similar to that of the hydrogen fluoride case. However, all of the errors are amplified: NPE as well as the absolute error. The NPE for the FXTCCSD method is remarkably small.

The active space selection for F_2 is done in the same fashion as for the FH example. The kernel density plots in Figure 6-7 show that there are already two well defined modes at 2.0 Å which can be attributed to the changing of orbitals from molecular to atomic character. It is easier seen in this example than in the previous one because there is only one type of atom present here. These two modes persist all the way through complete dissociation at 8.0 Å. As before, in the case of multiple modes, only the mode which contains the distribution of the larger energy gaps is used to determine the cutoff. The distribution of $ln(R(n))$ is normal according to the QQ plots (not shown in the interest of space).

The reduced active space fraction of the total space is more favorable for F_2 than FH due having larger atoms involved. Because of this, some of the speedup values in Table 6-6 reach two orders of magnitude. Starting with the cc-pVQZ basis set the minimum extended active space choice and an intersection extended active space choice diverges; for the equilibrium geometry in particular. The dissociation point tends to have the larger cutoff values just as in the FH example.

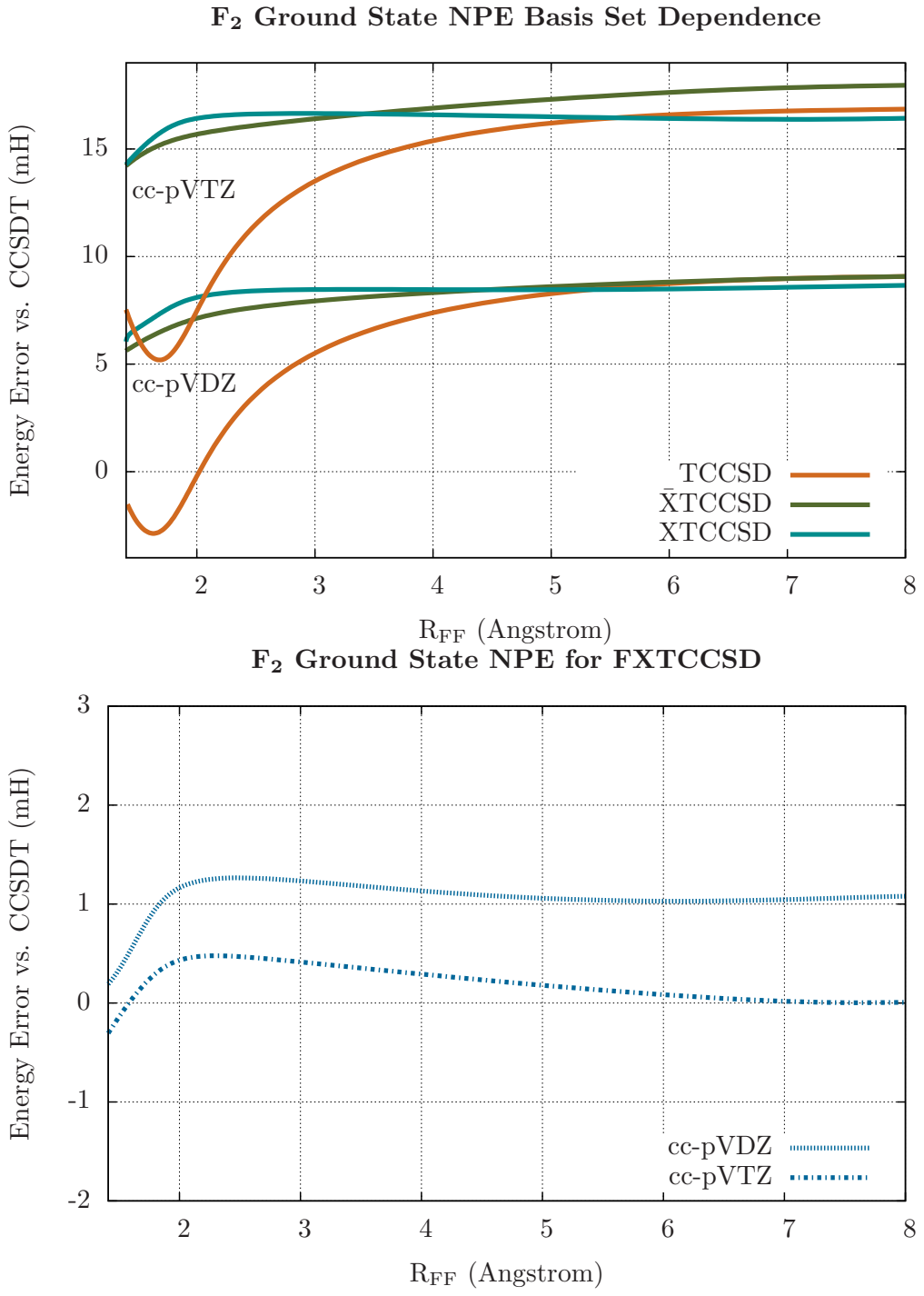

Figure 6-6. Dissociative PES energy error with respect to CCSDT of F_2 from 1.40 Å to 8.00 Å computed with TCCSD, $\bar{X}$TCCSD, and XTCCSD. Basis sets are cc-pVXZ(X=2,3).

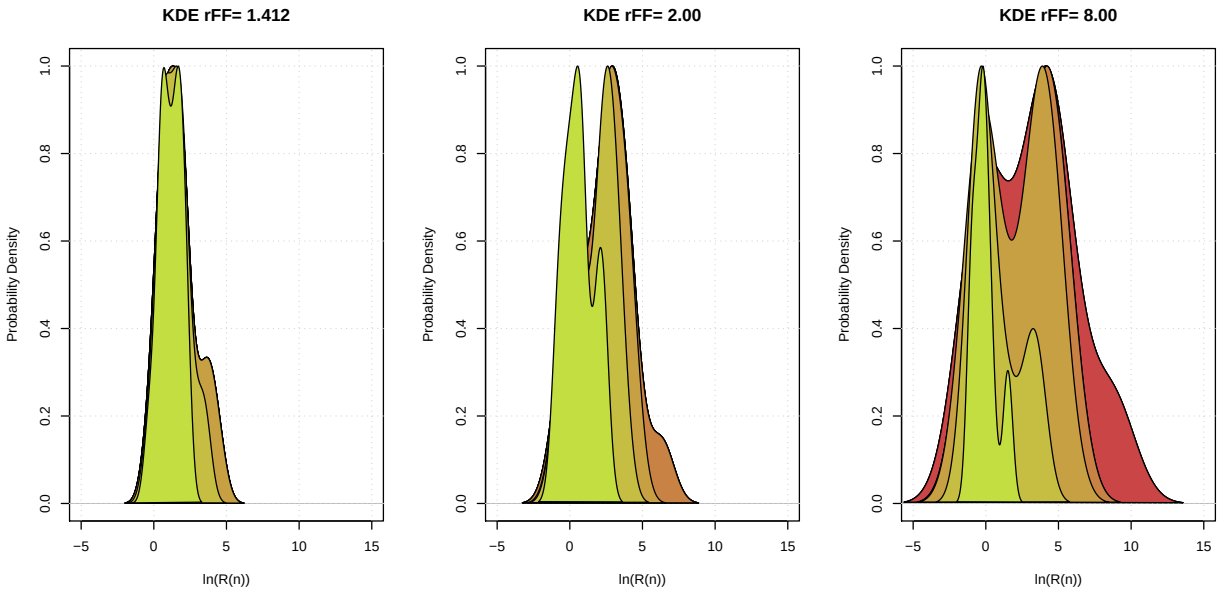

Figure 6-7. Graphical output from ASDA is shown for the equilibrium, 2.0 Å, and dissociation limit geometries of F_2 at cc-pVTZ basis. The KDE plot of $ln(R(n))$ is plotted for data which includes all energy differences (pink) and progresses toward the data set which includes only the large energy differences (green).

Table 6-6. Orbital space and performance for molecular fluorine.

cc-pVXZ[a]	[e,o]^{FS}	[e,o]^{AS}	% Reduced	Speedup[b]	Abs. Err.[c]	D_e Err.[c]
D	[18,28]	[14,16]	43	5x	0.89	0.19
T	[18,60]	[14,32]	47	25x	0.31	0.31
Q$^{\cap}$	[18,110]	[14,58]	47	62x	1.95	0.16
Q	[18,110]	[14,31]	72	314x	0.05	2.17
5$^{\cap}$	[18,182]	[14,101]	45	24x	2.50	0.18
5	[18,182]	[14,57]	69	511x	2.49	0.20

[a] The $\cap$ superscript stands for results obtained with the lowest common cutoff; [b] The calculation used for the speed benchmark is the energy computation at equilibrium geometry;
[c] With respect to the CCSDT reference values in mE_h units.

The results in Table 6-6 are fairly consistent with the exception of the cc-pVQZ basis where the energy at the dissociation limit is off from the CCSDT value by 2.11 mE_h and, strangely, the equilibrium energy is closer to the CCSDT with a smaller extended active space (0.05 mE_h) than with the larger extended active space (1.95 mE_h). This behavior leads to the D_e being significantly better for the latter calculation but only because both points are in ≈ 2 mE_h error compared to the reference. There is nothing out of the ordinary observed in the convergence or the amplitudes in the cc-pVQZ calculation. This is the only occurrence thus far of a failure to get within a mE_h of the reference D_e for no apparent reason.

The XTCCSD is much less sensitive to the choice of the extended active space since only a small portion of it ($t_1\{\sigma,\sigma^*\}$, and $t_2\{\sigma,\sigma^*\}$) is saved. For that reason, it will always use the minimal space provided by the ASDA and will have the fastest possible execution times. The TCCSD method is about 500x faster than CCSDT with a cc-pV5Z basis but at the expense of accuracy: 14.08 mE_h absolute error and 6.91 mE_h D_e error from the CCSDT reference.

6.3 Ethylene

6.3.1 Background

The ethylene twist is a somewhat different type of bond breaking since only the π-bond is broken while the σ-bond remains intact. Single reference methods tend to produce a cusp in the PES at the 90° angle while multi-reference methods show a transition state with a stationary point. The twisted ethylene singlet has become a popular example for electronic structure methods which concern themselves with describing non-dynamic correlation. Something as simple as introducing a second determinant into a Hartree-Fock calculation will produce reasonable PES and torsional barrier height provided the basis set is large enough[146, 160]. Small basis set calculations have been performed with Spin-Flip methods[77], VOO-CCSD[78], various multi-reference methods in Hoffmann et al.[61], multi-reference Fock space[115],

and Equation-of-Motion formalism[116]. Larger basis set calculations which should produce experimental results have been performed with CASPT2 by Molina *et al.*[109], with multi-reference perturbation theory[159], and with state-specific multi-reference perturbation theory[102]. Not all of the calculations above relax the bond-lengths and angles along the PES which does not produce highly accurate values for the barrier height[50]. In fact, many experimental publications on ethylene state that the changes bond lengths and angles are important in determining an accurate barrier height[18, 35, 107, 155].

The challenge of computing large-basis energy values for the ethylene barrier of rotation are twofold. First, the number of basis functions grows quickly due to its size. Second, the geometry of the CCH angle and the CC and CH bonds need to be relaxed which puts further time pressure in obtaining high-level correlated results with large basis sets. Since non-iterative corrections (such as CCSD(T)) do not produce the correct PES behavior at the twisted geometry, some type of inexpensive active space method is desirable. There were several methods proposed in the recent literature which obtain correct PES behavior with small basis sets, however their performance with large basis sets remain untested.

The TCCSD method faces a particular challenge with ethylene (as it will with most polyatomic molecules). Since only the [2,2] determinant is solved in the first step, any coupling between the electrons belonging to this determinant and the rest of the space are excluded. Normally, for single bond breaking of a diatomic, it can be assumed that this coupling is negligible due to the relatively small overlaps of the orbitals. In polyatomic structures with less symmetry, there is more prevalent orbital overlap and stronger correlation coupling between the electrons in the bond being broken and other electrons in the system.

6.3.2 Results

Twisted ethylene presents a challenge for single reference theory due to the bi-radical nature acquired by the carbon-carbon bond at the transition state. Also, the density of excited states at that point makes it difficult for all of the methods employed in this study to converge to the ground state solution. It is possible that these features of the transition state also translate into the physical realm since the experimental measurements of the barrier of rotation of ethylene in the ground state are not in agreement with each other (see the values and references in Table 6.3.2).

In order to obtain the correct energy for the barrier of rotation, r_{CC}, r_{CH}, and $\angle_{HCH}$ coordinates are optimized as the dihedral angle changes from 0 degrees to 90 degrees. The geometry optimization is done with each method and basis set where possible and the results are summarized in Table 6-7. The experimental geometry at the equilibrium is: $r_{CC} = 1.339$, $r_{CH} = 1.086$, $\angle_{HCH} = 117.6^{\circ}$ [57].

The average errors calculated in Table 6-7 is done with respect to the CCSDT calculation in that basis set in the units of $1000\times$a.u. such that the scale of geometry comparison is on the same scale as mE_h is for energies. While the CCSD(T) method provides the expected precision to CCSDT at equilibrium, it clearly deviates at the twisted geometry. CCSD performs as expected. The TCCSD method systematically provides geometries which are slightly closer to the CCSDT than those from the XTCCSD method but the difference between the two methods is small enough that it could fall within statistical error. The FXTCCSD geometries have the smallest errors with the CCSDT geometries across the board.

It is prohibitively time consuming to obtain the CCSDT geometries with the cc-pVQZ basis set in the serial ACES II program. It is estimated that each geometry optimization

would require approximately 75 days[1] At the equilibrium geometry, the expectation is that the CCSD(T) geometry is virtually as good as the CCSDT geometry so that offers a comparison. In the case of the twisted geometry the active space methods described here are considered predictive of what the true CCSDT values would have been.

There appears to be a lack of agreement in the literature as to the value of the rotational barrier of ethylene (Table 6.3.2). Based on the analysis accomplished thus far, the most definitive value for the rotation barrier would be using the FXTCCSD/cc-pVQZ geometry and energy: 110.05 mE_h. In order to determine if this value is at the basis set limit, a single point FXTCCSD energy calculation is performed using the FXTCCSD/cc-pVQZ geometries with cc-pV5Z basis set. Equations 6–4 and 6–3 are used to estimate the CBS value: 110.26 mE_h which means that in all likelihood the orbital space has been exhausted.

The theoretical value for the rotation barrier is 10 to 20 mE_h higher than the experimental values listed in Table 6.3.2. These values are estimated from vibrational spectroscopy experiments and we suggest a gas phase NMR experiment be done. The challenge with the NMR experiment is that one would need a probe of 800 °C to reach the needed kinetic range and the hottest current probes go no higher than 550 °C[2] .

The experimental geometry at the equilibrium is: $r_{CC} = 1.339$, $r_{CH} = 1.086$, $\angle_{HCH} = 117.6°$ [57].

[1] 30 hours per CCSDT single point; 6 points per geometry step; estimated 10 geometry steps for convergence

[2] personal communication with Dr. Alex Marchione at DuPont Central Research and Development

Table 6-7. Optimized geometry of ethylene. Distances are in Å and angles are in degrees. Units of error are 1000×a.u.

		cc-pVDZ		cc-pVTZ		cc-pVQZ	
		$\measuredangle_{HCCH} = 0°$	$\measuredangle_{HCCH} = 90°$	$\measuredangle_{HCCH} = 0°$	$\measuredangle_{HCCH} = 90°$	$\measuredangle_{HCCH} = 0°$	$\measuredangle_{HCCH} = 90°$
CCSDT	r_{CC}	1.3509	1.4687	1.3329	1.4513	NA.	NA.
	r_{CH}	1.0975	1.1028	1.0788	1.0826	NA.	NA.
	$\angle_{HCH}$	117.00	116.58	117.18	116.76	NA.	NA.
CCSD(T)	r_{CC}	1.3507	1.4955	1.3330	1.4749	1.3308	1.4667
	r_{CH}	1.0975	1.1002	1.0787	1.0806	1.0797	1.0821
	$\angle_{HCH}$	117.02	117.68	117.20	117.66	117.10	117.30
	Avg. Err.	0.15	11.59	0.15	9.76	NA.	NA.
CCSD	r_{CC}	1.3454	1.4549	1.3271	1.4347	1.3329	1.4274
	r_{CH}	1.0961	1.1020	1.0771	1.0826	1.0788	1.0839
	$\angle_{HCH}$	116.92	116.10	117.08	116.04	117.18	115.84
	Avg. Err.	1.68	5.37	1.90	7.10	NA.	NA.
TCCSD	r_{CC}	1.3511	1.4654	1.3324	1.4503	1.3248	1.4488
	r_{CH}	1.0975	1.1015	1.0770	1.0812	1.0778	1.0822
	$\angle_{HCH}$	117.00	116.58	117.20	116.90	117.00	116.70
	Avg. Err.	0.45	0.81	0.52	1.24	NA.	NA.
XTCCSD	r_{CC}	1.3474	1.4612	1.3293	1.4448	1.3249	1.4413
	r_{CH}	1.0960	1.1016	1.0771	1.0813	1.0780	1.0828
	$\angle_{HCH}$	116.94	116.32	117.08	116.50	116.98	116.38
	Avg. Err.	1.23	3.05	1.52	2.89	NA.	NA.
FXTCCSD	r_{CC}	1.3493	1.4612	1.3312	1.4500	1.3289	1.4454
	r_{CH}	1.0973	1.1027	1.0793	1.0835	1.0808	1.0859
	$\angle_{HCH}$	116.96	116.55	117.16	116.74	117.10	116.56
	Avg. Err.	0.55	0.28	0.51	0.51	NA.	NA.

Table 6-8. Barrier of rotation for ethylene. Energies are reported in mE_h units.

	cc-pVDZ	cc-pVTZ	cc-pVQZ
CCSD	130.78	137.53	136.81
CCSD(T)	107.66	116.38	118.42
CCSDT	103.94	109.24	NA.
TCCSD	110.97	116.09	114.04
XTCCSD	104.81	109.38	109.24
FXTCCSD	105.00	108.74	110.05
experimental values	103[a]	95.3[b]	90.8[c]
theoretical values	100.7[d]	91.9[e]	108.2[f] 104.8[f]

[a] From Ref. [35]; [b] From Ref. [155];
[c] From Ref. [18]; [d] From Ref. [160];
[e] From Ref. [109]; [f] From Ref. [159].

6.4 Bicyclo[1,1,0]butane

6.4.1 Background

The isomerization of bicyclo[1,1,0]butane to *trans*-buta-1,3-diene has been experimentally shown to proceed through a conrotary transition state [145]. There is also a forbidden pathway to *trans*-buta-1,3-diene through a high-energy biradical disrotary transition state [70, 96, 118]. Both transition states are shown in Figure 6-8.

Recently, Kinal and Piecuch published the activation barrier energies for both pathways using a CASSCF(10,10)/cc-pVDZ geometries[70] followed by a variety of multi-reference methods for the computation of the energy gap[96]. The zero-point energies (ZPE) and the geometries was determined with CASSCF(10,10)/cc-pVDZ in all calculations in the latter paper. The isomerization pathway of bicyclo[1,1,0]butane has since then been examined with two-electron reduced density matrix (2-RDM) by Mazziotti[106] and with optimal multireference-diffusion Monte Carlo (OMR-DMC) by Berner and Lüchow[15].

Only the conrotary pathway activation barrier and the geometry of bicyclo[1,1,0]butane are is experimentally known. While it appears to be possible to obtain a correct geometry and barrier energy of the conrotary pathway with single reference methods[15,

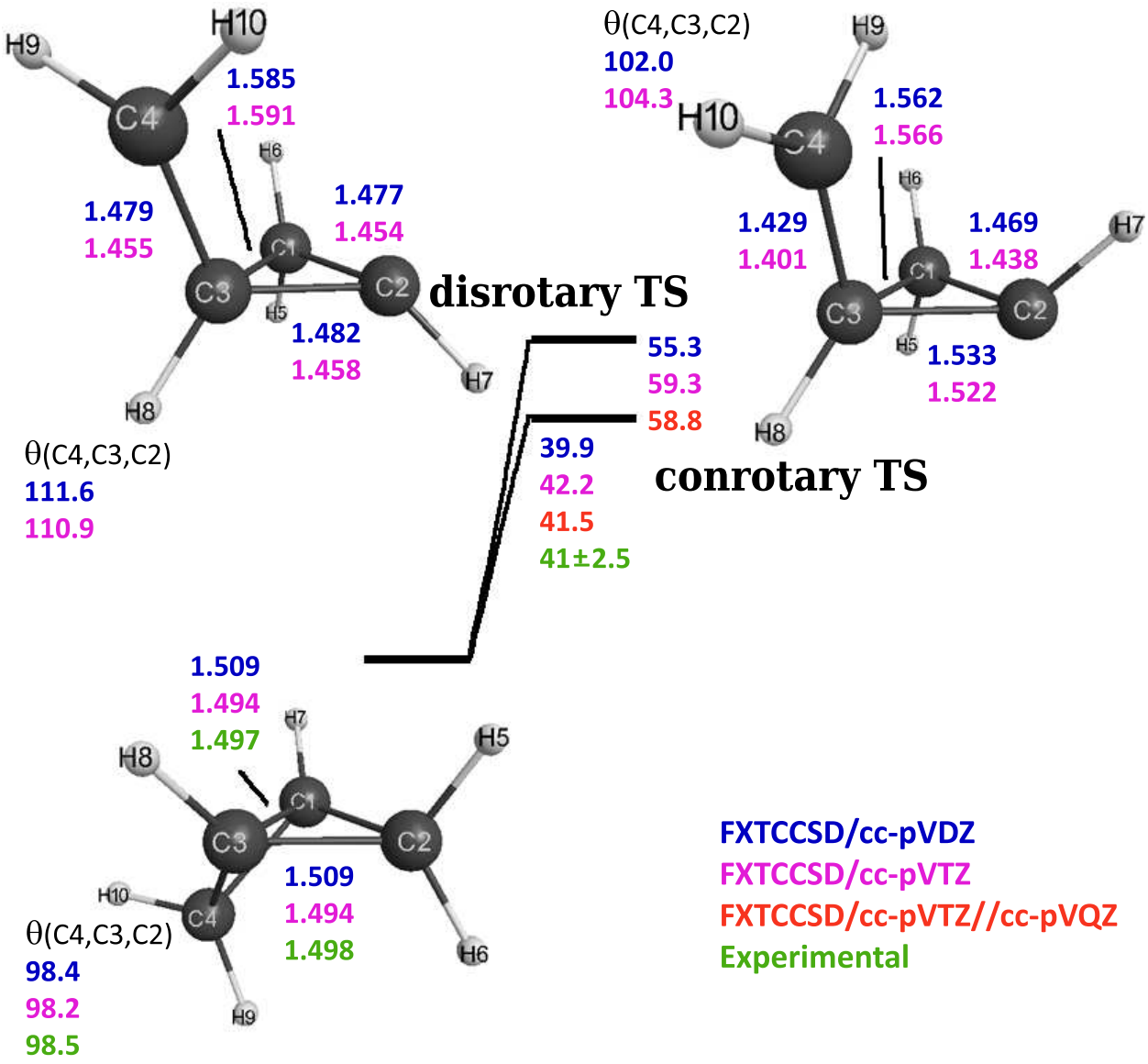

Figure 6-8. Select geometry parameters of isomerization of bicyclo[1,1,0]butane and the transition states. The bond lengths are in Angstroms and energies are in kcal/mol.

96] due to only a small multi-reference character of the corresponding transition state, the disrotary transition state appear to require a muti-referece treatment to correctly predict its geometry and energy[15].

Based on the geometry results from the ethylene study, we propose that the FXTCCSD optimized geometry with the largest possible basis set will provide an excellent geometry and energy for the disrotary transition state.

6.4.2 Results

The geometries of bicyclo[1,1,0]butane, conrotary TS and disrotary TS are optimized using the FXTCCSD method with cc-pVDZ and cc-pVTZ basis sets. The orbital space partitioning is done in accordance with the ASDA described previously. Vibrational frequencies and the ZPE are calculated with cc-pVDZ basis set but not higher due to computational time constraints[3] . A single point calculation is done with cc-pVQZ basis set at each cc-pVTZ geometry for a better total energy.

In the cc-pVDZ basis set the full space of 15 occupied and 71 virtual orbitals is reduced to 11 occupied and 30 virtual active space orbitals. In the cc-pVTZ basis set the full space of 15 occupied and 189 virtual orbitals is reduced to 11 occupied and 35 virtual active space orbitals. In the cc-pVQZ basis set the full space of 15 occupied and 385 virtual orbitals is reduced to 11 occupied and 68 virtual active space orbitals. These orbital spaces are generated automatically by the ASDA. The drastic reduction in the virtual space creates the possibility that a CCSDT-quality result, unobtainable without access to a large HPC cluster, may be acquired in a matter of days on a modern laptop computer.

The geometry where the experimental values are available [30] is in excellent agreement with the cc-pVTZ values and we assume that the transition state geometries

[3] 600 single point calculations needed for a Hessian with approximately 2 hours per point would take about 50 days

Table 6-9. Select bond lengths of bicyclo[1,1,0]butane isomers. The carbon-carbon bond lengths of bicyclo[1,1,0]butane and conrotary and disrotary transition states are listed in Å.

		FXTCCSD/ cc-pVDZ	FXTCCSD/ cc-pVTZ	CASSCF(10,10)/[a] cc-pVDZ	Experiment[b]
bicyclo[1,1,0]butane	$C_4 C_3$	1.509	1.494	1.522	1.498
	$C_1 C_3$	1.509	1.494	1.528	1.497
conrotary TS	$C_4 C_3$	1.429	1.401	1.455	NA.
	$C_3 C_2$	1.533	1.522	1.527	NA.
	$C_1 C_3$	1.562	1.566	1.563	NA.
	$C_1 C_2$	1.469	1.438	1.497	NA.
disrotary TS	$C_4 C_3$	1.479	1.455	1.511	NA.
	$C_3 C_2$	1.482	1.458	1.511	NA.
	$C_1 C_3$	1.585	1.591	1.561	NA.
	$C_1 C_2$	1.477	1.454	1.504	NA.

[a] The CASSCF(10,10)/cc-pVDZ values are from [70].
[b] The experimental values are from [30].

are of a similar quality. Select geometry parameters are shown in Figure 6-8 and in Table 6.4.2.

Based on the results presented in Table 6.4.2, the CASSCF(10,10) tends toward overestimating the carbon bond lengths for this system but the FXTCCSD/cc-pVTZ geometry is in good agreement with the available experimental geometry. Furthermore, the vibrational frequencies and ZPE (discussed in detail in the next section) from a cc-pVDZ calculation are in excellent agreement with the experimental values [157]. Harmonic ZPE values are not particularly sensitive to basis set choice for a system of comparable size [74] so the cc-pVDZ value is used with confidence that the difference between the available ZPE values and cc-pVTZ values is under a kcal/mol.

The cc-pVDZ ZPE values calculated with anharmonically-scaled frequencies for bicyclo[1,1,0]butane and conrotary and disrotary transition states are: 52.34 kcal/mol, 49.47 kcal/mol and 48.86 kcal/mol respectively. The experimental ZPE for bicyclo[1,1,0]butane is 52.43 kcal/mol. This leads to the following activation barriers (ΔH) using cc-pVTZ energy and geometry: 42.16 kcal/mol for the conrotary pathway and 59.28 kcal/mol for the disrotary pathway. These results are summarized in Table 6-10.

Single point FXTCCSD energy calculations are done at the FXTCCSD/cc-pVTZ geometries with cc-pVQZ basis set to obtain the values for conrotary and disrotary transition states: 41.54 kcal/mol and 58.78 kcal/mol with anharmonically-scaled frequencies.

Select previous theoretical results for the conrotary pathway include: ΔE = 42.2 kcal/mol and ΔH = 41.5 kcal/mol PT2F energy at MCSCF(10,10) geometry with 6-31G* basis (for details see [118]); ΔH = 41.3 kcal/mol CR-CC(2,3)/CBS with CASSCF(10,10) geometry and ZPE [96]; ΔH = 41.2 kcal/mol 2-RDM/6-311G**[106]; ΔH = 40.4 kcal/mol OMR3-DMC[15]. For the disrotary pathway: ΔE = 60.3 kcal/mol and ΔH = 56.3 kcal/mol PT2F//MCSCF(10,10)/6-31G* basis [118]; ΔH = 67.1 kcal/mol CR-CC(2,3)/CBS with CASSCF(10,10) geometry and ZPE [96]; ΔH = 55.7 kcal/mol 2-RDM/6-311G**[106]; ΔH = 58.7 kcal/mol OMR3-DMC[15].

The experimental value for ΔH for the conrotary pathway is 41(2.5) [145] but the value for the disrotary pathway is unknown.

All of the previous methods from literature, experimental value and the values in this work are in good agreement regarding the activation energy barrier of the conrotary path. However, the more difficult to compute disrotary path is not as consistent. Our value for ΔH is in better agreement with the value of Nguyen and Gordon as opposed to Lutz and Piecuch. However, one must point out that this agreement is likely fortuitous due to a difference in the basis sets employed as well as a substantial difference between the FXTCCSD/cc-pVTZ geometries and the MCSCF(10,10)/6-31G* geometries which were closer to the CASSCF(10,10)/cc-pVDZ geometries in [70].

In order to find some conformation of the FXTCCSD result, a ΛCCSD(T) calculation was performed. The ΛCCSD(T) method is capable in overcoming some of the multi-reference difficulties of the regular CCSD(T) method [151, 152]. Table 6-10 includes the results from the ΛCCSD(T) calculation which is in agreement with the FXTCCSD result. The ΔE value is the difference between total energy and the ΔH value

Table 6-10. Energetics of bicyclo[1,1,0]butane isomerization. All energy units are in kcal/mol. The cc-pVQZ values are energies with cc-pVTZ geometries.

		FXTCCSD/ cc-pVDZ	FXTCCSD/ cc-pVTZ	FXTCCSD/ cc-pVQZ	ΛCCSD(T)/ cc-pVDZ	ΛCCSD(T)/ cc-pVTZ
bicyclo[1,1,0]butane	ZPE	54.24			54.16	
	ZPE_{sc}	52.34			52.30	
Through conrotary TS	ΔE	42.79	45.03	44.28	43.59	45.37
	ZPE	51.39			51.43	
	ΔH	39.93	42.18	41.56	40.86	42.64
	ZPE_{sc}	49.47			49.56	
	$ΔH_{sc}$	39.92	42.16	41.54	40.85	42.63
Through disrotary TS	ΔE	58.77	62.76	62.22	60.86	64.91
	ZPE	50.74			50.83	
	ΔH	55.26	59.26	58.81	57.53	61.59
	ZPE_{sc}	48.86			48.90	
	$ΔH_{sc}$	55.29	59.28	58.78	57.46	61.51

includes correction for ZPE. The ZPE is only calculated with the cc-pVDZ basis and the the sc subscript denotes an anharmonically-scaled value. The 2-RDM activation barrier energy for the disrotary TS as well as the OMR3-DMC are both very close to the FXTCCSD and even ΛCCSD(T) values when done with a comparable basis set.

6.5 Frequencies and ZPE

Vibrational frequencies calculated in ACES II are based on a harmonic potential. The most inexpensive way to correct for the difference in energy between harmonic energy levels and anharmonic energy levels is to empirically derive a scaling factor using experimental frequencies. The scaling factor varies for different methods and basis sets. A wide variety of the scaling factors is available on the Computational Chemistry Comparison and Benchmark DataBase (CCCBDB)[4] .

The ZPE which is one half the sum of all frequencies should also be scaled. Since the active space methods presented here are novel and there is no entry on the CCCBDB for them, we derive our own scaling factors based on the examples at hand: ethylene and bicyclo[1,1,0]butane with the caveat that only those frequencies which

[4] http://cccbdb.nist.gov/

Table 6-11. Vibrational frequencies of bicyclo[1,1,0]butane isomerization.

	Experiment	FXTCCSD/cc-pVDZ			FXTCCSD/cc-pVDZ - scaled		
	BIC	BIC	CON	DIS	BIC	CON	DIS
	423	408*			408*		
	657	661*	409*	352*	661*	409*	352*
	737	755	578*	386*	724	555	386*
	838	861	637	579	826	611	555
	839	873	704	682*	837	675	682*
	909	924	761*	746*	886	761*	746*
	935	942*	890*	842	942*	890*	808
	980	986*	918	893	986*	880	856
	1063	1083*	945	994	1083*	906	954
	1081	1104	1009	1018	1059	968	977
	1081	1105	1037*	1034*	1060	1037*	1034*
	1092	1136	1050	1094	1136	1007	1049
	1110	1171	1115	1144	1123	1069	1097
	1172	1186	1201	1156	1138	1153	1109
	1261	1293	1272	1226	1241	1220	1176
	1266	1335	1361	1381	1280	1305	1325
	1485	1487	1479	1470	1426	1419	1410
	1501	1528	1508	1481	1465	1446	1421
	2935	3087	3089	3098	2961	2963	2972
	2969	3090	3154	3108	2964	3026	2981
	3044	3196	3177	3136	3066	3048	3008
	3044	3198	3189	3198	3068	3059	3068
	3120	3261	3195	3219	3128	3064	3088
	3131	3273	3268	3252	3140	3135	3120
scaling factor	0.959						
ZPE	52.43	54.24	51.39	50.74	52.34	49.47	48.86

are dominated by a stretch are to be used in the determination of the scaling factor and subsequently scaled. Bending and torsional frequencies generally have potentials which are best described by trigonometric functions and therefore should not be unilaterally scaled.

Table 6-11 shows all of the vibrational frequencies, scaling factors and ZPE values used in the determination of the scaled ΔH values. The experimental values are from [157]. The * signify modes which are identified to be primarily bending and/or twisting and thus are not scaled.

The scaling factor is derived by:

$$scaling.factor = \frac{\sum \tilde{\nu}_{exp}\tilde{\nu}_{calc}}{\tilde{\nu}^2_{calc}} \tag{6–5}$$

where only the predominantly stretching frequencies are used in the summation. This is repeated with the ΛCCSD(T) for which the scaling factor is 0.960. Finally, the same procedure is repeated with the ethylene (experimental frequency values from [86]) at FXTCCSD/cc-pVDZ and the scaling factor remains consistent at 0.959.

6.6 Conclusion

Single reference coupled cluster methods are shown to have the ability to successfully address multi-reference problems as seen in the two cases demonstrated in this work when CCSDT provides a good treatment of a single bond dissociation. For higher MR character examples such as ozone vibrational frequencies or double bond dissociation, one would expect the same can be accomplished with CCSDTQ and higher.

We have outlined a procedure that brings the cost of high order coupled cluster calculation down considerably without a significant loss of accuracy, so that more challenging multi-reference problems can now be tackled with a large enough basis set to yield useful results.

The active space selection procedure is automated and will perform with very little intervention from the user. We believe, philosophically, that this is the best way to assure a truly predictive theory, not biased to the users' chemical knowledge or experience with quantum chemistry software.

At this point, there is reason to believe that the contractions used in the Dunning basis sets yield a less than optimal energy manifold of the virtual orbitals which tends to cause the ASDA to make earlier cutoffs than necessary. When compared to a large ANO basis set, the statistical analysis yields more consistent results: no early cutoffs and no large amplitudes which go outside the extended space.

CHAPTER 7
CONCLUSIONS AND FUTURE WORK

There are several novel approaches described in this dissertation which greatly aid chemists in performing computationally demanding calculation at a lower cost but with little to no sacrifice in accuracy. STEOM is a well established method which tends to be underutilized due to its limited availability. Future implementation of STEOM in the parallel ACES III software will greatly increase its usability and presence in the literature.

The analytic fitting to vibtrational normal modes followed by a solution of the Hamiltonian in a discrete variable representation produces a good vibronic spectrum, even when some of the normal modes are dissociative; which is the main advantage of the DVR approach. The mode-mode coupling is hidden in the potential energy surfaces and is introduced perturbatively and analytically.

The active space partitioning of the Hilbert space may not be a new concept. However, an automatic approach without user bias or knowledge of chemistry is novel. Generally, those who use CAS and CCSDtq methods tend to pick active spaces based on their prior knowledge of the system or until the theoretical and the experimental results reach agreement. The ASDA provides a philosophically different approach by using the statistical analysis of the Hilbert space to determine the active space cutoffs.

The ASDA is superbly demonstrated with several simple but novel active space methods in which the correlation in the active space is solved with CCSDT and the correlation in the full space is solved with CCSD subject to the constant amplitudes from the CCSDT calculation. This approach yields excellent CCSDT-quality results without incurring the CCSDT cost. These methods are easily amendable to many other combinations: CCSDTQ/CCSD, CCSDT-1/CCSD, CCSD/MBPT(2), *etc*., all depending on the level of accuracy desired. Furthermore, the ASDA allows the Hilbert space to be partitioned in many layers providing a possibility to perform a CCSDQ/CCSD/MBPT(2) calculation for a large system and expect the results to be close to CCSDTQ in quality.

Finally, an interesting application of all of the techniques proposed in this dissertation is to use the FXTCCSD method to calculate the ground state PES along with STEOM-CCSD to compute the excited state PES in order to obtain dissociative absorption cross sections. The RHF-UHF PES discontinuity observed in the NaOH example would be mitigated and it should lead to significantly better analytic potential fits. The final product would be a stand-alone DVR program written in a high-level language (such as R or MatLab) which would include input parsing, curve-fitting, solving the DVR vibrational Hamiltonian, and generating the plots of the vibronic cross section.

REFERENCES

[1] Agmon, Noam. “Elementary Steps in Excited-State Proton Transfer.” *The Journal of Physical Chemistry A* 109 (2005).1: 13–35. PMID: 16839085.

[2] Andrews, L. “Ultraviolet-absorption studies of alkali-metal atom oxygen molecule matrix reaction.” *Journal of Molecular Spectroscopy* 61 (1976).3: 337–345.

[3] Bartlett, Rodney J. “Coupled-cluster approach to molecular structure and spectra: a step toward predictive quantum chemistry.” *Journal of Physical Chemistry* 93 (1989).5: 577.

[4] Bartlett, Rodney J. *Coupled cluster theory: An overview of recent developments*. Singapore: World Scientific Publishing Co. Ltd., 1995.

[5] Bartlett, Rodney J. and Musiał, Monika. “Coupled-cluster theory in quantum chemistry.” *Rev. Mod. Phys.* 79 (2007): 291–352.

[6] Bartlett, Rodney J. and Nooijen, Marcel. “A new method for excited states: Similarity transformed equation- of-motion coupled-cluster theory.” *Journal of Chemical Physics* 106 (1997): 6441–6448.

[7] Bartlett, Rodney J. and Purvis, George D. “Electron correlation in large molecules with many-body methods.” *Annals of the New York Academy of Sciences* 367 (1981).1: 62–82.

[8] Bartlett, Rodney J. and Purvis III, G. D. “Many-body perturbation theory, coupled-pair many-electron theory, and the importance of quadrupole excitations for the correlation problem.” *International Journal of Quantum Chemistry* 14 (1978).5: 561.

[9] Bartlett, Rodney J. and Purvis III, G. D. “Molecular applications of coupled cluster and many-body perturbation methods.” *Physcia Scripta* 21 (1980): 255.

[10] Bartlett, Rodney J. and Stanton, John F. *Applications of post-Hatree-Fock methods: a tutorial*. New York: VCH Publishers, 1994.

[11] Bartlett, Rodney J., Watts, J.D., Kucharski, S.A., and Noga, J. “Non-iterative fifth-order triple and quadruple excitation energy corrections in correlated methods.” *Chemical Physics Letters* 165 (1990).6: 513 – 522.

[12] Becke, Axel D. “Density-functional thermochemistry. III. The role of exact exchange.” *The Journal of Chemical Physics* 98 (1993).7: 5648–5652.

[13] Bene, Janet Del and Jaffé, H. H. “Use of the CNDO Method in Spectroscopy. III. Monosubstituted Benzenes and Pyridines.” *The Journal of Chemical Physics* 49 (1968).3: 1221–1229.

[14] Berger, R., Fischer, C., and Klessinger, M. “Calculation of the Vibronic Fine Structure in Electronic Spectra at Higher Temperatures. 1. Benzene and Pyrazine.” *Journal of Physical Chemistry A* 102 (1998): 7157–7167.

[15] Berner, R. and Lüchow, A. “Isomerization of Bicyclo[1.1.0]butane by Means of the Diffusion Quantum Monte Carlo Method.” *Journal of Physical Chemistry A* 114 (2010): 13222–13227.

[16] Bode, Brett M. and Gordon, Mark S. “Macmolplt: a graphical user interface for GAMESS.” *Journal of Molecular Graphics and Modelling* 16 (1998).3: 133 – 138.

[17] Bolovinos, A., Tsekeris, P., Philis, J., Pantos, E., and Andritsopoulos, G. “Absolute vacuum ultraviolet absorption spectra of some gaseous azabenzenes.” *Journal of Molecular Spectroscopy* 103 (1984): 240–256.

[18] Borrelli, Raffaele and Peluso, Andrea. “The vibrational progressions of the N –> V electronic transition of ethylene: A test case for the computation of Franck-Condon factors of highly flexible photoexcited molecules.” *The Journal of Chemical Physics* 125 (2006).19: 194308.

[19] Brucker, G. A. and Kelley, D. F. “Excited state intermolecular proton transfer in matrix isolated beta-naphthol/ammonia complexes.” *The Journal of Chemical Physics* 90 (1989).10: 5243–5251.

[20] Buenker, Robert and Peyerimhoff, Sigrid. “Individualized configuration selection in CI calculations with subsequent energy extrapolation.” *Theoretical Chemistry Accounts: Theory, Computation, and Modeling (Theoretica Chimica Acta)* 35 (1974): 33–58.

[21] Bytautas, Laimutis, Nagata, Takeshi, Gordon, Mark S., and Ruedenberg, Klaus. “Accurate ab initio potential energy curve of F[sub 2]. I. Nonrelativistic full valence configuration interaction energies using the correlation energy extrapolation by intrinsic scaling method.” *The Journal of Chemical Physics* 127 (2007).16: 164317.

[22] Calvert, Jack G. and Pitts Jr., James N. *Photochemistry*. New York: John Wiley & Sons, 1966.

[23] Chase Jr., M. W. *J. Phys. Chem. Ref. Data* (1998).9: 1.

[24] Cheshnovsky, Ori and Leutwyler, Samuel. “Excited-state proton transfer in neutral microsolvent clusters: naphthol(NH3)n.” *Chemical Physics Letters* 121 (1985).1-2: 1 – 8.

[25] Cheshnovsky, Ori and Leutwyler, Samuel. “Proton transfer in neutral gas-phase clusters: alpha-Naphthol [center-dot] (NH[sub 3])[sub n].” *The Journal of Chemical Physics* 88 (1988).7: 4127–4138.

[26] Chutjian, A., Hall, R. I., and Trajmar, S. “Electron-impact excitation of H[sub 2]O and D[sub 2]O at various scattering angles and impact energies in the energy-loss range 4.2–12 eV.” *The Journal of Chemical Physics* 63 (1975).2: 892–898.

[27] Cizek, J. “Use of the cluster expansion and the technique of diagrams in calculations of correlation effects in atoms and molecules.” *Advances in Chemical Physics* 14 (1969): 35.

[28] Cizek, J., Paldus, J., and Shavitt, I. “Correlation problems in atomic and molecular systems. IV. Extended coupled-pair many-electron theory and its application to the borane molecule.” *Physical Review A: Atomic, Molecular, and Optical Physics* 5 (1972).3: 50.

[29] Colbert, Daniel T and Miller, William H. “A novel discrete variable representation for quantum scattering via the S-matrix Kohn method.” *Journal of Chemical Physics* 96 (1992): 1982–1991.

[30] Cox, Kent W., Harmony, Marlin D., Nelson, Gordon, and Wiberg, K. B. “Microwave Spectrum and Structure of Bicyclo[1.1.0]butane.” *The Journal of Chemical Physics* 50 (1969).5: 1976–1980.

[31] Coxon, John A. and Hajigeorgiou, Photos G. “The B1+ and X1+ Electronic States of Hydrogen Fluoride: A Direct Potential Fit Analysis.” *J. Phys. Chem. A* 110 (2006).19: 6261.

[32] Daigoku, Kota, ichi Ishiuchi, Shun, Sakai, Makoto, Fujii, Masaaki, and Hashimoto, Kenro. “Photochemistry of phenol–(NH[sub 3])[sub n] clusters: Solvent effect on a radical cleavage of an OH bond in an electronically excited state and intracluster reactions in the product NH[sub 4](NH[sub 3])[sub n - 1] (n <= 5).” *The Journal of Chemical Physics* 119 (2003).10: 5149–5158.

[33] David, O., Dedonder-Lardeux, C., and Jouvet, C. “Is there an Excited State Proton Transfer in phenol (or 1 -naphthol)-ammonia clusters? Hydrogen Detachment and Transfer to Solvent: A key for non-radiative processes in clusters.” *International Reviews in Physical Chemistry* 21 (2002).3: 499–523.

[34] Dessent, Caroline E. H. and MÃijller-Dethlefs, Klaus. “Hydrogen-Bonding and van der Waals Complexes Studied by ZEKE and REMPI Spectroscopy.” *Chemical Reviews* 100 (2000).11: 3999–4022.

[35] Douglas, John E., Rabinovitch, B. S., and Looney, F. S. “Kinetics of the Thermal Cis-Trans Isomerization of Dideuteroethylene.” *The Journal of Chemical Physics* 23 (1955).2: 315–323.

[36] Droz, Thierry, Knochenmuss, Richard, and Leutwyler, Samuel. “Excited-state proton transfer in gas-phase clusters: 2-Naphthol(NH3n).” *The Journal of Chemical Physics* 93 (1990).7: 4520–4532.

[37] Dunning Jr., Thom H. “Gaussian basis sets for use in correlated molecular calculations. I. The atoms boron through neon and hydrogen.” *Journal of Chemical Physics* 90 (1989): 1007–1023.

[38] Evangelista, Francesco A. “Alternative single-reference coupled cluster approaches for multireference problems: The simpler, the better.” *The Journal of Chemical Physics* 134 (2011).22: 224102.

[39] Evangelista, Francesco A., Allen, Wesley D., Schaefer, Henry F., and III. “Coupling term derivation and general implementation of state-specific multireference coupled cluster theories.” *The Journal of Chemical Physics* 127 (2007).2: 024102.

[40] Evangelista, Francesco A., Prochnow, Eric, Gauss, Jürgen, Schaefer, Henry F., and III. “Perturbative triples corrections in state-specific multireference coupled cluster theory.” *The Journal of Chemical Physics* 132 (2010).7: 074107.

[41] Feller, David, Peterson, Kirk A., and Hill, J. Grant. “On the effectiveness of CCSD(T) complete basis set extrapolations for atomization energies.” *The Journal of Chemical Physics* 135 (2011).4: 044102.

[42] Feller, David and Sordo, Jose A. “Performance of CCSDT for diatomic dissociation energies.” *The Journal of Chemical Physics* 113 (2000).2: 485–493.

[43] Flaud, J. M., Peyret, C. C., Johns, J. W. C., and Carli, B. “The far infrared spectrum of H[sub 2]O[sub 2]. First observation of the staggering of the levels and determination of the cis barrier.” *Journal of Chemical Physics* 91 (1989): 1504–1510.

[44] Fleisher, A. J., Morgan, P. J., and Pratt, D. W. “Charge transfer by electronic excitation: Direct measurement by high resolution spectroscopy in the gas phase.” *The Journal of Chemical Physics* 131 (2009).21: 211101.

[45] Flowers, Bradley A, Stanton, John F, and Simpson, William R. “Wavelength Dependence of Nitrate Radical Quantum Yield from Peroxyacetyl Nitrate Photolysis: Experimental and Theoretical Studies.” *Journal of Physical Chemistry A* 111 (2007): 11602–11607.

[46] Foresman, James B., Head-Gordon, Martin, Pople, John A., and Frisch, Michael J. “Toward a systematic molecular orbital theory for excited states.” *The Journal of Physical Chemistry* 96 (1992).1: 135–149.

[47] Förster, T. *Z. Elektrochem* 54 (1949): 42.

[48] Furche, Filipp and Ahlrichs, Reinhart. “Adiabatic time-dependent density functional methods for excited state properties.” *The Journal of Chemical Physics* 117 (2002).16: 7433–7447.

[49] Ghose, Keya B., Piecuch, Piotr, and Adamowicz, Ludwik. “Improved computational strategy for the state-selective coupled-cluster theory with semi-internal triexcited clusters: Potential energy surface of the HF molecule.” *The Journal of Chemical Physics* 103 (1995).21: 9331–9346.

[50] Giroux, L., Back, M.H., and Back, R.A. “A comment on the rotational isomerization of ethylene.” *Chemical Physics Letters* 154 (1989).6: 610 – 612.

[51] Granucci, Giovanni, Hynes, James T., Milloé, Philippe, and Tran-Thi, Thu-Hoa. “A Theoretical Investigation of Excited-State Acidity of Phenol and Cyanophenols.” *Journal of the American Chemical Society* 122 (2000).49: 12243–12253.

[52] Gurvich, V., Bergman, G. A., Gorokhov, N., and Vungman, V. S. “Thermodynamic Properties of Alkali Metal Hydroxides. Part 1. Lithium and Sodium Hydroxides.” *Journal of Physical Chemistry Reference Data* 25 (1996): 1211–1276.

[53] Halkier, Asger, Helgaker, Trygve, Jörgensen, Poul, Klopper, Wim, Koch, Henrik, Olsen, Jeppe, and Wilson, Angela K. “Basis-set convergence in correlated calculations on Ne, N2, and H2O.” *Chemical Physics Letters* 286 (1998): 243 – 252.

[54] Hariharan, P.C. and Pople, J.A. “The influence of polarization functions on molecular orbital hydrogenation energies.” *Theoretica chimica acta* 28 (1973): 213–222.

[55] Harrison, Robert J., Fitzgerald, George B., Laidig, William D., and Barteltt, Rodney J. “Analytic MBPT(2) second derivatives.” *Chemical Physics Letters* 124 (1986).3: 291 – 294.

[56] Henseler, Debora, Tanner, Christian, Frey, Hans-Martin, and Leutwyler, Samuel. “Intermolecular vibrations of 1-naphthol(NH3) and d3-1-naphthol(ND3) in the S0 and S1 states.” *The Journal of Chemical Physics* 115 (2001).9: 4055–4069.

[57] Herzberg, G. *Infrared and Raman Spectra of Polyatomic Molecules*. New York: Van Nostrand Reinhold, New York, 1945.

[58] Hineman, M. F., Brucker, G. A., Kelley, D. F., and Bernstein, E. R. “Excited-state proton transfer in 1-naphthol/ammonia clusters.” *The Journal of Chemical Physics* 97 (1992).5: 3341–3347.

[59] Hino, Osamu, Kinoshita, Tomoko, Chan, Garnet Kin-Lic, and Bartlett, Rodney J. “Tailored coupled cluster singles and doubles method applied to calculations on molecular structure and harmonic vibrational frequencies of ozone.” *The Journal of Chemical Physics* 124 (2006).11: 114311.

[60] Hirao, K. “Multireference Möller-Plesset method.” *Chemical Physics Letters* 190 (1992).3-4: 374 – 380.

[61] Hoffmann, Mark R., Datta, Dipayan, Das, Sanghamitra, Mukherjee, Debashis, Ágnes Szabados, Rolik, Zoltán, and Surján, Péter R. “Comparative study of multireference perturbative theories for ground and excited states.” *The Journal of Chemical Physics* 131 (2009).20: 204104.

[62] Huber, K. J. and Herzberg, G. *Molecular Spectra and Molecular Structure: Constants of Diatomic Molecules*. New York: Van Nostrand Reinhold, New York, 1979.

[63] Humphrey, Susan J. and Pratt, David W. “Acid–base chemistry in the gas phase: The trans-1-naphthol [center-dot] NH[sub 3] complex in its S[sub 0] and S[sub 1] electronic states.” *The Journal of Chemical Physics* 104 (1996).21: 8332–8340.

[64] Ivanov, Vladimir V. and Adamowicz, Ludwik. “CASCCD: Coupled-cluster method with double excitations and the CAS reference.” *The Journal of Chemical Physics* 112 (2000).21: 9258–9268.

[65] Jacoby, Christoph, Hering, Peter, Schmitt, Michael, Roth, Wolfgang, and Kleinermanns, Karl. “Investigations of OHN- and NHO-type hydrogen-bonded clusters by UV laser spectroscopy.” *Chemical Physics* 239 (1998).1-3: 23 – 32.

[66] Jenkin, Michael E., Boyd, Andrew A., and Lesclaux, Robert. “Peroxy Radical Kinetics Resulting from the OH-Initiated Oxidation of 1,3-Butadiene, 2,3-Dimethyl-1,3-Butadiene and Isoprene.” *Journal of Atmospheric Chemistry* 29 (1998): 267–298.

[67] Johnson, J. R., Jordan, K. D., Plusquellic, D. F., and Pratt, D. W. “High resolution S1 <– S0 fluoescence excitation spectra of the 1- and 2-hydroxynaphthalenes. Distinguishing the cis and trans rotamers.” *The Journal of Chemical Physics* 93 (1990).4: 2258–2273.

[68] Jouvet, C., Lardeux-Dedonder, C., Richard-Viard, M., Solgadi, D., and Tramer, A. “Reactivity of molecular clusters in the gas phase: proton-transfer reaction in neutral phenol-(ammonia)n and phenol-(ethanamine)n.” *The Journal of Physical Chemistry* 94 (1990).12: 5041–5048.

[69] Kimura, K. and Nagakura, S. “Vacuum ultra-violet absorption spectra of various mono-substituted benzenes.” *Molecular Physics* 9 (1965).2: 117–135.

[70] Kinal, Armagan and Piecuch, Piotr. “Computational Investigation of the Conrotatory and Disrotatory Isomerization Channels of Bicyclo[1.1.0]butane to Buta-1,3-diene: A Completely Renormalized Coupled-Cluster Study.” *The Journal of Physical Chemistry A* 111 (2007).4: 734–742. PMID: 17249766.

[71] Kinoshita, Tomoko, Hino, Osamu, and Bartlett, Rodney J. “Coupled-cluster method tailored by configuration interaction.” *The Journal of Chemical Physics* 123 (2005).7: 074106.

[72] Knochenmuss, Richard. “Excited-state proton transfer in 1-naphthol(NH3n complexes: the threshold size is n=4.” *Chemical Physics Letters* 293 (1998).3-4: 191 – 196.

[73] Knochenmuss, Richard and Fischer, Ingo. “Excited-state proton transfer in naphthol/solvent clusters: the current state of affairs.” *International Journal of Mass Spectrometry* 220 (2002).2: 343 – 357.

[74] Kolmann, Stephen J. and Jordan, Meredith J. T. “Method and basis set dependence of anharmonic ground state nuclear wave functions and zero-point energies: Application to SSSH.” *The Journal of Chemical Physics* 132 (2010).5: 054105.

[75] Koput, Jacek. “An ab initio study on the equilibrium structure and torsional potential energy function of hydrogen peroxide.” *Chemical Physics Letters* 236 (1995): 516–520.

[76] Kou, Zhuangfei, Shen, Jun, Xu, Enhua, and Li, Shuhua. “Hybrid coupled cluster methods: Combining active space coupled cluster methods with coupled cluster singles, doubles, and perturbative triples.” *The Journal of Chemical Physics* 136 (2012).19: 194105.

[77] Krylov, Anna I. and Sherrill, C. David. “Perturbative corrections to the equation-of-motion spin–flip self-consistent field model: Application to bond-breaking and equilibrium properties of diradicals.” *The Journal of Chemical Physics* 116 (2002).8: 3194–3203.

[78] Krylov, Anna I., Sherrill, C. David, Byrd, Edward F. C., and Head-Gordon, Martin. “Size-consistent wave functions for nondynamical correlation energy: The valence active space optimized orbital coupled-cluster doubles model.” *The Journal of Chemical Physics* 109 (1998).24: 10669–10678.

[79] Kuchitsu, K. *Structure of Free Polyatomic Molecules - Basic Data*. Berlin: Springer Netherlands, 1998.

[80] Kuś, Tomasz, Lotrich, Victor F., and Bartlett, Rodney J. “Parallel implementation of the equation-of-motion coupled-cluster singles and doubles method and application for radical adducts of cytosine.” *The Journal of Chemical Physics* 130 (2009).12: 124122.

[81] Larsen, N.W. “Microwave spectra of the six mono-13C-substituted phenols and of some monodeuterated species of phenol. Complete substitution structure and absolute dipole moment.” *Journal of Molecular Structure* 51 (1979).0: 175 – 190.

[82] Le Roy, R. J. “LEVEL 8.0, A Computer Program for Solving the Radial Schrödinger Equation for Bound and Quasibound Levels.”

[83] Lee, Edmond P F and Wright, Timothy G. “Heats of Formation of NaOH and NaOH + : Ionization Energy of NaOH.” *Journal of Physical Chemistry A* 106 (2002): 8903–8907.

[84] Lee, Yoon S., Kucharski, Stanislaw A., and Bartlett, Rodney J. “A coupled cluster approach with triple excitations.” *The Journal of Chemical Physics* 81 (1984): 5906–5912.

[85] Lee, Young-Shin, Yu, Hyunung, Kwon, Oh-Hoon, and Jang, Du-Jeon. “Photo-induced proton-transfer cycle of 2-naphthol in faujasite zeolitic nanocavities.” *Phys. Chem. Chem. Phys.* 10 (2008): 153–158.

[86] Lerberghe, D. Van, Wright, I.J., and Duncan, J.L. “High-resolution infrared spectrum and rotational constants of ethylene-H4.” *Journal of Molecular Spectroscopy* 42 (1972).2: 251 – 273.

[87] Li, Xiangzhu and Paldus, Josef. “Reduced multireference CCSD method: An effective approach to quasidegenerate states.” *The Journal of Chemical Physics* 107 (1997).16: 6257–6269.

[88] Li, Xiangzhu and Paldus, Josef. “Reduced multireference couple cluster method. II. Application to potential energy surfaces of HF, F[sub 2], and H[sub 2]O.” *The Journal of Chemical Physics* 108 (1998).2: 637–648.

[89] Li, Xiangzhu and Paldus, Josef. “General-model-space state-universal coupled-cluster method: excitation energies of water.” *Molecular Physics* 104 (2006).5-7: 661–676.

[90] Light, J. C., Hamilton, I. P., and Lill, J. V. “Generalized discrete variable approximation in qunatum mechanics.” *Journal of Chemical Physics* 82 (1985): 1400–1409.

[91] Loch, Marta W., Lodriguito, Maricris D., Piecuch, Piotr, and Gour, Jeffrey R. “Two new classes of non-iterative coupled-cluster methods derived from the method of moments of coupled-cluster equations.” *Molecular Physics* 104 (2006).13-14: 2149–2172.

[92] Lotrich, V.F., Ponton, J.M., Perera, A.S., Deumens, E., Bartlett, R.J., and Sanders, B.A. “Super instruction architecture of petascale electronic structure software: the story.” *Molecular Physics* 108 (2010).21-23: 3323–3330.

[93] Lotrich, Victor F., Flocke, N., Ponton, M., Yau, A. D., Perera, A., Deumens, E., and Bartlett, R. J. “Parallel implementation of electronic structure energy, gradient, and Hessian calculations.” *The Journal of chemical physics* 128 (2008): 194104.

[94] Lüchow, Arne and Anderson, James B. “Accurate quantum Monte Carlo calculations for hydrogen fluoride and the fluorine atom.” *The Journal of Chemical Physics* 105 (1996).11: 4636.

[95] Läuter, H. “Silverman, B. W.: Density Estimation for Statistics and Data Analysis. Chapman and Hall, London âĂŞ New York 1986.” *Biometrical Journal* 30 (1988).7: 876–877.

[96] Lutz, Jesse J. and Piecuch, Piotr. “Extrapolating potential energy surfaces by scaling electron correlation: Isomerization of bicyclobutane to butadiene.” *The Journal of Chemical Physics* 128 (2008).15: 154116.

[97] Lyakh, Dmitry I. and Bartlett, Rodney J. “An adaptive coupled-cluster theory: @CC approach.” *The Journal of Chemical Physics* 133 (2010).24: 244112.

[98] Lyakh, Dmitry I., Ivanov, Vladimir V., and Adamowicz, Ludwik. “State-specific multireference complete-active-space coupled-cluster approach versus other quantum chemical methods: dissociation of the N2 molecule.” *Molecular Physics* 105 (2007).10: 1335–1357.

[99] Lyakh, Dmitry I., Musiał, Monika, Lotrich, Victor, and Bartlett, Rodney J. “Multireference nature of chemistry: The coupled-cluster view.” *Chem. Revs.* (2012).112: 182–243.

[100] Madronich, S., Hastie, D. R., Ridley, B. A., and Schiff, H. I. “Calculations of the Temperature Dependence of the NO 2 Photodissociation Coefficient in the Atmosphere.” *Journal of Atmospheric Chemistry* 1 (1984): 151–157.

[101] Mahapatra, Uttam Sinha, Chattopadhyay, Sudip, and Chaudhuri, Rajat K. “Molecular applications of state-specific multireference perturbation theory to HF, H2O, H2S, C2, and N2 molecules.” *The Journal of Chemical Physics* 129 (2008).2: 024108.

[102] Mahapatra, Uttam Sinha, Chattopadhyay, Sudip, and Chaudhuri, Rajat K. “Second-order state-specific multireference Möller Plesset perturbation theory: Application to energy surfaces of diimide, ethylene, butadiene, and cyclobutadiene.” *Journal of Computational Chemistry* 32 (2011).2: 325–337.

[103] Marston, Clay C. and Balint-Kurti, G., Gabriel. “The Fourier grid Hamiltonian method for bound state eigenvalues and eigenfunctions.” *Journal of Chemical Physics* 91 (1989): 3571–3576.

[104] Matsumoto, Y, Ebata, T, and Mikami, N. “Structures and vibrations of 2-naphthol(NH3)n (n=1-3) hydrogen-bonded clusters investigated by IR/UV double-resonance spectroscopy.” *Journal of Molecular Structure* 552 (2000): 257 – 271.

[105] Mayor, E. and Velasco, A. M. “Photodissociation of the d(0,0) and d(1,0) bands of nitric oxide in the stratosphere and the mesosphere: A molecular-adapted quantum defect orbital calculation of photolysis rate constants.” *Journal of Geophysical Research* 112 (2007): D13304.

[106] Mazziotti, D. A. “Energy Barriers in the Conversion of Bicyclobutane to gauche-1,3-Butadiene from the Anti-Hermitian Contracted SchroÌĹdinger Equation.” *Journal of Physical Chemistry A* 112 (2008): 13684–13690.

[107] Merer, A. J. and Mulliken, Robert S. “Ultraviolet spectra and excited states of ethylene and its alkyl derivatives.” *Chemical Reviews* 69 (1969).5: 639–656.

[108] Mikami, Naohiko, Okabe, Akihiro, and Suzuki, Itaru. “Photodissociation of the hydrogen-bonded [phenol-ammonia]+ heterodimer ion.” *The Journal of Physical Chemistry* 92 (1988).7: 1858–1862.

[109] Molina, Vicent, Merchan, Manuela, Roos, Bjorn O., and Malmqvist, Per-Ake. “On the low-lying singlet excited states of styrene: a theoretical contribution.” *Phys. Chem. Chem. Phys.* 2 (2000): 2211–2217.

[110] Monnerville, M and Robbe, J M. “Optical potential coupled to discrete variable representation for calculations of quasibound states: Application interaction to the CO predissociating.” 101 (1994): 7580–7591.

[111] Mota, R., Parafita, R., Giuliani, A., Hubin-Franskin, M.-J., Lourenaso, J.M.C., Garcia, G., Hoffmann, S.V., Mason, N.J., Ribeiro, P.A., Raposo, M., and Limato-Vieira, P. “Water VUV electronic state spectroscopy by synchrotron radiation.” *Chemical Physics Letters* 416 (2005): 152 – 159.

[112] Mulliken, Robert S. “Molecular Compounds and their Spectra. III. The Interaction of Electron Donors and Acceptors.” *The Journal of Physical Chemistry* 56 (1952): 801–822.

[113] Bartlett, Rodney J and Musiał, Monika. “Coupled-cluster theory in quantum chemistry” *Review of Modern Physics* 79 (2007): 291–352.

[114] Musiał, Monika and Bartlett, Rodney J. “Charge-transfer separability and size-extensivity in the equation-of-motion coupled cluster method: EOM-CCx” *The Journal of Chemical Physics* 134 (2011): 034106.

[115] Musiał, Monika and Bartlett, Rodney J. “Multi-reference Fock space coupled-cluster method in the intermediate Hamiltonian formulation for potential energy surfaces.” *The Journal of Chemical Physics* 135 (2011): 044121.

[116] Musiał, Monika, Perera, Ajith, and Bartlett, Rodney J. “Multireference coupled-cluster theory: The easy way.” *The Journal of Chemical Physics* 134 (2011).11: 114108.

[117] Nagakura, S. and Gouterman, M. “Effect of Hydrogen Bonding on the Near Ultraviolet Absorption of Naphthol.” *The Journal of Chemical Physics* 26 (1957).4: 881–886.

[118] Nguyen, Kiet A. and Gordon, Mark S. “Isomerization Of Bicyclo[1.1.0]butane to Butadiene.” *Journal of the American Chemical Society* 117 (1995).13: 3835–3847.

[119] Nix, Michael G. D., Devine, Adam L., Cronin, Bríd, Dixon, Richard N., and Ashfold, Michael N. R. “High resolution photofragment translational spectroscopy studies of the near ultraviolet photolysis of phenol.” *The Journal of Chemical Physics* 125 (2006).13: 133318.

[120] Nooijen, Marcel. “Electronic Excitation Spectrum of s-Tetrazine:An Extended-STEOM-CCSD Study.” *The Journal of Physical Chemistry A* 104 (2000).19: 4553–4561.

[121] Nooijen, Marcel and Hazra, Anirban. “VIBRON-A Program for Vibronic Coupling and Franck-Condon Calculations. With contributions from J. F. Stanton and K. Sattelmeyer.” 2003.

[122] Olsen, Jeppe, Roos, Björn O., rgensen, Poul Jø, and rgen Aa. Jensen, Hans Jø. “Determinant based configuration interaction algorithms for complete and restricted configuration interaction spaces.” *The Journal of Chemical Physics* 89 (1988).4: 2185–2192.

[123] Paldus, J. *Methods in Computational Molecular Physics*. New York: Plenum Press, 1992.

[124] Piecuch, Piotr. “Active-space coupled-cluster methods.” *Molecular Physics* 108 (2010).21-23: 2987–3015.

[125] Piecuch, Piotr, aw A. Kucharski, Stanisł, and Bartlett, Rodney J. “Coupled-cluster methods with internal and semi-internal triply and quadruply excited clusters: CCSDt and CCSDtq approaches.” *The Journal of Chemical Physics* 110 (1999).13: 6103–6122.

[126] Piecuch, Piotr, Kowalski, Karol, Pimienta, Ian S. O., and Mcguire, Michael J. “Recent advances in electronic structure theory: Method of moments of coupled-cluster equations and renormalized coupled-cluster approaches.” *International Reviews in Physical Chemistry* 21 (2002).4: 527–655.

[127] Pino, G., Gregoire, G., Dedonder-Lardeux, C., Jouvet, C., Martrenchard, S., and Solgadi, D. “A forgotten channel in the excited state dynamics of phenol-(ammonia) clusters: hydrogen transfer.” *Phys. Chem. Chem. Phys.* 2 (2000): 893–900.

[128] Plane, J. M. C. “The role of sodium bicarbonate in the nucleation of noctilucent clouds.” *Annales Geophysicae* 18 (2000): 807–814.

[129] Plusquellic, D. F., Tan, X.-Q., and Pratt, D. W. “Acid-base chemistry in the gas phase. The cis- and trans-2-naphthol(NH3) complexes in their S0 and S1 states.” *The Journal of Chemical Physics* 96 (1992).11: 8026–8036.

[130] Pope, Francis D, Hansen, Jaron C, Bayes, Kyle D, Friedl, Randall R, and Sander, Stanley P. “Ultraviolet absorption spectrum of chlorine peroxide, ClOOCl.” *The journal of physical chemistry. A* 111 (2007): 4322–32.

[131] Purvis III, G. D. and Bartlett, Rodney J. “A full coupled-cluster singles and doubles model: the inclusion of disconnected triples.” *Journal of Chemical Physics* 76 (1982).4: 1910–1918.

[132] Puzari, Panchanan, Swathi, Rotti S, Sarkar, Biplab, and Adhikari, Satrajit. “A quantum-classical approach to the photoabsorption spectrum of pyrazine.” *The Journal of chemical physics* 123 (2005): 134317.

[133] Rauhut, Guntram. “Efficient calculation of potential energy surfaces for the generation of vibrational wave functions.” *The Journal of chemical physics* 121 (2004): 9313–22.

[134] Redmon, Lynn T., Purvis, George D., and Bartlett, Rodney J. “Accurate binding energies of diborane, borane carbonyl, and borazane determined by many-body perturbation theory.” *Journal of the American Chemical Society* 101 (1979).11: 2856–2862.

[135] Rosta, Edina and Surján, Péter R. “Two-body zeroth order Hamiltonians in multireference perturbation theory: The APSG reference state.” *The Journal of Chemical Physics* 116 (2002).3: 878–890.

[136] Sadlej, Andrzej J. “Medium-size polarized basis sets for high-level-correlated calculations of molecular electric properties.” *Theoretica Chimica Acta* 79 (1991): 123–140.

[137] Schmidt, Michael W., Baldridge, Kim K., Boatz, Jerry A., Elbert, Steven T., Gordon, Mark S., Jensen, Jan H., Koseki, Shiro, Matsunaga, Nikita, Nguyen, Kiet A., Su, Shujun, Windus, Theresa L., Dupuis, Michel, and Montgomery, John A. “General atomic and molecular electronic structure system.” *Journal of Computational Chemistry* 14 (1993).11: 1347–1363.

[138] Sears, John S., Sherrill, C. David, and Krylov, Anna I. “A spin-complete version of the spin-flip approach to bond breaking: What is the impact of obtaining spin eigenfunctions?” *The Journal of Chemical Physics* 118 (2003).20: 9084–9094.

[139] Self, Daniel E. and Plane, John M. C. “Absolute photolysis cross-sections for NaHCO 3 , NaOH, NaO, NaO 2 and NaO 3 : implications for sodium chemistry in the upper mesosphere.” *Physical Chemistry Chemical Physics* 4 (2002): 16–23.

[140] Shen, Jun, Xu, Enhua, Kou, Zhuangfei, and Li, Shuhua. “A coupled cluster approach with a hybrid treatment of connected triple excitations for bond-breaking potential energy surfaces.” *The Journal of Chemical Physics* 132 (2010).11: 114115.

[141] Siebrand, Willem, Zgierski, Marek Z., Smedarchina, Zorka K., Vener, Mikhail, and Kaneti, Jose. “The structure of phenol-ammonia clusters before and after proton transfer. A theoretical investigation.” *Chemical Physics Letters* 266 (1997).1-2: 47 – 52.

[142] Sobolewski, Andrzej L. and Domcke, Wolfgang. “Photoinduced Electron and Proton Transfer in Phenol and Its Clusters with Water and Ammonia.” *The Journal of Physical Chemistry A* 105 (2001).40: 9275–9283.

[143] Solgadi, D., Jouvet, C., and Tramer, A. “Resonance-enhanced multiphoton ionization spectra and ionization thresholds of phenol-(ammonia)n clusters.” *The Journal of Physical Chemistry* 92 (1988).12: 3313–3315.

[144] Solntsev, Kyril M., Huppert, Dan, and Agmon, Noam. “Solvatochromism of beta-Naphthol.” *The Journal of Physical Chemistry A* 102 (1998).47: 9599–9606.

[145] Srinivasan, R., Levi, A. A., and Haller, I. “The Thermal Decomposition of Bicyclo[1.1.0]butane.” *The Journal of Physical Chemistry* 69 (1965).5: 1775–1777.

[146] Staemmler, Volker. “Note on open shell restricted SCF calculations for rotation barriers about C-C double bonds: Ethylene and allene.” *Theoretical Chemistry Accounts: Theory, Computation, and Modeling (Theoretica Chimica Acta)* 45 (1977): 89–94. 10.1007/BF00552543.

[147] Stanton, J. F., J Gauss, J. T., Perera, S. A., Watts, J. D., Yau, A. D., Nooijen, M., Oliphant, N., Szalay, P. G., Lauderdale, W. J., Gwaltney, S. R., Beck, S., Balkova, A., Bernholdt, D. E., Baeck, K. K., Rozyczko, P., Sekino, H., Huber, C., Pittner, J., and Cencek, W. “ACES II is A Program Product Of The Quantum Theory Project University Of Florida. packages Included Are VMOL (J. Almlof, P. R. Taylor); VPROPS (P. Taylor); ABACUS (T. Helgaker, H.J. Aa. Jensen, P. Jørgensen, J. Olsen, P.R. Taylor); HONDO/GAMESS (M.W. Schmidt, K.K. Baldridge, J.A. Boatz, S.T. Elbert, M.S. Gordon, J.J. Jensen, S. Koseki, N. Matsunaga, K.A. Nguyen, S. Su, T.L. Windus, M. Dupuis, J.A. Montgomery.”

[148] Stanton, John F and Bartlett, Rodney J. “The equation of motion coupled-cluster method. A systematic biorthogonal approach to molecular excitation energies, transition probabilities, and excited state properties.” *The Journal of Chemical Physics* 98 (1993).9: 7029.

[149] Suppan, Paul. “Invited review solvatochromic shifts: The influence of the medium on the energy of electronic states.” *Journal of Photochemistry and Photobiology A: Chemistry* 50 (1990).3: 293 – 330.

[150] Tanner, Christian, Henseler, Debora, Leutwyler, Samuel, Connell, Leslie L., and Felker, Peter M. “Structural study of the hydrogen-bonded 1-naphthol(NH32 cluster.” *The Journal of Chemical Physics* 118 (2003).20: 9157–9166.

[151] Taube, Andrew G. and Bartlett, Rodney J. “Improving upon CCSD(T): Lambda CCSD(T). I. Potential energy surfaces.” *The Journal of Chemical Physics* 128 (2008).4: 044110.

[152] Taube, Andrew G. and Bartlett, Rodney J. “Improving upon CCSD(T): Lambda CCSD(T). II. Stationary formulation and derivatives.” *The Journal of Chemical Physics* 128 (2008).4: 044111.

[153] Tolbert, Laren M. and Solntsev, Kyril M. “Excited-State Proton Transfer: From Constrained Systems to Super Photoacids to Superfast Proton Transfer.” *Accounts of Chemical Research* 35 (2002).1: 19–27. PMID: 11790085.

[154] Trost, Barbara, Stutz, Jochen, and Platt, Ulrich. “UV-absorption cross sections of a series of monocyclic aromatic compounds.” *Atmospheric Environment* 31 (1997).23: 3999 – 4008.

[155] Wallace, R. “The torsional energy levels of ethylene: A re-evaluation.” *Chemical Physics Letters* 159 (1989).1: 35 – 36.

[156] Watanabe, K. and Zelikoff, M. “Absorption Coefficients of Water Vapor in the Vacuum Ultraviolet.” *J. Opt. Soc. Am.* 43 (1953).9: 753–754.

[157] Wiberg, Kenneth B., Waddell, Sherman T., and Rosenberg, Robert E. “Infrared intensities: bicyclo[1.1.0]butane. A normal coordinate analysis and comparison with cyclopropane and [1.1.1]propellane.” *Journal of the American Chemical Society* 112 (1990).6: 2184–2194.

[158] Widmark, Per Olof, Malmqvist, Per Ake, and Roos, Bjorn O. “Density matrix averaged atomic natural orbital (ANO) basis sets for correlated molecular wave functions.” *Theoretica Chimica Acta* 77 (1990): 291–306.

[159] Witek, Henryk A., Nakano, Haruyuki, and Hirao, Kimihiko. “Multireference perturbation theory with optimized partitioning. II. Applications to molecular systems.” *Journal of Computational Chemistry* 24 (2003).12: 1390–1400.

[160] Wood, M.H. “The barrier to rotation for the ground state of ethylene: a DC SCF approach.” *Chemical Physics Letters* 24 (1974).2: 239 – 242.

[161] Woon, David E. and Dunning Jr., Thom H. “Gaussian basis sets for use in correlated molecular calculations. V. Core-valence basis sets for boron through neon.” *Journal of Chemical Physics* 103 (1995): 4572–4585.

[162] Yang, Jie, Hao, Yusong, Li, Juan, Zhou, Chang, and Mo, Yuxiang. “A combined zero electronic kinetic energy spectroscopy and ion-pair dissociation imaging study of the F2+ structure.” *The Journal of Chemical Physics* 122 (2005).13: 134308.

[163] Yoshino, K., Esmond, J.R., Parkinson, W.H., Ito, K., and Matsui, T. “Absorption cross section measurements of water vapor in the wavelength region 120 to 188 nm.” *Chemical Physics* 211 (1996): 387 – 391.

[164] Yu, Hua-Gen. “A coherent discrete variable representation method for multidimensional systems in physics.” *The Journal of chemical physics* 122 (2005): 164107.

[165] Zemke, Warren T., c. Stwalley, William, Langhoff, Stephen R., Valderrama, Giuseppe L., and Berry, Michael J. “Radiative transition probabilities for all vibrational levels in the $X^1/Sigma^+$ state of HF.” *The Journal of Chemical Physics* 95 (1991).11: 7846.

[166] Zwier, Timothy S. “The spectroscopy of solvation in hydrogen-bonded aromatic clusters.” *Annual Review of Physical Chemistry* 47 (1996).1: 205–241.

BIOGRAPHICAL SKETCH

Ann was born in the USSR in 1982 in the Republic of Ukraine. She spent her childhood in Brooklyn, NY where she attended the Brooklyn Technical High School and graduated with NYS honors in 2000. Ann graduated with a B.A. in chemistry from Carnegie Mellon University in 2003 and went on to the University of Hawai'i at Manoa to obtain a M.S. in chemistry under the tutelage of Dr. John Head.

In 2006 Ann started her doctorate degree with Dr. Rodney Barlett in the Quantum Theory Project at the University of Florida. In 2013 Ann graduated with a Ph.D. in chemistry and a M.S. in electrical and computer engineering. She is currently employed at the Intel Corporation.